Research Square

Preprints are preliminary reports that have not undergone peer review.
They should not be considered conclusive, used to inform clinical practice,
or referenced by the media as validated information.

Dual-specificity protein phosphatase 1 (DUSP1/MKP1) enhances Radiation Efficacy in Triple-Negative Breast Cancer

Suryakant Niture

Suryakant-Niture@ou.edu

University of Oklahoma Health Sciences https://orcid.org/0009-0004-9503-5659

Dee Wu

University of Oklahoma Health Sciences

Blaine Mooers

Stephenson Cancer Center, University of Oklahoma Health Sciences

Andrew Thompson

Stephenson Cancer Center, University of Oklahoma Health Sciences

Muhammad Khan

Stephenson Cancer Center, University of Oklahoma Health Sciences

Carlos Vargas

Mayo Clinic Comprehensive Cancer Center

Saranya Chumsri

Mayo Clinic Comprehensive Cancer Center

Jennifer Kachergus

Mayo Clinic Comprehensive Cancer Center

Christina Henson

University of Oklahoma Health Sciences

Danushka Seneviratne

University of Oklahoma Health Sciences

Article

Keywords: Dual-specificity protein phosphatase 1, MAPKs, Breast cancer, Triple-negative breast cancer, Epithelial-mesenchymal transition, Radiation therapy

Posted Date: November 23rd, 2026

DOI: https://doi.org/10.21203/rs.3.rs-11408748/v1

License: This work is licensed under a Creative Commons Attribution 4.0 International License.
Read Full License

Additional Declarations: (Not answered)

Dual-specificity protein phosphatase 1 (DUSP1/MKP1) enhances Radiation Efficacy in Triple-Negative Breast Cancer

Suryakant Niture[1,2]*, Dee H. Wu[3], Blaine H. M. Mooers[2,4,5], Andrew Thompson[2], Muhammad Mansoor Khan[2], Carlos E Vargas[6], Saranya Chumsri[7], Jennifer M Kachergus[7], Christina Henson[1], and Danushka Seneviratne[1,2]*

[1]Department of Radiation Oncology, University of Oklahoma Health Sciences, Oklahoma City, OK 73104, USA

[2]Stephenson Cancer Center, University of Oklahoma Health Sciences, Oklahoma City, OK 73104, USA

[3]Department of Radiological Sciences, University of Oklahoma Health Sciences, Oklahoma City, OK 73104, USA

[4]Department of Biochemistry and Physiology, University of Oklahoma Health Sciences, Oklahoma City, OK 73104, USA

[5]Laboratory of Biomolecular Structure and Function, University of Oklahoma, Oklahoma City, OK 73104, USA

[6]Department of Radiation Oncology, Mayo Clinic Comprehensive Cancer Center, Phoenix, AZ 85054. USA

[7]Department of Radiation Oncology, Mayo Clinic Comprehensive Cancer Center, Jacksonville, FL 32224, USA

***Corresponding authors**

Suryakant Niture, MS, PhD

Stephenson Cancer Center

Department of Radiation Oncology, University of Oklahoma Health Sciences

800 N.E. 10th Street, Oklahoma City, OK 73104

Email: Suryakant-Niture@ouhsc.edu

Phone: 405-271-3016

Danushka Seneviratne, MD, PhD

Stephenson Cancer Center

Department of Radiation Oncology, University of Oklahoma Health Sciences

800 N.E. 10th Street, Oklahoma City, OK 73104

Email danushka-seneviratne@ouhsc.edu

Phone: 405-271-3016

Running title: *DUSP1 increased RT efficacy in TNBC*

Abstract

DUSP1/MKP-1 is a dual-specificity phosphatase that regulates MAPK signaling by dephosphorylating phosphothreonine and phosphotyrosine residues. This study investigated the regulation of DUSP1 following radiation therapy (RT) and its clinical significance in breast cancer (BC), particularly triple-negative breast cancer (TNBC). TCGA and immunohistochemistry analyses showed that reduced DUSP1 expression in hormone receptor-positive (HR+) BC and TNBC was associated with disease progression and aggressive tumor characteristics. NanoString RNA sequencing of BC patients' tumors receiving ultra-hypofractionated RT showed that RT induced DUSP1 expression, and increased DUSP1 levels were observed in the serum of TNBC patients treated with RT after breast conservation surgery (BCS). In vitro, RT-mediated induction or overexpression of DUSP1 suppressed TNBC-associated malignant characteristics by regulating MAPK signaling and promoting apoptosis. Mechanistically, RT induced phosphorylation of DUSP1 at S359, resulting in nuclear localization and modulating MAPK activity, thereby contributing to apoptotic responses. Transient and chronic RT exposure also altered DUSP1 and MAPK activity and regulated epithelial–mesenchymal transition (EMT) and cancer stem cell (CSC) markers. Pharmacological inhibition of DUSP1 and PARP in combination with RT altered TNBC cell proliferation, three-dimensional spheroid growth, and hypoxia. RNA-seq analysis further revealed enrichment of cell-cycle, autophagy, MAPK signaling, and metabolic pathways after RT or DUSP1 inhibition combined with RT. Overall, these findings indicate that DUSP1 loss is associated with poor prognosis and aggressive TNBC. RT-induced DUSP1 appears to enhance radiation efficacy through MAPK regulation and apoptosis, supporting DUSP1 as a potential prognostic biomarker and therapeutic target for TNBC treatment.

Keywords: Dual-specificity protein phosphatase 1, MAPKs, Breast cancer, Triple-negative breast cancer, Epithelial-mesenchymal transition, Radiation therapy.

Introduction

Dual-specificity protein phosphatases (DUSPs) consist of 11 members that play an important role in dephosphorylation and control of MAPK (ERK, JNK, and p38) signaling in the loop (DUSPs/MAPKs) [1, 2]. In response to external stresses, the phosphorylation of threonine and tyrosine residues of the catalytic domain (TXY motif) of MAPKs enhances MAPK activities [3, 4]. Activated MAPKs regulate gene transcription, mRNA and protein stability/localization, and control several cellular functions such as cell proliferation/ differentiation/ survival, autophagy, and cell apoptosis [5, 6]. To maintain cellular homeostasis, DUSP1-mediated dephosphorylation of MAPKs is required to reduce prolonged stress response, inflammation, and cellular dysfunction [7]. On the other hand, high DUSP1 expression is associated with numerous human diseases, such as dysregulation of adaptive and innate immune systems [8, 9], obesity-related metabolic control [10], suppression of osteoclast formation in mice [11], development of central nervous system (CNS) related disease and depressive disorder [12, 13].

In cancers, DUSP1 plays a context-dependent role and participates in tumor suppression, therapy resistance, and immune modulation in the tumor microenvironment (TME) [14]. DUSP1 is involved in the modulation of the TME by the invasion of tumor-associated macrophages [15, 16]. Elevated DUSP1 levels in prostate, pancreatic, gastric, colon, bladder, and lung cancers enhanced tumor growth [15, 17]. On the other hand, loss of DUSP1 levels in hepatocarcinoma (HCC) and head/neck squamous cell carcinoma suppressed tumor growth [18, 19]. Therefore, its function shifts from tumor promoter to suppressor depending on the cancer type and stage. Emerging studies suggest that dysregulation of DUSP1 expression impacts chemotherapeutic drug resistance [20-24], RT resistance [25-28], immunotherapy resistance [26, 29], as well as immune response [30-32].

BC is a heterogeneous disease, and patients with TNBC show a worse prognosis with a lower overall survival rate (78%) compared to other subtypes [33]. Loss of DUSP1 expression in BC is associated with increased aggressiveness and metastasis in TNBC [34, 35]. Because TNBC lacks the estrogen receptor (ER), progesterone receptor (PR), and human epidermal growth factor receptor 2

(HER2), hormonal therapy and immunotherapy cannot target TNBC and thus mostly rely on chemotherapy and radiotherapy. In this study, we investigated how RT regulates DUSP1 activity and downstream MAPK signaling, and how DUSP1 increases RT efficacy in HR+ BC vs TNBC.

Results

DUSP1 expression in HR + BC and TNBC tumors

To understand DUSP1 regulation in BC, we used the invasive breast carcinoma dataset (BRCA-TCGA), which suggests that *DUSP1* and *DUSP6* transcript expression were significantly downregulated (p<0.001) in BC tumors compared with normal breast tissues (Fig. 1A&B, left panels). The overall impact of *DUSP1* and *DUSP6* expressions (low or high) on BC patient survival has not significantly changed (Fig. 1A&B, right panels), whereas alteration *DUSP1*-expression shows 100% disease-specific survival rate (n=11) compared to unaltered *DUSP1* expression (60%) (n= 1052, p = 0.432) (Fig. 1C). Further compared to normal breast tissues, *DUSP1* is one of the top genes that is drastically downregulated (3.63-fold) in BC, and also co-related (Spearman rank correlation) with the downregulation of *APOD*, *TXNIP*, *GSN*, *FOS*, *ANXA1*, *DCN*, *SCGB2A2*, etc. and not with *ESR1* (ER), *PGR* (PR), and *ERBB2* (HER2) (Fig. S1A-D). TMA/IHC analysis further validated downregulation of DUSP1 protein expression with increasing stage in HR+ BC (p=0.65) and TNBC (p=0.51) compared with normal breast tissue (n=12) (Fig. 1D-F). Approximately 30% of TNBC tumors show upregulated DUSP1 expression compared with HR+BC (Fig. 1E). At higher BC stages, epithelial cell area and epithelial DUSP1 expression increased, while stromal cell area and DUSP1 expression decreased in tumors (Fig. 1G-I, all panels). At higher stages of HR+ or TNBC tumors, we observed increased DUSP1+ area, a higher percentage (~20 to 40%) of DUSP1-positive tissue, and significant DUSP1 expression in tumor epithelial cells rather than stromal cells (Fig. S2A-D and S3A-D). Finally, we analyzed DUSP1 expression in normal human breast cells, MCF 10A (ER/PR/Her2 -), and BC cell lines, including MCF7 HR+ (ER/PR+, Her2-) and TNBC cells, human MDA-MB-231 and mouse 4T1 cells (Fig. 1J). Immunoblotting data suggest that both TNBC cell lines showed significantly (p<0.05) upregulated

DUSP1 expression and dysregulated pJNK and pERK MAPK levels (Fig. 1J). Collectively, TCGA and IHC data support this hypothesis and suggest that DUSP1 loss may be associated with BC progression.

RT induced the expression of DUSP1 in BC tumors

To investigate the impact of radiotherapy (RT) on differential gene expressions (DGEs), we analyzed breast cancer (BC) patient cohort samples [36, 37] . NanoString BC360 and IO360 panel sequencing followed by DGE analysis demonstrated that RT significantly increased *DUSP1*, *DUSP6*, *CDKN1A (p21)*, *BAX*, *FOS*, *JUN*, *VIM*, *EGR1*, *HIF1A*, *CD163*, *HLA-DPA1*, and *ATF3* expression compared with pre-RT (biopsy) samples (Fig. 2A–C). *DUSP1* transcripts were not detected by the BC360 panel, likely because of their short half-life (15–30 min) [39]. TCGA-BRCA data suggest that reduced DUSP1 expression in BC tumors was also associated with decreased *FOS*, *FOSB*, *JUN*, *COL14A1*, *NR4A1*, and *SPRY1* expression (Fig. S1, A-C). Conversely, RT-induced *DUSP1/DUSP6* upregulation was accompanied by increased *FOS* and *JUN* expression (Fig. 2B, C). Ingenuity Pathway Analysis revealed associations between DUSP expression and MAPK, EMT, hypoxia, cell-cycle regulation (CDKN1A), TCF4, and BAX, as well as pro-inflammatory cytokines, EGFR, and BMP2 (Figs. S4A, B). KEGG analysis indicated that RT enriched TGF-β, EGFR tyrosine kinase inhibitor resistance, JAK–STAT, PI3K–AKT, Hippo, Wnt, RAS, PD-1 checkpoint, and chemokine signaling pathways (Fig. 2D).

In addition, BC patient (n=20) treated with RT after post BCS, the serum DUSP1 levels remained similar before and after RT in overall BC patients (average, 3.75 ng/mL; n=20) in HR+ patient 4.5% decreased (n=14), whereas TNBC patients showed an approximately 25.65% increase after RT (n=6; p=0.73) (Fig. 2E). *DUSP1* transcripts increased 2.05-fold (median) in HR-positive BC patients PBMCs but were unchanged in TNBC PBMCs (Fig. 2F). RT also dose-dependently induced DUSP1 protein and mRNA expression in TNBC MDA-MB-231 cells ($p<0.05$) (Fig. 2G). Collectively, these findings demonstrate RT induced DUSP1expressio in TNBC tumor cells and patients' serum after BCS.

RT affects TNBC cell survival/proliferation through DUSP1/MAPKs regulation

To assess radiosensitivity in BC cells, we exposed normal MCF7 10A, MCF7, and MDA-MB-231 cells to 4 and 8 Gy of RT. The immunoblotting data show that DUSP1 and cPARP expression increased across all cell types (Fig. 3A, all panels). RT induced early, late, or total apoptosis in MCF7 and TNBC cells differentially (Fig. 3B, both panels) and reduced the percentage of cell area/growth in MCF10A and MDA-MB-231 cells compared to MCF7 cells (Fig. 3C, both panels). RT reduced cell survival, colony formation, and migration but not cell proliferation in TNBC cells compared to HR+ MCF7 cells (Fig. 3D-G and Fig. S5A and B), suggesting that RT-mediated upregulation of DUSP1 in TNBC cells may confer higher radiosensitivity than in HR+ (ER+, PR+, HER2-) MCF7 cells.

To examine the molecular mechanism by which DUSP1 may have sensitized TNBC cells to RT, we analyzed the impact of RT on DUSP1-S323 and DUSP1-S359 phosphorylation and on downstream MAPK signaling. Immunoblotting data demonstrate that RT increased DUSP1-pS359 and DUSP1-pS323 in HR+ BC and TNBC cell lines (Fig. 3H and I). RT increased phosphorylation of pERK (pp44/42) in MCF7 and MDA-MB-231cells, and pJNK in all cell lines, whereas pp38 phosphorylation was decreased in MCF7 and MDA-MB-231 cells (Fig. 3H), Further, immunocytochemistry analysis suggest increased DUSP1-pS323 in all three cell lines significantly and DUSP1-pS359 in MCF 10A and MCF7 cells, and pJNK ($p=0.0001$) and pERK ($p=0.0007$) levels are significantly upregulated in MDA-MB-231 cells after RT exposure (Fig. 3J and K). Because DUSP1 possesses a C-terminal nuclear localization signal (NLS; 13LRALL14) (Fig. 3L), immunoblotting of cytosolic and nuclear extracts clearly suggests that RT treatments increase nuclear accumulation of DUSP1, DUSP1-pS359, and DUSP1-pS359 in MDA-MB-231 and MCF7 cells and suppress nuclear pJNK and pERK expression (Fig. 3M). Overall, our data suggest that RT-mediated induction and nuclear accumulation of DUSP1-pS359 predominantly suppress MAPKs and potentially enhance radiosensitivity in TNBC cells.

Alteration/inactivation of DUSP1 regulates radiosensitivity

Transient transfection of the *DUSP1* plasmid increased *DUSP1* transcripts ($p<0.001$), DUSP1 protein, and altered the expression of pJNK, pERK, and cPARP. It reduced cell survival in MDA-MB-231

cells more effectively than in MCF7 cells (Fig. 4A-C). DUSP1 overexpression and RT treatment increased pJNK, decreased pp38, and pERK in MCF7 cells. DUSP1 overexpression decreased pJNK and p-p38 and stabilized pERK in MDA-MB-231 cells and reduced MDA-MB-231 cell survival/proliferation compared to MCF7 (Fig. 4D and E, both panels). In contrast, DUSP1 knockdown and RT treatment increased pERK and decreased pJNK, pp38, and cPARP in MDA-MB-231 cells, significantly restoring cell survival and proliferation in MDA-MB-231 cells to levels comparable to those in MCF7 cells (Fig. 4F and G, both panels).

Structurally, DUSP1 consists of an N-terminal rhodanese/CH2 domain, a catalytic DSPD domain, and a long C-terminal tail containing Ser323, S359, and S364, the potential phosphorylation sites (Fig. 4H). In DSPD domain Cys-258, Arg-264, and Asp-227 are essential for catalysis. Cys-258 modulates nucleophilic attack on the phosphorus of the substrate (pERP, pJNK) to form a thiol-phosphate intermediate; Arg-264 binds the substrate pTyr and pThr and stabilizes the transition state, whereas Asp-227 increases catalysis by protonating the leaving-group oxygen. Mechanistically, ERK-mediated phosphorylation of Ser359 and Ser364 in DUSP1 enhances DUSP1 stability, and phosphorylation of Ser296/323 triggers degradation, as we analyzed earlier (14). However, an earlier study suggests that DUSP1 lacking 53 C-terminal residues shows higher substrate affinity or a faster catalytic rate than its full-length counterpart [38]. BCI is an allosteric inhibitor of DUSP1/6 that binds the DSPD domain of zebrafish DUSP6. BCI interacts with Trp262, Asn335, and Phe336 side chains [39]. In hDUSP1, BCI may probably interact with the acidic group of Asp-227 and, through conformational changes, halt catalytic activity, whereas phosphorylation at Ser359 and S323 affects DUSP1 stability (Fig. 4H). Immunoblotting data suggest that BCI-mediated DUSP1 inhibition increased pERK, pJNK, and p38 as expected, indicating BCI potency, and that BCI plus RT further exacerbated MAPK phosphorylation in MDAMB-231 cells. BCI treatment did not change the levels of DUSP1-pSer323 and DUSP1 in both cell lines; however, DUSP1-pSer359 was induced to some extent in MDA-MB-231 after BCI and RT exposure (Fig. 4I). Importantly, BCI and RT reduced cPARP expression in MDA-MB-231 cells (Fig 4I

and J). Annexin V5 staining demonstrates that, compared to DMSO-treated cells, total apoptosis in MCF7 cells was 8.2%, in MDA-MB-231 cells was 6.52%, and in 4T1 cells was 5.61% when cells were treated with BCI+RT (Fig. 4K and Fig. S6A). In 4T1 cells, BCI+RT treatment potentially decreased DUSP1-pS359 cPARP, like MDA-MB-231 cells, and showed upregulated pERK (Fig. S6B), and RT alone induced c-PARP, c-Caspase 3, Bax expression, and decreased Bcl-2 (Fig. S6C, both panels). RT alone suppressed cell survival in MCF7 and MDA-MB-231 cells, whereas BCI+RT suppressed cell survival in MCF7 but significantly increased it in MDA-MB-231 cells (Fig. 4L). Collectively, these data suggest that DUSP1 activity is potentially required for radiosensitization and for enhancing apoptosis in TNBC cells.

DUSP1 expression regulates EMT and CSC marker expression

NanoString (BC360 and I0360) targeted sequencing suggests that *CDH1* (E-Cad) expression decreased and subsequently increased *CDH2* (N-Cad), along with EMT-associated genes such as *VIM*, *TWIST1*, *ZEB2*, *DCN*, *FSTL1*, *FGFR1*, *CDH11*, and *VCAN* after post-RT in BC tumors (Fig. 5A). KEGG analysis reveals that the enrichment of these genes in post-RT BC tumors is associated with ECM-receptor interaction, cell adhesion, extracellular matrix organization, mesenchymal cell differentiation, and cell migration (Fig. 5B), suggesting RT regulates EMT. Because DUSPs participate in EMT [40], we examine its functional role in EMT. E-Cad and N-Cad dysregulation in BC cell lines (Fig. 5C) prompted us to examine whether alterations in DUSP1 and RT affect E-Cad and N-Cad expression. To do so, we overexpressed, knocked down, or inactivated DUSP1 in MCF7 and MDA-MB-231 cells and analyzed levels of E-Cad-M, E-Cad-C, N-Cad-P, and N-Cad-M. Overall immunoblotting data suggest that DUSP1 overexpression and RT induced N-Cad-M and regulated EMT in MDA-MB-231 cells (Fig. 5D-H). Moreover, RT/qPCR data suggest that BCI alone or BCT+RT induced *N-CAD* and *VIM* expression in MDA-MB-231 cells and *SNAIL1* and *VIM* gene expression in MCF7 cells (Fig. S7A-D).

Because EMT regulates tumor recurrence and metastasis [41], here, we examined the significance of low and chronic doses of RT on MCF7 and MDA-MB-231 cell morphology (Fig. 5I). Four weeks of low-dose RT exposure induced morphological changes in both cell lines and neutrophil extracellular trap

(NET) formation in MDA-MB-231 cells (Fig. 5J). Since NET formation regulates EMT [42], our RT/qPCR data suggest alterations in the expression of *DUSP1*, *E-CAD,* and *DUSP1, N-CAD* in MCF7 and MDA-MB-231 cells after each week of RT exposure, respectively (Fig. 5K). The EMT genes *SNAIL1*, *ZEB1*, and *VIM* were also differentially regulated after RT exposure in MCF7 cells (Fig. S7E), whereas *SNAIL1*, *ZEB1*, and *VIM* were undetected in MDA-MB-231 cells (data not shown). Further, immunoblotting data demonstrated that chronic low-dose RT exposure induced DUSP1-pS323, pp38, pJNK, and pERK in MDA-MB-231 cells but not in MCF7 cells (Fig. 5L). We observed increased E-CAD-C in MCF7 and N-Cad-M in MDA-MB-231 cells, with no change in cPARP expression, particularly after 3 and 4 weeks of RT (Fig. 5M). Importantly, chronic RT exposure also induced cancer stem cell biomarker expression, including CD44, CD133, ALDH1, and OCT4, in MDA-MB-231 cells, compared to MCF7 cells (Fig. 5N). Indeed, our data suggests that low doses and prolonged RT exposure upregulate DUSP1 activity, modulate MAPK-ERK signaling and EMT, and increase CSC marker expression; they might be involved in radioresistance in TNBC cells and need further investigation.

DUSP1and PARP inhibition enhances radioresistance and restore cell proliferation in MDA-MB-231 cells

RT induces DNA damage, and PARP inhibitors halt DNA repair, thereby triggering cellular apoptosis. We used two PARP inhibitors, olaparib and niraparib, and examined their effects on the cell proliferative activity of MCF7 and MDA-MB-231 cells following DUSP1 inactivation or RT exposure. Overall, the data suggest that in MCF7 cells, pre-treatment with BCI (1μM) + niraparib (5μM) restored 24% of cell proliferation compared to niraparib (5 μM) alone, and no restoration of cell proliferation was observed when cells were exposed to RT (Fig. 6A&B, both panels). MDA-MB-231 cells showed no significant overall effect on cell proliferation when exposed to PARP inhibitors, either alone or as a pre-BCI treatment plus PARP inhibitors (Fig. 6C, both panels). In MDA-MB-231 cells, olaparib or niraparib (5 μM) followed by RT suppressed cell proliferation by ~42.8% and ~47.78%, respectively, compared with DMSO + RT-exposed cells. However, combining BCI with olaparib and with niraparib (5 μM)

treatments, followed by RT, restored 18.8% and 16.5% cell proliferation, respectively, compared to olaparib plus RT and niraparib plus RT exposure (Fig. 6D, left and right panels). Immunoblotting data demonstrated that olaparib and niraparib treatment induced cPARP and pJNK, which decreased after PARP inhibition and RT exposure in MCF7 cells. In contrast, PARP inhibition followed by RT exposure in MDA-MB-231 cells stabilized DUSP1, DUSP1-pS359, DUSP1-pS323, the mature form of N-Cad and decreased pJNK and pERK (Fig. 6E, left and right panels). Overall, these data suggest that DUSP1 activation and PARP inhibition are required for RT-mediated suppression of cell proliferation in MDA-MB-231 cells.

RT reduced hypoxia and suppressed TNBC-derived spheroids' growth after DUSP1 and PARP inhibition

To test DUSP1's role in a physiologically relevant tumor model, we generated 3D spheroids from MCF7 and MDA-MB-231 cells to mimic *in vivo* solid tumors and assess RT efficacy after DUSP1 and PARP inhibition. Comparative analysis demonstrated that RT exposure alone reduced spheroid area by 32.8% and 43.7% in MCF7 cells, and by 19.5% and 9.9% (ns) in MDA-MB-231 cells at days 7 and 15, respectively (Fig. 7A and B; Fig. S8A and B). DUSP1, or DUSP1 plus PARP inhibition followed by RT, significantly increased MCF7 spheroid area by ~10-22% compared to DMSO and RT treatments in MCF7 cells on day 7 or 15. In contrast, MDA-MB-231-derived spheroids showed significant decreases in spheroid area at day 7 and 15 (Fig. 7A and B both panels). Spheroid cell proliferation activity increased significantly in MCF7. However, we observed no significant change in spheroid cell proliferation activity in MDA-MB-231 cells after treatment with BCI and PARP inhibitors (Fig. 7C, upper and lower panels). We also analyzed HIF-1-related hypoxia in MCF7-derived spheroids on day 15 (Fig. 7D). Our data showed no significant change in hypoxia after treatment or RT. However, PARP and DUSP1 inhibition followed by RT significantly reduced HIF-1-related hypoxia in MDA-MB-231 spheroids (Fig. 7E, right panel). Spheroid expression of DUSP1, EMT markers, and cPARP after DUSP1 and PARP inhibition and RT treatment suggests that DUSP1 or PARP inhibition alone did not induce RT-mediated apoptotic

cPARP expression. However, combining DUSP1 and PARP inhibition induced RT mediated apoptotic c-PARP expression in MDA-MB-231-derived spheroids (Fig. S9). In spheroids, endogenous control markers (GAPDH and α-tubulin) are highly dysregulated due to the hypoxic spheroid environment. The overall data indicate that RT reduced hypoxia in MDA-MB-231 spheroids following DUSP1 and PARP inhibition.

DUSP1 inhibition followed by RT exposure differentially enriched gene expression in HR+ MCF7 and TNBC cells

We compared and analyzed the differential gene expression (DGEs) after DUSP1 inhibition, RT treatment alone, or in combination and presented top 50 DGEs (Fig. S10A). In MCF7 cells, comparative DGE analysis (log2FC vs -log10 FDR p-ad) followed by KEGG analysis revealed that BCI treatment enriched metabolic pathways, and RT exposure enriched ER-related protein processing, oxidative phosphorylation, and metabolic pathways. BCI treatment followed by RT exposure enriched p53 signaling, autophagy, oxidative phosphorylation, spliceosome, nucleocytoplasmic transport, and metabolic pathways in MCF7 cells (Fig. 8A-C). Similarly, in MDA-MB-231 cells, although BCI treatment did not affect many DGEs, RT alone enriched MAPK pathways, autophagy, focal adhesion, and metabolic pathways. BCI+RT exposure enriched mTOR, AMPK, autophagy, and cellular senescence-related pathways (Fig. 8D-E). Other treatment comparisons also suggest similar pathway enrichments. (Fig. S10B and C). Collective RNA-seq data suggest that BCI treatment affects 57 genes, RT treatment affects 456 genes, and BCI+RT exposure affects 210 genes that are commonly and differentially regulated in MCF7 and MDA-MB-231 cells (Fig. S10D). These genes may modulate the RT response in HR+ MCF7 and TNBC MDA-MB-231 cells and are currently under investigation in our laboratory.

Discussion

BC is a heterogeneous cancer comprising various cancer cells and immune cells [43, 44]. Neoadjuvant RT is a common clinical practice that utilizes high-energy RT to damage tumor DNA, which activates the

caspases and induces PARP cleavage and tumor cell apoptosis [45]. However, RT responses in HR+BC vs TNBC with respect to radiosensitivity, radioresistance, and tumor recurrence remain poorly defined. Therefore, in the current manuscript, we investigated the impact of RT on HR+ BC vs TNBC. Although DUSP1 plays a context-dependent role in cancer, overall DUSP1 expression was downregulated in advanced BC, including TNBC [45]. This is not due to *DUSP1* gene promoter methylation but possibly due to exon or intron methylation, and transcriptional instability [33]. Treatment with 5-ADC, a potent inhibitor of DNA methyltransferases (DNMTs), did not affect DUSP1 protein expression in normal breast cells or BC cell lines (Fig. S11). However, DUSP1 promoter methylation was detected in peripheral blood leukocytes from TNBC patients as reported earlier and was associated with TNBC risk [46].

Here, we analyzed the impact of hypofractionated RT on BC tumors, and our overall data suggest that RT induced *DUSP* and other genes. These include *ATF3, CDKN1A, BAX, FOS, JUN, VIM, EGR1, HIF1A, CD163,* and regulate oncogenic and immunogenic signaling pathways in BC tumors [37]. These genes are highly expressed in epithelial cells, lymphocytes, and macrophages after RT [47-49]. Our data suggest that RT not only induces *DUSP1* expression but also induces macrophages (M2) associated with *CD163* transcript in BC tumors, which may promote immunosuppressive TEM and radioresistance [44]. On the other hand, higher DUSP1 expression in high-grade TNBC tumor-specific epithelial cells may play an important role in reducing malignancy and improving prognosis in TNBC patients during RT, as TNBC cells exhibit higher levels of HRD and genomic instability [50, 51]. Our data suggest that RT mediated the induction and stabilization of DUSP1 radiosensitized TNBC cells by inhibiting MAPKs, although DUSP1's role in HR+ BC and TNBC subtypes differs [14].

DUSP1 is a stress-induced protein that acts as a negative regulator of MAPKs signaling [52]. RT-induced DNA damage and cellular inflammation lead to DUSP1 phosphorylation and nuclear accumulation. Phosphorylation of DUSP1 at S323 and S359 is critical for DUSP1 proteasomal degradation and stability, respectively [53-55]. Nuclear DUSP1 also modulated EMT by co-localizing with the histone-active promoter markers H3K9me1 and H3K4me3. This leads to regulating histone methylation,

heterochromatin formation, and gene silencing related to EMT in TNBC cells [40]. DUSPs are involved in CSC ($CD44^{hi}/CD24^{lo}/EpCAM^{+}$) phenotype formation in BC [56]. Our data suggests that inhibition of PARP and DUSP1 reduced RT-mediated HIF-1, corresponding hypoxia in TNBC spheroids, whereas RT induced *HIF-1* in BC tumor, which may exacerbate metastasis and tumor recurrence [57-59].

Since RT-induced DNA damage is repaired by Poly(ADP-ribose) polymerase (PARP) enzymes, combining RT with PARP inhibition is a powerful strategy for cancer therapy [60]. To assess DUSP1's role under RT, we used an allosteric inhibitor of DUSP1/6 [60, 61] and PARP inhibitors olaparib and niraparib (which have stronger approval data for breast cancer treatment) [62]. Interestingly, treatment with BCI plus olaparib or niraparib restored proliferative activity in TNBC cells, suggesting that DUSP1 activity is required during combination therapies; although MDA-MB-231 cells have a *TP53* missense mutation, they lack the classic *BRCA1/2* mutations and high HRD [61, 62]. Earlier reports suggest that p53 controls DUSP1 expression during oxidative stress [62], induces autophagy [62], and that its expression affects lipid metabolic pathways in obese mice [63]. Our RNA/seq data from HR+ BC cells and TNBC after DUSP1 inhibition and RT exposure suggest that in MCF7 cells, the cell cycle, cellular senescence, p53, ribosome, and metabolic pathways are enriched. In contrast, in TNBC MDA-MB-231 cells, the spliceosome, autophagy, MAPK signaling, cellular senescence, and focal adhesion-related pathways are enriched, suggesting that targeting DUSP1-associated upstream and downstream pathways may be the best strategy for controlling aggressive TNBC during RT.

Future research should include developing a preclinical DUSP1 stable overexpression TNBC xenograft model and analyzing the impact of RT on tumorigenesis, immune invasion, and animal survival. We will develop strategies to activate DUSP1 activity in TNBC by transactivating its upstream transcription factors. We will assess the molecular mechanistic impact of a DUSP1/PARP inhibitor on RT-mediated regulation of TNBC tumor hypoxia to improve locoregional tumor control and, potentially, patient survival and outcomes.

Materials and Methods

Tissue microarray (TMA) and immunohistochemistry (IHC) analysis

Unstained tissue microarray (TMA) slides containing HR+ BC tumors with adjacent normal breast tissues (Cat # BC081116f) and TNBC tumor tissues with normal adjacent breast tissues (Cat # BR1102) were obtained from Tissue Microarray (Derwood, MD). IHC was performed at the University of North Carolina, Pathology Services Core, Lineberger Comprehensive Cancer Center (Chapel Hill, NC). Chromogenic immunohistochemistry (IHC) was performed on paraffin-embedded tissue sections (four-micron). We performed this IHC using the Leica Bond Rx Autostainer system. Slides were deparaffinized in Bond Dewax solution (AR9222) and hydrated in Bond Wash solution (AR9590). Heat-induced antigen retrieval was performed at 100ºC in Bond-Epitope Retrieval solution 1 pH 6.0 (AR9961) for 20 minutes. After pretreatment, slides were blocked and incubated with DUSP1 primary antibody (M02276, Boster Bio) at an optimized 1:500 dilution for 60 minutes, followed by ready-to-use Novolink Polymer (RE7260-CE). We detected secondary antibody binding with 3,3'-diaminobenzidine (DAB) using the Bond Intense R detection system (DS9263). Stained slides were dehydrated and coverslipped with Cytoseal 60 (23-244256, Fisher Scientific). A positive control slide was included for this assay. Stained slides were digitally imaged in the Aperio AT2 (Leica Microsystems) using a 20x objective. Aperio AT2 Digital Pathology Slide Scanner (Leica Biosystems, Deer Park, IL) was used to image the TMA slides at 20X magnification. All slides and ROI annotations were uploaded to HALO AI® (Indica Labs, Inc., version 4.0.5107.527) for analysis by a trained analyst. Examples of classes used to create a classifier were provided to HALO AI® to train a MiniNet AI classifier until the classification achieved greater than 95% visual accuracy.

Next, a specific algorithm type, such as the multiplex IHC algorithm (HALO AI® multiplex IHC version 3.4.9), was designed for the DUSP1 stain. For this algorithm, the magnification was set to 1, and a nuclear algorithm was employed to detect cell nuclei using hematoxylin and DUSP1, with nuclear detection weights of 1 and 2, respectively. The minimum nuclear optical density for DUSP1 was 0, and

nuclear size was set between 0 and 508.9286 μm in diameter. The minimum nuclear roundness was 0, and nuclear segmentation aggressiveness was 0.576. DUSP1 nuclear detection thresholds were set to 0.2455, 0.2455,1.0937, and 1.8638 for low, medium, and darkly stained cells. Output values were presented as the percentage of positively stained DUSP1 compared to negative DUSP1 cells, as well as the percentage of stained tissue area in stroma versus epithelial cells. A board-certified veterinary pathologist validated the algorithms through a visual, randomized, semi-quantitative assessment of relative stain intensity and the percentage of cells stained.

Breast cancer tumor collection and RNA sequencing

We recruited breast cancer (BC) patients at Mayo College of Medicine in Jacksonville, FL. The study was conducted under the title of "A Pilot/Phase II Trial of Hypofractionated Radiotherapy to the Whole Breast Alone before Breast Conserving Surgery" in accordance with the Declaration of Helsinki, and the protocol was approved by the Ethics Committee of Mayo College of Medicine, Jacksonville, FL, Institutional Review Board (IRB) with protocol code 17-004130 and IRB modification # Mod17-004130-59 on 24 December 2024. All patients signed consent forms permitting use of donated BC tissue, and the IRB reviewed and approved them. We enrolled patients with cT0-T2, N0, M0 BC and treated them with ultra-hypofractionated whole-breast radiotherapy (RT), 5 fractions (total 25 Gy), before breast conservation surgery (BCS), as described earlier [36, 37, 64]. RT was delivered with proton beam therapy (PBT) or photons, and no RT boost or regional nodal RT was allowed [64]. The earlier study describes detailed patient and cohort characteristics [37]. We prepared and pooled FFPE block tumor sections (five slides per case), and isolated total RNA from pre-RT (Biopsy) and post-RT (surgical) samples using the RNeasy FFPE Kit (Qiagen Cat #73504). We sent samples to NanoString (Bothell, WA, USA) for further gene expression analysis and data analysis. We used the nCounter BC-specific 360 panel (BC360) and immune-oncology 360 (IO360) panCancer panels for analyzing the RT effect on BC-specific onco-markers and immuno-oncogenic markers (gene expression) analysis, as described earlier [37]. The RNA

sequencing data for the BC360 and IO360 panels were deposited in the GEO database under accession number GSE307387.

ELISA

To detect serum DUISP1 protein expression, we enrolled BC patients who have undergone surgery and are seeking post-surgery RT treatment under an IRB-approved protocol (16611-056). Supplementary Table S1 presents patients' identification, ER/PR/HER2 status, and Ki-67 status. We collected 15 mL of blood from BC patients after surgery and before RT (basal) and after RT (endpoint) using an EDTA blood collection tube. The pre-RT and post-RT blood collection periods had an average 30-day interval. We have collected blood samples from 20 patients and processed them to isolate serum and PBMCs. We centrifuged blood samples for 15 min at 2500 rpm, collected clear serum from the supernatant, and stored it at -80°C. 100 microliters of serum were used to quantify DUSP1 levels. A colorimetric ELISA was used. We used the Human MKP-1/DUSP1 ELISA kit (Antibodies, Cat # A76457) to determine DUSP1 concentrations using standards, as per the manufacturer's guidelines. ELISA color was measured by reading the plate at 450 nm using a SpectraMax mini plate reader (Molecular Devices, San Jose, CA).

Cell culture

Normal human breast MCF 10A cells, human breast cancer MCF7 cells, and human triple-negative breast cancer (TNBC) cells MDA-MB-231 were obtained from Elizabeth Wellberg's laboratory, Stephenson Cancer Center, Oklahoma University, Oklahoma City, USA. Mouse TNBC 4T1 cells were purchased from American Type Culture Collection (ATCC; Cat # CRL-2539). MCF 10A cells were grown in Dulbecco's Modified Eagle's Medium (DMEM) containing 5% horse serum, Epidermal Growth Factor (EGF) (10 ng/ml), Hydrocortisone (0.5 µg/ml), Cholera Toxin (100 ng/ml), Insulin (10 µg/ml), and Penicillin-Streptomycin (1%). Breast cancer MCF7 cells were grown in DMEM containing human insulin (10 µg/ml), Penicillin-Streptomycin (1%), and 10% Fetal Bovine Serum (FBS). Human triple-negative breast cancer (TNBC) cells (MDA-MB-231) and mouse TNBC cells were cultured in DMEM

supplemented with 10% FBS and 1% Penicillin-Streptomycin. Cells were incubated at 37 °C in a cell culture incubator supplied with 5% CO_2 and used for experiments once they reached 70-80% confluence. Mycoplasma contamination was tested using the MycoAlert Kit (Lonza cat # LT07-518) confirming the absence of contamination across all cell lines and all cell lines utilized within ten passages.

Western blot

BC cells were counted with Countess 3 (Invitrogen), and cells (1×10^5) were grown in 6-well plates for 24 h. Cells were treated or exposed to RT with indicated doses or transfected with indicated plasmids. Cells were washed twice with sterile DEPC-treated PBS, and cells were lysed with cell lysis buffer (Cell Signaling, Danvers, MA) containing protease inhibitor mixture (Roche, Indianapolis, IN) and Phenylmethylsulfonyl fluoride (PMSF) (0.1 mM). After centrifugation at 10000 rpm for 15 min, collect the supernatant cell lysates, and determine protein concentrations using the Bio-Rad protein assay reagent (Bio-Rad, Hercules, CA). The proteins (60 µg) were separated by electrophoresis (NuPAGE 4–12% Bis-Tris-SDS gel; Invitrogen) and blotted on a PVDF membrane (Thermo Scientific, Rockford, IL). After blotting, membranes were blocked in 1X blocking buffer (Sigma-Aldrich, St. Louis, MO) for 1 h and incubated with the indicated primary antibodies overnight at 4 °C. The following antibodies were purchased from Cell Signaling Technology: anti-E-cadherin (Cat # 3195), anti-N-cadherin (Cat# 13116), anti-JNK/SAPK (Cat# #9252), anti-phospho-Thr183/Tyr185-JNK/SAPK (Cat # 4668), anti-p38 MAPK (Cat # 8090), anti-phospho-Thr180/Tyr182-p38 MAPK (Cat# 4511), anti-p44/42 (ERK1/2; Cat# 4695), anti-phospho-Thr202/Tyr204-p44/42 MAPK (phospho-ERK1/2) (Cat# 4370), anti-GAPDH (Cat # 5174), anti-PARP (9542), anti-ALDH1A1(Cat#12035), anti-Oct-4A (Cat# 2840), anti-CD44 (Cat# 37259), anti-CD133 (Cat# 64326), anti-Bcl2 (Cat# 3498), anti-Bax (Cat# 14796), and anti-Cleaved caspase3 (Cat# 9661). Anti-DUSP1/MKP 1 antibody (Cat # M02776) was obtained from Boster Bio (Pleasanton, CA), anti-phospho-Ser359-MKP-1(Cat # PA5-105159) and anti-phospho-Ser323-MKP-1(Cat # AB1065) from Antibodies LLC (St. Louis, MO). All antibodies (dilutions) were used as per the manufacturer's suggestions. After washing the membranes three times with Tris-buffered saline with 0.1% Tween 20

(TBST), the membranes were incubated in the appropriate (Rabbit or mouse) secondary antibody (1:10,000 dilution) (Jackson ImmunoResearch, PA) conjugated with horseradish peroxidase for 1 h at room temperature. The immunoreactive bands were visualized using ECL chemiluminescence detection reagents (Signagen Laboratories, Rockville, MD). The blots were developed using the Azure 500 biosystem, with band detection within the linear range, and presented. In some cases, band intensities were quantified using ImageJ (NIH), and protein expression was plotted.

Cytoplasmic and nuclear fractionation

MCF10A, MCF7, and MDA-MB-231 cells were plated in 100 mm tissue culture plates at a density of 1×10^6 cells/well for 24 h. Cells were treated with 8 Gy of RT and further incubated at 37 °C for 16 h. Cells were trypsinized and washed with cold PBC containing protease inhibitor, and cell pellets were used to isolate cytoplasmic and nuclear protein fractions. The Active Motif (Carlsbad, CA) nuclear extract kit (Cat # 40010) was used for cytoplasmic and nuclear protein extraction according to the manufacturer's instructions. Six micrograms of cytoplasmic and nuclear proteins were immunoblotted with anti- DUSP1, anti-pS323DUSP1, anti-pS359DUSP1, anti-pJNK, anti-pERK, anti-alpha-tubulin, anti-GAPDH, and anti-Lamin B antibodies as indicated.

RNA isolation and RT/qPCR

MCF 10A, MCF7, MDA-MB-231, and 4T1 cells were plated in 6-well plates at a density of 1×10^5 cells/well overnight and exposed to RT or treated as indicated. Cells were washed with PBS, and total RNA was isolated using TRIZOL Reagent (Invitrogen, Carlsbad, CA). We analyzed DUSP1, E-Cad, N-Cad, Snail, ZEB1, and Vimentin expression using specific primers (Supplementary Table S2) followed by RT/qPCR as described previously [65]. Briefly, RNA (1 μg) was reverse transcribed using a High-Capacity cDNA Reverse Transcription kit (Applied Biosystems, Carlsbad, CA). We mixed the cDNA with Power SYBR Green PCR master mix (Applied Biosystems) and forward- and reverse-specific primers. We amplified GAPDH or β-actin as an internal control. We ran the PCR mixtures on a QuantStudio-3

PCR System (Applied Biosystems) using relative quantitation according to the manufacturer's protocols. Similarly, in BC patients who underwent RT, we isolated post-BCS peripheral blood mononuclear cells (PBMCs) from blood and extracted total RNA using TRIZOL Reagent; we then reverse transcribed RNA (1 μg) using a High-Capacity cDNA Reverse Transcription kit (Applied Biosystems, Carlsbad, CA). The cDNA was mixed with Power SYBR Green PCR master mix (Applied Biosystems), and DUSP1 and GAPDH expression was analyzed by RT-qPCR.

Plasmid and siRNA transfections

We obtained a full-length human DUSP1 (NM_004417) ORF Clone-RC205220 Myc-DDK-tagged DNA plasmid from Origene Technologies (Rockville, MD). The plasmid encodes 367 amino acids of the DUSP1 protein. For transfection, MCF7 10A, MCF7, and MDA-MB-231 cells were plated in 6-well plates at a density of 1×10^5 cells/well for 24 h. Cells were transfected with 1–2 μg of the pcDNA3.1 empty vector (EV) or DUSP1plasmid DNA using Lipofectamine LTX-plus transfection reagent (Invitrogen Cat # 15338030) according to the manufacturer's instructions. After 24 h of transfection, we harvested cells and assessed DUSP1 protein overexpression by RT-qPCR and immunoblotting. For siRNA transfection, we used human pool ON-TARGETplus GAPDH control siRNA (Cat # D-001830-10-05) or human ON-TARGETplus DUSP1(1843) siRNA (Cat# J-003484-21-0050) and DharmaFECT 1 Transfection Reagent (Cat #T-2001-01) purchased from Horizon Discovery Biosciences Limited (Cambridge, UK). Cells were transfected with 100 nM control or DUSP1 siRNA using DharmaFECT 1 transfection reagent according to the manufacturer's instructions. Following 24 h of transfection, cells were harvested, and DUSP1 knockdown and downstream signaling were analyzed by immunoblotting.

MTT and WST assay

MTT cell survival assay was performed in 96-well plates using MTT (3-(4,5-dimethylthiazol-2-yl)-2,5-diphenyl tetrazolium bromide) reagent (MP Biomedicals, Solon, OH). BC cells were exposed to RT or transfected with EV or DUSP1 plasmid DNA. After 72 h, cells were treated with 5 μl MTT reagent/well

(stock: 5 mg/ml in PBS) and incubated at 37 °C for 1 h. Cells were washed with PBS, and formazan crystals were dissolved in DMSO. Cell survival was measured by reading the plate at 570 nm using a SpectraMax mini plate reader (Molecular Devices, San Jose, CA). Cell proliferation was performed in 96-well plates using the WST-1 reagent (Roche Applied Science, Indianapolis, IN, USA). The BC cells were exposed to RT, treated with a PARP inhibitor, or transfected with EV or DUSP1 plasmid DNA. Cell proliferation was measured by adding 10 µl of WST-1 reagent according to the manufacturer's instructions. Cell proliferation was measured at 450 nm using a SpectraMax mini plate reader (Molecular Devices, San Jose, CA).

Cell colony formation and migration assay

MCF 10A, MCF7, MDA-MB-231, and 4T1 cells were plated (1×10^5) and grown in 6-well plates for overnight and irradiated with different doses of RT. After 16 h, irradiated cells were trypsinized, and 5,000 cells were replated in 6-well plates in triplicate and allowed to grow for 7–10 days. Cells were fixed with cold methanol and stained with 0.5% crystal violet for 30 min. Cells were washed with distilled water and allowed to dry. Blue colonies were counted and plotted. For the cell migration assay, MCF10A, MCF7, MDA-MB-231, and 4T1 cells (1×10 ^5) were cultured in 6-well plates overnight and irradiated with different RT doses. After 16 h, the monolayer was scraped using a micropipette tip and photographed (A_0). After 24h post-wounding (A_{24}), cells were photographed again, and the cell migration gap length was calculated using ImageJ (https://imagej.nih.gov/ij/). The percent wound closure (migration) was calculated using the formula $[(A_0 - A_{24})/A_0] \times 100$ and plotted.

Annexin V5 cell apoptosis assay

MCF 10A, MCF7, MDA-MB-231, and 4T1 cells (1×105) were grown in 6-well plates in triplicate overnight and either irradiated with different RT doses or treated with the DUSP1 inhibitor (BCI), as indicated. After 48h, irradiated cells were trypsinized and suspended in annexin-binding buffer (10 mM HEPES, 140 mM NaCl, and 2.5 mM CaCl2, pH 7.4). A hundred µl aliquot of cells (1×10^5 cells/mL)

was mixed with 10 ul of Annexin V/PI conjugate (ThermoFisher Cat # A23202) and incubated for 15 min at room temperature. Cells were diluted to a final volume of 400 µl with annexin-binding buffer and mixed. Cell apoptosis was monitored by FACS, and early, late, and total apoptosis were plotted.

Immunocytochemistry

MCF 10A, MCF7, and MDA-MB-231 cells (1×10^5) were grown on coverslips in 6-well plates overnight and irradiated with 8 Gy RT. After 24 h, untreated and RT-treated cells were fixed with 4% paraformaldehyde for 15 min at 4°C, permeabilized with 0.3% Triton X-100 for 15 min, and blocked with 2% bovine serum albumin for 1 h. For immunostaining, cells were incubated with anti-DUSP1, anti-pS323DUSP1, anti-pS359DUSP1, anti-pJNK, and anti-pERK rabbit primary antibodies (1:500 dilution) at 4 °C for 18h. Cells were washed twice with PBS and incubated with Alexa Fluor® 594-conjugated anti-rabbit antibody (Invitrogen) for 2h. Following immunostaining and washing, cells were mounted with ProLong™ Gold Antifade mounting with DAPI (Life Technologies). Images were captured with a Leica SP8 Confocal microscope and analyzed using LAS-X software. Immunostaining was quantified using ImageJ and plotted.

Spheroids assay

MCF7 and MDA-MB-231 cells (2000/well) were seeded in a 96-well round-bottom ultra-low attachment plate containing appropriate 200 ul medium containing BCI (1 µM), olaparib (5 µM), niraparib (5 µM) separately or BCI (1 µM) plus olaparib (5 µM) and BCI (1 µM) plus olaparib (5 µM) as indicated. Control cells were treated with DMSO. Plates were centrifuged at 1000 RPM for 5 min and cultured at 37 °C for 24h as described previously [66]. After 24h, one set of cells was treated with 8Gy of RT and incubated at 37 °C to generate spheroids. On days 7 and 15, spheroid images were captured using a light microscope (EvosXL core; Invitrogen), and spheroid areas were calculated using ImageJ. Under similar conditions, after 15 days of spheroid generation, spheroid cell proliferation was measured using the WST-1 reagent (10 µl) and the plate was read at 450 nm with a SpectraMax mini plate reader (Molecular

Devices, San Jose, CA). The expressions of DUSP1, pS323DUSP1, PARP, E-Cad, and N-Cad were analyzed from pooled spheroid samples (n=6) by immunoblotting.

Hypoxia assay

MCF7 and MDA-MB-231 cells (2000/well) were seeded in a 96-well round-bottom ultra-low-attachment plate containing the appropriate medium. Control cells were treated with DMSO or BCI (1 μM), olaparib (5 μM), niraparib (5 μM) separately or BCI (1 μM) plus olaparib (5 μM) and BCI (1 μM) plus olaparib (5 μM) as indicated. On day 15, spheroids were stained with Image-iT Red, a cell-permeable fluorescence hypoxia reagent (Invitrogen Cat # H10498), and Hoechst-33342 reagent (Thermofisher Cat # R37605) for 90 min at 37°C. Images were captured with a Leica SP8 Confocal microscope and analyzed using LAS-X software. Spheroid area and red fluorescence intensity correspond to HIF-1α expression and were quantified using ImageJ and plotted.

RNA seq and data analysis

MCF7 and MDA-MB-231 cells were grown in three independent experiments and treated with BCI (1 μM) and RT (8 Gy) alone, or after 16 h of BCI treatment, cells were exposed to RT as indicated. After 24h, total RNA was isolated using TRIZOL reagents (Sigma), and RNA samples were quantified using the NanoDrop ND-1000 Spectrophotometer (Thermo Scientific). We sent RNA samples to the Oklahoma Medical Research Foundation (OMRF) for RNA-seq analysis. Poly-dT oligo beads were used for the isolation of mRNA from total RNA. The mRNA is fragmented, reverse-transcribed into cDNA, end-repaired, adenylated, ligated, and libraries were used for sequencing (Illumina). High-coverage expression profiling (counts) of protein-coding genes in eukaryotes was performed. RNA-seq counts were analyzed using DESeq2 with the experimental group as the main factor. Differential expression was assessed using the standard DESeq2 workflow. Counts were variance-stabilized (VST), and genes showing the greatest variation across all treatment-versus-control comparisons were selected. Expression values were Z-score normalized by gene to highlight relative expression changes. The top 50 variable genes were visualized

using heatmaps with correlation-based gene clustering and samples shown in experimental order. For differentially expressed genes (DGEs), adjusted p-values <0.05 and absolute log2 fold changes were used for each comparison. The human Gene Ontology list was used to cluster genes by biological process and to assess their statistical significance. The RNA sequencing data were deposited in the GEO database with accession number GSE337733.

Reagents preparation and cell treatments

Olaparib (Cat # S1060), Niraparib (Cat # S2741), 5-AZDC (Decitabine (5-Aza-2'-Deoxycytidine; Cat# S1200) and DUSP1/DUSP6 Inhibitor: (E)-2-benzylidene-3-(cyclohexyl amino)-2,3- dihydro-1H-inden-1-one / BCI (Cat # S2837) were purchased from Selleck Chemicals LLC, Houston, TX. Reagents were dissolved in DMSO and treated with cells as indicated.

Statistical analysis

Results are from independent duplicate or triplicate experiments and presented as means ± SEM. Differences between groups were analyzed using a two-tailed Student's t-test. We considered $p < 0.05$ statistically significant. We used GraphPad Prism 9 software (La Jolla, CA) for analysis.

Abbreviations

DUSP1: Dual-specificity protein phosphatase 1
MAPKs: Mitogen-activated protein kinases
TMA: Tumor microarray
IHC: Immunohistochemistry
FFPE: Formalin-fixed, paraffin-embedded
TNBC: Triple-negative breast cancer
HR+: Hormone receptor positive
HER2: Human epidermal growth factor receptor 2
DGEs: Differential genes expression
pJNK: Phospho-JNK

pp44/42: Phospho-ERK

pp38: Phospho-p38

EMT: Epithelial-mesenchymal transition

E-Cad-M: E-Cadherin matured

E-Cad-C: E-Cadherin cleaved

N-Cad-P: N-Cadherin precursor

N-Cad-M: N-Cadherin matured

c-PARP: Cleaved-PARP

RT: Radiation/radiation therapy / radiotherapy

BC subtypes: Breast cancer subtypes

TME: Tumor microenvironment

BCI:(E)-2-benzylidene-3-(cyclohexylamino)-2,3- dihydro-1H-inden-1-one

5-ADC: 5-AZDC (Decitabine (5-Aza-2'-Deoxycytidine

CSCs: Cancer stem cells

HRD: Homologous recombination deficiency

Author Contribution

Conceptualization, S.N.; investigation, S.N. and D.S.; D.H.W., B.H.M.; A. T., M.M.K.; writing – original draft preparation, S.N. and D.S.; review and editing, S.N., D.S., C.E.V., S.C., J. M. K and C.H. All authors have read and agreed to the current version of the manuscript.

Acknowledgements:

We are sincerely thankful for the investigator-initiated trials grant (MDSCC309) to D.S. from Stephenson Cancer Center, University of Oklahoma. We are sincerely thankful for support from Stephenson Cancer Center Support Grant NCI-NIH: P30 CA225520 (PI: R. Mannel). We thank Nicholas Pankow and the Pathology Services Core (PSC) for expert technical assistance with Histopathology. The PSC is supported in part by an NCI Center Core Support Grant (P30CA016086).

Data Availability

All sequencing and expression data from the current study are available in the GEO database and can be retrieved through the accession codes GSE307387 and GSE337733. All data generated or analyzed during this study are included in this article and its supplementary information files. The data set used and/or analyzed during the study is available to the corresponding authors upon request.

Conflict of Interest

The authors declare no competing interests

References

1. Dickinson, R.J. and S.M. Keyse, *Diverse physiological functions for dual-specificity MAP kinase phosphatases.* J Cell Sci, 2006. **119**(Pt 22): p. 4607-15.
2. Cargnello, M. and P.P. Roux, *Activation and function of the MAPKs and their substrates, the MAPK-activated protein kinases.* Microbiol Mol Biol Rev, 2011. **75**(1): p. 50-83.
3. Kyriakis, J.M. and J. Avruch, *Mammalian mitogen-activated protein kinase signal transduction pathways activated by stress and inflammation.* Physiol Rev, 2001. **81**(2): p. 807-69.
4. Kondoh, K. and E. Nishida, *Regulation of MAP kinases by MAP kinase phosphatases.* Biochimica et Biophysica Acta (BBA) - Molecular Cell Research, 2007. **1773**(8): p. 1227-1237.
5. Chen, H.F., H.C. Chuang, and T.H. Tan, *Regulation of Dual-Specificity Phosphatase (DUSP) Ubiquitination and Protein Stability.* Int J Mol Sci, 2019. **20**(11).
6. Wang, J., et al., *Role for DUSP1 (dual-specificity protein phosphatase 1) in the regulation of autophagy.* Autophagy, 2016. **12**(10): p. 1791-1803.
7. Dickinson, R.J. and S.M. Keyse, *Diverse physiological functions for dual-specificity MAP kinase phosphatases.* Journal of Cell Science, 2006. **119**(22): p. 4607-4615.
8. Salojin, K.V., et al., *Essential role of MAPK phosphatase-1 in the negative control of innate immune responses.* J Immunol, 2006. **176**(3): p. 1899-907.
9. Liu, Y., E.G. Shepherd, and L.D. Nelin, *MAPK phosphatases--regulating the immune response.* Nat Rev Immunol, 2007. **7**(3): p. 202-12.
10. Wu, J.J., et al., *Mice lacking MAP kinase phosphatase-1 have enhanced MAP kinase activity and resistance to diet-induced obesity.* Cell Metab, 2006. **4**(1): p. 61-73.
11. Liu, B., et al., *Dusp1 in osteolytic diseases-mechanisms and therapeutic potential.* Scientific Reports, 2025. **15**(1): p. 20887.
12. Eljaschewitsch, E., et al., *The endocannabinoid anandamide protects neurons during CNS inflammation by induction of MKP-1 in microglial cells.* Neuron, 2006. **49**(1): p. 67-79.

13. Duric, V., et al., *A negative regulator of MAP kinase causes depressive behavior*. Nat Med, 2010. **16**(11): p. 1328-32.
14. Niture, S., et al., *Dual-specificity protein phosphatase 1: A potential therapeutic target in cancer*. iScience, 2025. **28**(11): p. 113706.
15. Shen, J., et al., *Role of DUSP1/MKP1 in tumorigenesis, tumor progression and therapy*. Cancer Med, 2016. **5**(8): p. 2061-8.
16. Zhang, X., et al., *DUSP1 phosphatase regulates the proinflammatory milieu in head and neck squamous cell carcinoma*. Cancer Res, 2014. **74**(24): p. 7191-7.
17. Niture, S., et al., *Dual-specificity protein phosphatase 1: A potential therapeutic target in cancer*. iScience, 2025. **28**(11).
18. Zhang, X., et al., *DUSP1 Phosphatase Regulates the Proinflammatory Milieu in Head and Neck Squamous Cell Carcinoma*. Cancer Research, 2014. **74**(24): p. 7191-7197.
19. Hao, P.-P., et al., *Disruption of a regulatory loop between DUSP1 and p53 contributes to hepatocellular carcinoma development and progression*. Journal of Hepatology, 2015. **62**(6): p. 1278-1286.
20. Teng, F., et al., *DUSP1 induces apatinib resistance by activating the MAPK pathway in gastric cancer*. Oncol Rep, 2018. **40**(3): p. 1203-1222.
21. Singh, M.K., et al., *Role of dual specificity phosphatases (DUSPs) in melanoma cellular plasticity and drug resistance*. Scientific Reports, 2022. **12**(1): p. 14395.
22. Kang, Y.S., et al., *DUSP1 induces paclitaxel resistance through the regulation of p-glycoprotein expression in human ovarian cancer cells*. Biochem Biophys Res Commun, 2016. **478**(1): p. 403-409.
23. Metin, S., et al., *DUSP1 protein's impact on breast cancer: Anticancer response and sensitivity to cisplatin*. Biochimica et Biophysica Acta (BBA) - Gene Regulatory Mechanisms, 2025. **1868**(3): p. 195103.
24. Metin, S., et al., *DUSP1 protein's impact on breast cancer: Anticancer response and sensitivity to cisplatin*. Biochim Biophys Acta Gene Regul Mech, 2025. **1868**(3): p. 195103.
25. Zandi, Z., et al., *Dual-specificity phosphatases: therapeutic targets in cancer therapy resistance*. Journal of Cancer Research and Clinical Oncology, 2022. **148**: p. 1-14.
26. Candas, D., et al., *Mitochondrial MKP1 is a target for therapy-resistant HER2-positive breast cancer cells*. Cancer Res, 2014. **74**(24): p. 7498-509.
27. Franklin, C.C., S. Srikanth, and A.S. Kraft, *Conditional expression of mitogen-activated protein kinase phosphatase-1, MKP-1, is cytoprotective against UV-induced apoptosis*. Proc Natl Acad Sci U S A, 1998. **95**(6): p. 3014-9.
28. Sharma, A.K., et al., *MKP1 phosphatase mediates G1-specific dephosphorylation of H3Serine10P in response to DNA damage*. Mutat Res, 2015. **778**: p. 71-9.
29. Candas, D. and J.J. Li, *MKP1 mediates resistance to therapy in HER2-positive breast tumors*. Mol Cell Oncol, 2015. **2**(4): p. e997518.
30. Castro-Sánchez, P., et al., *Regulation of CD4(+) T Cell Signaling and Immunological Synapse by Protein Tyrosine Phosphatases: Molecular Mechanisms in Autoimmunity*. Front Immunol, 2019. **10**: p. 1447.

31. Patysheva, M.R., et al., *Dual-Specificity Phosphatases in Regulation of Tumor-Associated Macrophage Activity.* Int J Mol Sci, 2023. **24**(24).
32. Park, J., et al., *TGF-β1 and hypoxia-dependent expression of MKP-1 leads tumor resistance to death receptor-mediated cell death.* Cell Death Dis, 2013. **4**(2): p. e521.
33. Niture, S., et al., *DUSP1: Triple-Negative Breast Cancer and Therapeutic Potential.* Curr Oncol, 2026. **33**(2).
34. Khoshnazar, S.M., et al., *Expression of DUSP1, LINC02202, and LINC01554 as a biomarker panel in the diagnosis and prognosis of breast cancer.* Medical Journal of Indonesia, 2025. **34**: p. 4-10.
35. Chen, F.M., et al., *The mitogen-activated protein kinase phosphatase-1 (MKP-1) gene is a potential methylation biomarker for malignancy of breast cancer.* Exp Mol Med, 2012. **44**(5): p. 356-62.
36. Thorpe, C.S., et al., *Pilot/Phase II Trial of Hypofractionated Radiation Therapy to the Whole Breast Alone Before Breast Conserving Surgery.* Adv Radiat Oncol, 2023. **8**(1): p. 101111.
37. Niture, S., et al., *Characterization of Oncogenic and Immunogenic Profiling in Patients with Breast Cancer Tumors After Radiation Therapy.* Int J Mol Sci, 2026. **27**(7).
38. Hutter, D., et al., *The carboxyl-terminal domains of MKP-1 and MKP-2 have inhibitory effects on their phosphatase activity.* Mol Cell Biochem, 2002. **233**(1-2): p. 107-17.
39. Molina, G., et al., *Zebrafish chemical screening reveals an inhibitor of Dusp6 that expands cardiac cell lineages.* Nat Chem Biol, 2009. **5**(9): p. 680-7.
40. McDonald, O.G., et al., *Genome-scale epigenetic reprogramming during epithelial-to-mesenchymal transition.* Nature Structural & Molecular Biology, 2011. **18**(8): p. 867-874.
41. Hashemi, M., et al., *EMT mechanism in breast cancer metastasis and drug resistance: Revisiting molecular interactions and biological functions.* Biomedicine & Pharmacotherapy, 2022. **155**: p. 113774.
42. Maddalena, M., et al., *Neutrophil extracellular traps as drivers of epithelial-mesenchymal transition in cancer cells.* Front Immunol, 2025. **16**: p. 1655019.
43. Januškevičienė, I. and V. Petrikaitė, *Heterogeneity of breast cancer: The importance of interaction between different tumor cell populations.* Life Sciences, 2019. **239**: p. 117009.
44. Niture, S., et al., *Tumor Microenvironment Dynamics of Triple-Negative Breast Cancer Under Radiation Therapy.* Int J Mol Sci, 2025. **26**(6).
45. Los, M., et al., *Activation and caspase-mediated inhibition of PARP: a molecular switch between fibroblast necrosis and apoptosis in death receptor signaling.* Mol Biol Cell, 2002. **13**(3): p. 978-88.
46. Li, J., et al., *DUSP1 promoter methylation in peripheral blood leukocyte is associated with triple-negative breast cancer risk.* Scientific Reports, 2017. **7**(1): p. 43011.
47. Ock, S.A., J.G. Knott, and I. Choi, *Involvement of CDKN1A (p21) in cellular senescence in response to heat and irradiation stress during preimplantation development.* Cell Stress Chaperones, 2020. **25**(3): p. 503-508.

48. Nettersheim, D., et al., *A signaling cascade including ARID1A, GADD45B and DUSP1 induces apoptosis and affects the cell cycle of germ cell cancers after romidepsin treatment*. Oncotarget, 2016. **7**(46): p. 74931-74946.
49. Lu, Y., et al., *Transcriptionally up-regulation of CDKN1A/p21 by TFE3 fusion proteins worsened TFE3-rearranged renal cell carcinoma*. Sci Rep, 2025. **15**(1): p. 30067.
50. Vedoya, G.M., M.M. López Nigro, and G.A. Martín, *The secretome of non-tumorigenic mammary cells MCF-10A elicits DNA damage in MCF-7 and MDA-MB-231 breast cancer cells*. Toxicology in Vitro, 2021. **70**: p. 105018.
51. Abrahams, B., A. Gerber, and D.C. Hiss, *Combination Treatment with EGFR Inhibitor and Doxorubicin Synergistically Inhibits Proliferation of MCF-7 Cells and MDA-MB-231 Triple-Negative Breast Cancer Cells In Vitro*. International Journal of Molecular Sciences, 2024. **25**(5): p. 3066.
52. Auger-Messier, M., et al., *Unrestrained p38 MAPK activation in Dusp1/4 double-null mice induces cardiomyopathy*. Circ Res, 2013. **112**(1): p. 48-56.
53. Gil-Redondo, J.C., et al., *DUSP1/MKP-1 represents another piece in the P2X7R intracellular signaling puzzle in cerebellar cells: our last journey with Mª Teresa along the purinergic pathways of Eden*. Purinergic Signal, 2024. **20**(2): p. 127-144.
54. Brondello, J.M., J. Pouysségur, and F.R. McKenzie, *Reduced MAP kinase phosphatase-1 degradation after p42/p44MAPK-dependent phosphorylation*. Science, 1999. **286**(5449): p. 2514-7.
55. Lin, Y.W., S.M. Chuang, and J.L. Yang, *ERK1/2 achieves sustained activation by stimulating MAPK phosphatase-1 degradation via the ubiquitin-proteasome pathway*. J Biol Chem, 2003. **278**(24): p. 21534-41.
56. Boulding, T., et al., *Differential Roles for DUSP Family Members in Epithelial-to-Mesenchymal Transition and Cancer Stem Cell Regulation in Breast Cancer*. PLoS One, 2016. **11**(2): p. e0148065.
57. Balamurugan, K., *HIF-1 at the crossroads of hypoxia, inflammation, and cancer*. Int J Cancer, 2016. **138**(5): p. 1058-66.
58. Kozal, K. and A. Krześlak, *The Role of Hypoxia-Inducible Factor Isoforms in Breast Cancer and Perspectives on Their Inhibition in Therapy*. Cancers (Basel), 2022. **14**(18).
59. Han, D., et al., *Targeting Hypoxia and HIF1α in Triple-Negative Breast Cancer: New Insights from Gene Expression Profiling and Implications for Therapy*. Biology (Basel), 2024. **13**(8).
60. Sun, C., et al., *PARP inhibitors combined with radiotherapy: are we ready?* Front Pharmacol, 2023. **14**: p. 1234973.
61. Junk, D.J., et al., *Different mutant/wild-type p53 combinations cause a spectrum of increased invasive potential in nonmalignant immortalized human mammary epithelial cells*. Neoplasia, 2008. **10**(5): p. 450-61.
62. Antberg, L., et al., *Pathway-centric analysis of the DNA damage response to chemotherapeutic agents in two breast cell lines*. EuPA Open Proteomics, 2015. **8**: p. 128-136.

63. Khadir, A., et al., *MAP kinase phosphatase DUSP1 is overexpressed in obese humans and modulated by physical exercise*. American Journal of Physiology-Endocrinology and Metabolism, 2015. **308**(1): p. E71-E83.
64. Thorpe, C.S., et al., *MC1732: Pilot/Phase II Trial of Hypofractionated Radiotherapy to the Whole Breast Alone Before Breast Conserving Surgery*. International Journal of Radiation Oncology*Biology*Physics, 2021. **111**(3, Supplement): p. S109.
65. Niture, S., et al., *Cytotoxicity Modulated by Cyanotoxins in Neuroblastoma SH-SY5Y Cells*. J Exp Pathol (Wilmington), 2025. **6**(1): p. 29-39.
66. Chen, G., W. Liu, and B. Yan, *Breast Cancer MCF-7 Cell Spheroid Culture for Drug Discovery and Development*. J Cancer Ther, 2022. **13**(3): p. 117-130.
67. Cho, M., et al., *OncoDB 2.0: a comprehensive platform for integrated pan-cancer omics analysis*. Nucleic Acids Research, 2025. **54**(D1): p. D1537-D1544.
68. Cerami, E., et al., *The cBio cancer genomics portal: an open platform for exploring multidimensional cancer genomics data*. Cancer Discov, 2012. **2**(5): p. 401-4.
69. Schneider, C.A., W.S. Rasband, and K.W. Eliceiri, *NIH Image to ImageJ: 25 years of image analysis*. Nat Methods, 2012. **9**(7): p. 671-5.
70. Ge, S.X., D. Jung, and R. Yao, *ShinyGO: a graphical gene-set enrichment tool for animals and plants*. Bioinformatics, 2020. **36**(8): p. 2628-2629.

Figure Legends

Figure 1: DUSP1 expression in HR+ BC and TNBC tumors. (A &B) Left panels: The expression of *DUSP1* and *DUSP6* RNA from breast cancer (BRCA) (n=1135) and adjacent normal breast tissues (n=114) was analyzed from the TCGA data set and presented (The OncoDB web portal: https://oncodb.org/), Right panels: The correlation between high and low *DUSP1* and *DUSP6* (n=541) expression and BC patient overall survival (OS) was analyzed from the TCGA data set as presented in the OncoDB web portal (https://oncodb.org/) [67]. (**C**) The effect of alteration of *DUSP1* RNA expression (TCGA data) of BC specific patient survival was analyzed and presented (https://www.cbioportal.org/) [68]. (**D**) Expression of DUSP1 protein in HR+ BC and TNBC was visualized using tumor microarray (TMA) and immunohistochemistry (IHC). DUSP1 staining in normal breast tissue, HR+ BC tumors, and TNBC at different stages was presented. (**E**) The expression of DUSP1 protein in normal breast tissue vs BC HR+ BC tumors and TNBC was quantified (optical density, OD) and presented. (**F**) Comparative quantification of DUSP1 protein expression in normal breast tissue, HR+ BC, and TNBC at different stages was grouped and presented. (**G** & **H**) DUSP1 protein expression in stromal and epithelial cells (arrow) at different stages of HR+ BC and TNBC was visualized, and the alteration of areas between

stromal (S) and epithelial (E) cells was presented. **(I)** The stromal and epithelial DUSP1 positive levels (weak +, moderate ++, and strong +++) in HR+ BC tumors and TNBC tumors were analyzed and plotted. (**J**) Expression of DUSP1, pJNK, and pERK protein levels in normal human breast cell MCF 10A (ER-, PR-, HER2-), breast carcinoma MCF7(ER+, PR+, HER2-), TNBC MDA-MB-231(ER-, PR-, HER2-), and mouse TNBC 4T1 cells were analyzed by immunoblotting and quantified by ImageJ [69]. * $P<0.05$, ** $P<0.01$, *** $P<0.001$.

Figure 2: Radiotherapy-induced DUSP1 expression in BC tumor. (**A**) The schematic model represents the patient cohort study design, RT strategy, and RNA sample collection strategy [biopsy (n=5) vs surgery (n=14 or 15)] for RNA analysis. A NanoString BC360 and IO360 panel strategy was used to analyze the impact of RT on differential gene expression (DGEs), as described in the materials and methods section. (**B**) Differential gene expression (DGE) analysis of BC360 and IO360 panels was performed between biopsy vs surgery. We determined gene expression (fold change) and adjusted p-values within each analysis using an unpaired t-test followed by Benjamini-Yekutieli False Discovery Rate (FDR) adjustment. Significantly adjusted ($p<0.05$) cut-off expression key genes were presented (red circles). We labeled the induction of *DUSP1* and *DUSP6*. (**C**) The impact of RT on the induction of transcripts of *DUSP1* and *DUSP6* was presented from NanoString data analysis. *P* values were presented in the figures. (**D**) Biopsy vs surgery BC tumor (BC360 and IO360) KEGG analysis represents enriched biological pathways (ShinyGO 0.77) [70] (https://bioinformatics.sdstate.edu/go77/; accessed April 25, 2026). (**E**) ELISA: BC patients who went RT after post-BCS, the expression of DUSP1 protein levels before RT and post-RT in total (n=20) BC patients, including HR+ BC (n=14) and TNBC (n=6; please note that two patients have low detectable levels of HER2 expression and ER- and PR- expression; here we considered them as TNBC), was analyzed by ELISA and plotted as described in the materials and methods section. (**F)** BC patients who underwent RT after post-BCS peripheral blood mononuclear cells (PBMCs) were isolated from blood, and total RNA was isolated using TRIZOL reagent, and the expression of DUSP1 and GAPDH was analyzed by RT/qPCR. **G**) The Effect of different RT doses on

DUSP1 protein and *DUSP1* mRNA expression in MCF-10A, MCF7, and MDA-MB-231 cells was analyzed by immunoblotting and RT/qPCR after 72 h and 30 h, respectively, as described in the Materials and Methods section.

Figure 3: RT-sensitized TNBC cells for apoptosis by MAPK regulation. (**A**) Left Panel: MCF 10A, MCF7, and MDA-MB-231 cells were exposed to 4Gy and 8 Gy of RT for 48 h, and cell lysates were immunoblotted with anti-DUSP1, anti-PARP, and anti-GAPDH antibodies. Right Panel: DUSP1 and cleaved-PARP expression were quantified from three independent experiments and plotted. (**B**) MCF7, MDA-MB-231, and 4T1 cells were exposed to 8Gy for RT, and after 48 h, Annexin V5 staining followed by flow cytometry quantified necrotic, early, late, and total cell apoptosis. * $P<0.05$, *** $P<0.001$ relative to unirradiated cells or early or total apoptotic cells, as indicated. (**C**) MCF 10A, MCF7, and MDA-MB-231 cells were cultured in six-well plates and exposed to the indicated dose of RT. After 72 h, the relative percentage of cell area /per microscopic field (n=3) was calculated (ImageJ). Left panel: representative images. Right panel: relative cell area. (**D-G**) MCF10A, MCF7, MDA-MB-231, and 4T1 cells (as indicated) were exposed to different doses of RT. Relative cell survival (D), colony-forming ability (E), cell migration (F), and cell proliferation (G) were analyzed using standard assays as described in the Materials and Methods section. * $P<0.05$, ** $P<0.01$, *** $P<0.001$ relative to unirradiated cells. The experiment was repeated in triplicate. (**H**) MCF 10A, MCF7, MDA-MB-231, and 4T1 cells were exposed to 4 and 8Gy of RT. After 72h, cells were lysed, and cell lysates were immunoblotted with anti-pS323-DUSP1, anti-pS359-DUSP1, anti-DUSP1, anti-pp44/42, total anti-p44/42, pp38, total anti-p38, anti-pJNK, total anti-JNK, and anti-GAPDH. (**I**) The ratio of expression of pS359-DUSP1/DUSP1 was quantified and plotted (ImageJ). (**J**&**K**) MCF 10A, MCF7, and MDA-MB-231 were grown on coverslips in 6-well plates and irradiated with 8 Gy RT. After 24h, cells were fixed and permeabilized. The effect of RT on the expression of cellular pS323-DUSP1, pS359-DUSP1, DUSP1, pp44/42, and pJNK was visualized after immunostaining, and staining was quantified by ImageJ (K) as described in the materials and methods section. (**L**) Key domains of the DUSP1 protein were represented, including CH1, CH2,

CDC25, substrate-binding domains, catalytic residues (DSPD), and the N-terminal nuclear localization signal (NLS). (**M**) The effect of RT on cytosolic and nuclear localization of pS323-DUSP1, pS359-DUSP1, and DUSP1 was analyzed by immunoblotting of cytosolic and nuclear extracts obtained from MCF 10A, MCF7, and MDA-MB-231 cells with and without RT treatment. GAPDH, alpha-tubulin cytosolic, and Lamin B were used as nuclear biomarkers.

Figure 4: Alteration of DUSP1 regulates radiosensitivity. (**A**) MCF7, MDA-MB-231, and 4T1 cells were transfected with empty vector (EV) or DUSP1 plasmid DNA for 48 h, and DUSP1 mRNA overexpression was analyzed by RT-qPCR. (**B**) MCF7, MDA-MB-231, and 4T1 cells were transfected with empty vector (EV) or DUSP1 plasmid DNA for 48h, and overexpression of DUSP1 protein and its effect on MAPKs phosphorylation were analyzed by immunoblotting of the cell lysates as indicated. (**C**) Overexpression of DUSP1 in MCF7 and MDA-MB-231 cells and its effect on cell survival/ metabolic activities were analyzed by MTT assay as described in the methods section. (**D** &**E**) MCF7 and MDA-MB-231 were transfected with empty vector (EV) or DUSP1 plasmid DNA for 24h. After 24h, cells were irradiated with 8Gy and further incubated for 24h. Cell lysates were immunoblotted with the indicated antibodies (D). Similarly, MCF7 and MDA-MB-231 cells were grown in six-well plates and transfected with an empty vector (EV) or a DUSP1 plasmid for 24 h. After 24h, cells were irradiated with 8Gy and further incubated for 24h. Transfected and irradiated cells were transferred to 96-well plates and incubated for 16 h, after which MTT and WST assays were performed as described in the methods section (E). (**F** & **G**) MCF7 and MDA-MB-231 were transfected with control siRNA or DUSP1 siRNA 24h. After 24h, cells were irradiated with 8Gy and further incubated for 24h. Cell lysates were immunoblotted with the indicated antibodies (F). MCF7 and MDA-MB-231 cells were grown in 96-well plates and transfected with control or DUSP1 siRNA for 24 h. After 24 h, cells were irradiated with 8Gy and incubated for an additional 24 h; MTT and WST assays were performed as described in the Methods section (G). * P<0.05, ** P<0.0, 1 *** P<0.001 relative to EV or control siRNA transfected cells. (**H**) We downloaded a DUSP1 AlphaFold structure from the GeneCards online portal

(https://alphafold.ebi.ac.uk/entry/P28562). We presented DUSP1 domains, catalytic key residues, N-terminal serine phosphorylation sites, and the BCI structure. **(I)** We analyzed the effect of the DUSP1 inhibitor and RT on the expression of pS323-DUSP1, pS359-DUSP1, DUSP1, pp44/42, total p44/42, pp38, total p38, pJNK, total JNK, and GAPDH after treating MCF7 and MDA-MB-231 cells for 72 h, as indicated. (**J** & **K**) The effect of the DUSP1 inhibitor and RT, alone or in combination, on cell apoptosis and PARP expression was analyzed by immunoblotting (J). The effects of the DUSP1 inhibitor and RT, alone or in combination, on cell apoptosis were analyzed by annexin V5 staining followed by flow cytometry, and early, late, and total apoptosis were plotted (K). (**L**) MCF 10A, MCF7, and MDA-MB-231 cells were treated with DMSO, BCI [DUSP1 inhibitor (0.5 and 1 μM)], RT (8Gy), or in combination for 48h. Cells were exposed to MTT reagent, and relative cell survival was calculated as described in the Materials and Methods section. * P<0.05, ** P<0.01, *** P<0.001 relative to DMSO-treated cells or RT (RT) treated cells.

Figure 5: DUSP1 regulates EMT and CSC marker expression. (**A**) The effect of RT on the comparative expression of EMT-associated genes was analyzed in BC tumor samples (pre-RT vs post-RT) using NanoString (BC360 and I0360) sequencing and presented. (**B**) An EMT-overrepresented gene set from BC360 and IO360, followed by KEGG analysis to identify enriched biological pathways and interconnections, was presented. The analysis was carried out using ShinyGO 0.77 (https://bioinformatics.sdstate.edu/go77/). (**C**)The relative expression of E-Cad and N-Cad EMT markers in MCF 10A, MCF7, MDA-MB-231, and 4T1 cells was analyzed by Western blotting. E-Cad M-Matured E-Cad, E-Cad-C- Cleaved E-Cad, N-Cad P-Precursor N-Cad, and N-Cad M-Matured N-Cad. (**D** & **E**) The effect of DUSP1 overexpression and RT on the expression of E-Cad and N-Cad in MCF7 and MDA-MB-231 cells was analyzed by Western blotting. (**F**) The effect of DUSP1 knockdown and RT on the expression of E-Cad and N-Cad in MCF7 and MDA-MB-231 cells was analyzed by Western blotting. (**G** & **H**) The effect of DUSP1 inactivation and DUSP1 inactivation plus RT on the expression of E-Cad and N-Cad in MCF7 and MDA-MB-231 cells was analyzed by Western blotting, as indicated. * P<0.05

relative to pre-RT BC tumors. (**I**) The schematic represents chronic RT treatment. MCF7 and MDA-MB-231 cells were exposed to 2 Gy for 4 weeks, with a 2-day halt as indicated, and samples were collected weekly. (**J**) Images of alterations in MCF7 and MDA-MB-231 cell morphology were captured in unirradiated and irradiated cells (4 weeks). The arrow indicated neutrophil extracellular trap (NET) formation in MDA-MB-231 cells. (**K**) The effect of chronic RT exposure on EMT markers in MCF7 and MDA-MB-231 cells was analyzed by RT/qPCR. (**L-N**) The effect of chronic RT exposure on DUSP1, pS323-DUSP1, pS359-DUSP1, MAPKs, EMT, and CSC marker expression in MCF7 and MDA-MB-231 cells was analyzed by immunoblotting as indicated in the materials and methods section. CW1; control weak 1, CW2; control weak 2, CW3; control weak 3, CW4; control weak 4; IRW1; irritated weak 1; IRW2; irritated weak 2; IRW3; irritated weak 3; IRW4; irritated weak 4. * P<0.05, ** P<0.01, *** P<0.001 relative to unirradiated respective weeks.

Figure 6: DUSP1 and PARP inhibitors induce redioresistance and restore TNBC cell proliferation. (**A** &**B**) MCF7 cells (5000 cells/ well; 96-well plate) were treated with increasing doses of olaparib and niraparib (0.5 μM – 6.0 μM separately in the presence or absence of BCI (1μM) for 72h, and the relative cell proliferation was analyzed by WST assay (n=6) (A). Similarly, MCF7 cells were treated with increasing doses of olaparib and niraparib (0.5 μM – 6.0 μM separately in the presence or absence of BCI (1μM) for 24h. Cells were exposed to 8 Gy of RT for 48h, and the relative cell proliferation was analyzed by WST assay (n=6) (B). (**C** & **D**) MDA-MB-231 cells were treated with increasing doses of olaparib and niraparib (0.5 μM – 6.0 μM separately in the presence or absence of BCI (1μM) for 72h, and the relative cell proliferation was analyzed by WST assay (n=6) (C). MDA-MB-231 cells (5000 cells/ well; 96-well plate) were treated with increasing doses of olaparib and niraparib (0.5 μM – 6.0 μM separately in the presence or absence of BCI (1μM) for 24h. Cells were exposed to 8 Gy of RT for 48h, and the relative cell proliferation was analyzed by WST assay (n=6) (D). (**E**) Effects of PARP inhibitors and RT on the expression of PARP, DUSP1, pERK, pJNK, and EMT markers were analyzed by immunoblotting

with the indicated antibodies. * P < 0.05, ** *P*<0.01, *** *P*<0.001 relative to DMSO or DMSO + RT-exposed cells.

Figure 7: Effect of PARP and DUSP1 inhibition and RT-mediated spheroid suppression. (**A & B**) MCF7 and MDA-MB-231 cells (2000/well) were seeded in a 96-well round-bottom ultra-low attachment plate and treated with BCI (1 μM), olaparib (5 μM), niraparib (5 μM) separately or BCI (1 μM) plus olaparib (5 μM) and BCI (1 μM) plus niraparib (5 μM) as indicated. One set of cells was treated with 8Gy of RT, and on days 7 and 15, the spheroid area was measured by ImageJ and plotted. (**C**) MCF7 and MDA-MB-231 spheroids' cell proliferation was measured on day 15 after treatments as indicated in A and B. (**D**&**E**) MCF7 and MDA-MB-231 were treated as indicated, and spheroids were generated. On day 15, spheroids were stained with Image-iT Red, a cell-permeable fluorescence hypoxia reagent and Hoechst-33342 reagent. Images were captured with a Leica SP8 Confocal microscope (d). Spheroid area and red fluorescence intensity correspond to HIF-1α expression and were quantified using ImageJ and plotted (**E**). * *P*<0.05, ** *P*<0.01, *** *P*<0.001, $ *P*<0.05, $$ *P*<0.01, $$$ *P*<0.001 relative to DMSO- or RT-exposed cells or appropriate treatment.

Figure 8: DUSP1 inhibition and RT exposure modulate distinct enrichment of gene expression and biological pathways in MCF7 and MDA-MB-231. RNA-seq analysis: (**A** to **F**) Left panels: Volcano plots represent DGE profiles after BCI and RT or BCI plus RT treatments in MCF7 and MDA-MB-231 cells. Left second panels: The heatmap represents the top 31 DGEs. Middle panel and middle-right panels: KEGG analysis shows enriched biological pathways; a hierarchical tree structure and network interconnections are presented. The analysis was carried out using ShinyGO 0.77 [70] (https://bioinformatics.sdstate.edu/go77/).

Supplementary figure legends

Figure S1: Downregulated major genes, including DUSP1, in invasive BC and DUSP correlation. (**A-B**) The expression profile of the top 20 genes in breast invasive carcinoma (n=1135) vs normal breast

(n=114) was analyzed from the TCGA dataset and presented (https://oncodb.org/cgi-bin/expression_profile.cgi; accessed January 15, 2026) (A&B). The significant downregulation of DUSP1 in breast cancer tumors compared to normal breast tissues was presented. (**C**) Spearman's correlation between *DUSP1* transcripts and *FOS*, *ZFP36*, *CCN1*, *SPARCL1*, *CXCL12*, *DCN*, *CAVIN1*, *TXNIP*, *ANXA1*, *ESR1*, *PGR*, and *ERBB2,* and *DUSP6* transcripts expression in BC were presented (https://www.cbioportal.org/, accessed February 12, 2026).

Figure S2: Expression of DUSP1 in HR+ BC TMA (BC081116f). (**A and B**) The DUSP1 expression area vs. total tissue area was analyzed for BC (HR+) stages (A), and the percentages of DUSP1-positive normal breast tissue and BC tumor tissues by stage were calculated and plotted (B). (**C**& **D**) The distribution of DUSP1 expression between stromal and epithelial cells in normal and HR+ BC tumors with stages was calculated (C), and the average optical density of DUSP1 in stromal and epithelial tissues in normal and HR+ BC tumors was plotted (D). * P<0.05, ** P<0.01, *** P<0.001 relative to normal breast tissues or stromal tissues as indicated.

Figure S3: Expression of DUSP1 in TNBC TMA (BR1102). (**A-B**) The DUSP1 expression tissue area vs. total tissue area in normal and TNBC tissues, stratified by stage, was calculated using TNBC TMA (A); the percentages of DUSP1-positive normal breast and TNBC tumor tissues, stratified by stage, were calculated and plotted (B). (**C** & **D**) The percentage distribution of DUSP1 expression between stromal and epithelial cells (C) and DUSP1 quantification (OD) (D) in normal breast tissue and TNBC tumors with stages were calculated and plotted. * P<0.05, ** P<0.01, *** P<0.001 relative to normal breast tissues (A-C) or stromal tissues as indicated.

Figure S4: DUSP1-related IPA analysis. (A) IPA analysis depicts the DUSP-related network and the interconnections among key genes (left panel). The BC360 IPA analysis represents the gene network and its interconnections (right panel) after pos-RT. (**B**) The IO360 IPA analysis depicts the DUSP1 gene network, including its interconnections and direct connections (left and right panels).

Figure S5: Effect of RT on cell colony formation and cell migration. (**A**) MCF 10A, MCF7, MDA-MB-231, and 4T1 cells were exposed to 2-12 Gy of RT for 48 h in 6-well plates, as described in the methods section, and then allowed to grow for 7–10 days. Cells were fixed, stained with 0.5% crystal violet, and photographed (**B**). Cell migration assay: MCF 10A, MCF7, MDA-MB-231, and 4T1 cells (1×10^5) were grown in 6-well plates overnight and irradiated with 4 and 8 Gy RT, and after 16 h, the monolayer was scraped using a micropipette tip and photographed(A_0). After 24h post-wounding (A_{24}), cells were again photographed and presented.

Figure S6: Effect of DUSP1 inhibition and RT on cell apoptosis. (**A**) 4T1 cells were treated with DMSO, DUSP1 inhibitor BCI (1 μM), RT (8Gy), or in combination for 48h. Necrotic, early, late, and total cell apoptosis were quantified by annexin V staining followed by flow cytometry. (**B**) 4T1 cells were treated with DMSO, BCI [DUSP1 inhibitor (1 μM)], RT (8Gy), or in combination for 48h. Cell lysates were immunoblotted with the indicated antibodies. (**C**) 4T1 cells were treated with 4 and 8Gy of RT, and expression of apoptotic markers were analyzed by immunoblotting and inflammatory gene expression by RT/qPCR. * P<0.05, *** P<0.001 relative to control cells.

Figure S7: Effect of DUSP1 inhibition and RT on EMT-related gene expression. (A-D) MCF7 and MDA-MB-231 cells were treated with DMSO, BCI [DUSP1 inhibitor (1 μM)], RT (RT) (8 Gy), or treated in combination for 48h. The expression levels of *DUSP1*, *E-CAD*, *N-CAD*, *ZEB1*, *SNAIL1*, and *VIMENTIN* were analyzed by RT-qPCR as described in the methods section. (**E**) The effect of chronic RT exposure on the expression of *ZEB1*, *SNAIL1*, and *VIMENTIN* in MCF7 cells was analyzed by RT-qPCR as described in the methods section. * P<0.05, ** P<0.01, *** P<0.001 relative to DMSO-treated cells.

Figure S8: Spheroid formation. (**A &B**) MCF7 and MDA-MB-231 cells (2000/well) were seeded in a 96-well round-bottom ultra-low attachment plate and treated with BCI (1 μM), olaparib (5 μM), niraparib (5 μM) separately or BCI (1 μM) plus olaparib (5 μM) and BCI (1 μM) plus olaparib (5 μM) as indicated. Plates were centrifuged at 1000 RPM for 5 min and cultured at 37 °C for 24h as described previously.

One set of cells was treated with 8Gy of RT and incubated at 37 °C to generate spheroids. On days 7 and 15, spheroid images were captured using a light microscope and presented.

Figure S9: Expression of spheroid-associated markers. The effects of PARP and DUSP1 inhibition and RT on the spheroid-associated DUSP1, PARP, and EMT marker expression were analyzed by immunoblotting as indicated.

Figure S10: RNA-seq analysis: (**A**) Heat map represents DMSO vs treatments (as indicated) comparative analysis of MCF7 and MDA-MB-231 DGEs after sequencing. Eukaryotic high-coverage expression profiling (counts) of protein-coding genes was performed, and relative gene expression was compared with that of DMSO-treated cells. The top 50 variable genes were visualized using heatmaps with correlation-based gene clustering. (**B** & **C**) Left panels: Volcano plots show the DGEs profiles after BCI vs RT and RT vs BCI+RT treatments in MCF7 and MDA-MB-231 cells. Left second panels: Middle panel and middle right panels: KEGG analysis represents enriched biological pathways; hierarchical structure tree and network interconnections were presented. The analysis was carried out using ShinyGO 0.77 (https://bioinformatics.sdstate.edu/go77/). (**D**) A Venn diagram represents the comparison of the BCI, RT, and BCI+RT effects on MCF7 vs MDA-MB-231 unique gene and common gene expression ($p<0.05$ t-test).

Figure S11: Effect of 5-Azacitidine (5-ADC), a DNA methyltransferase inhibitor, on DUSP1 expression. MCF 10A, MCF7, and MDA-MB-231 cells were treated with DMSO or 5-ADC (2.5 and 5 μM) for 48h. The expressions of DUSP1, pS323-DUSP1, and pS359-DUSP1 was analyzed by immunoblotting.

Fig. 1

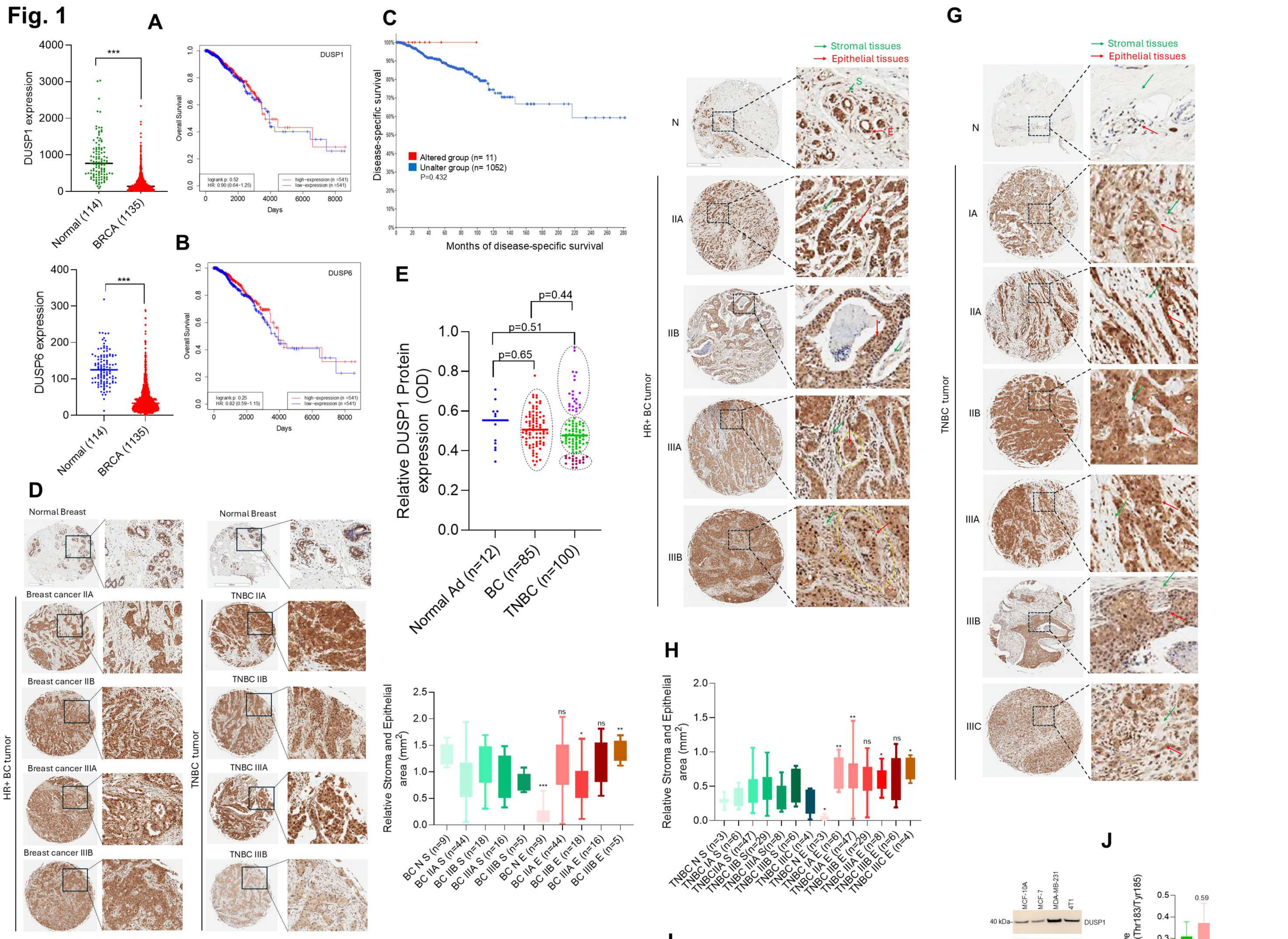
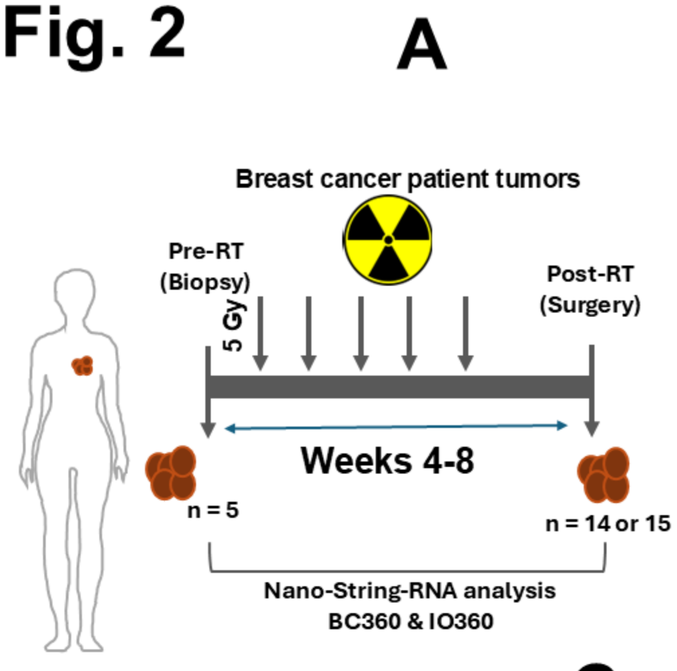
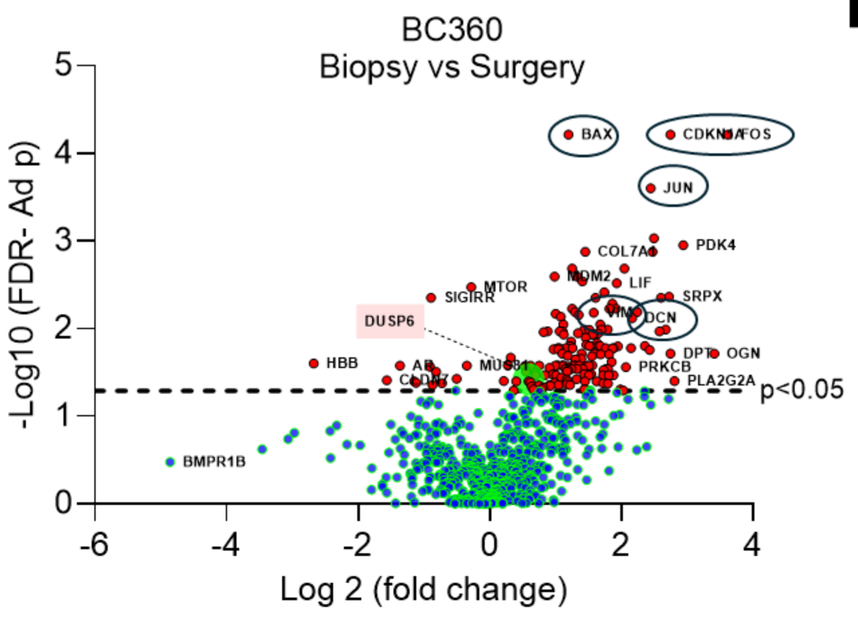
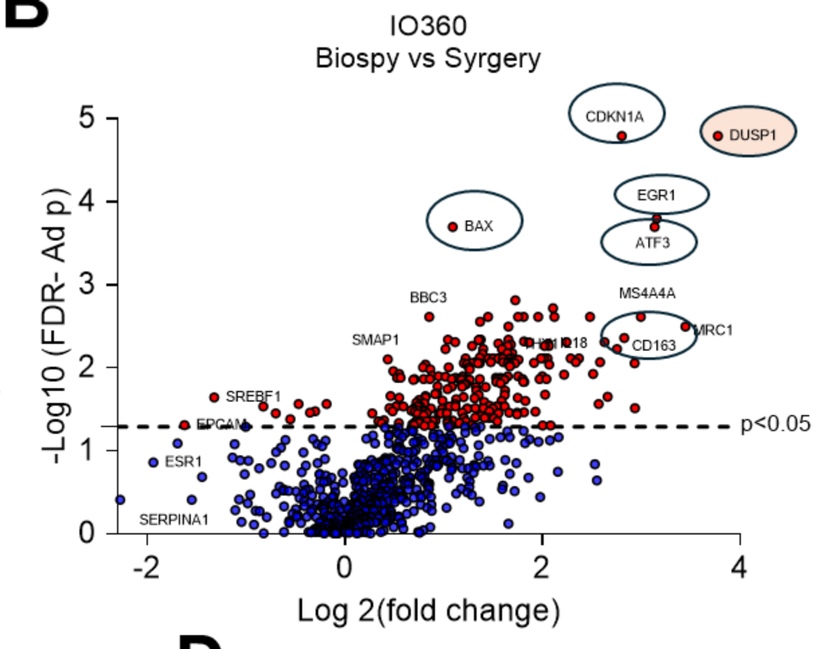
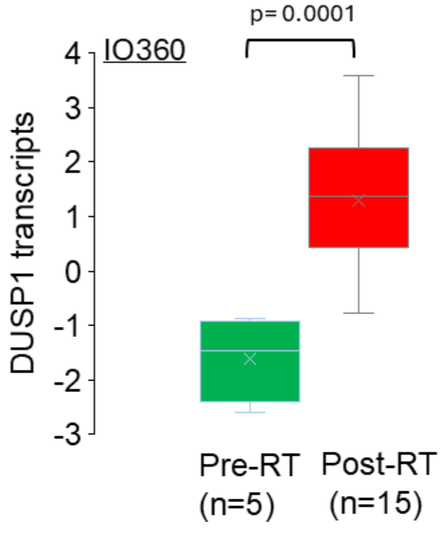

A
DUSP1 expression
***
Normal (114)
BRCA (1135)
DUSP1
Overall Survival
logrank p: 0.52
HR: 0.90 (0.64~1.25)
high~expression (n =541)
low~expression (n =541)
Days
B
DUSP6 expression
DUSP6
logrank p: 0.25
HR: 0.82 (0.59~1.15)
C
Disease-specific survival
Altered group (n= 11)
Unalter group (n= 1052)
P=0.432
Months of disease-specific survival
D
Normal Breast
Breast cancer IIA
Breast cancer IIB
Breast cancer IIIA
Breast cancer IIIB
TNBC IIA
TNBC IIB
TNBC IIIA
TNBC IIIB
HR+ BC tumor
TNBC tumor
E
Relative DUSP1 Protein expression (OD)
p=0.44
p=0.51
p=0.65
Normal Ad (n=12)
BC (n=85)
TNBC (n=100)
Relative Stroma and Epithelial area (mm2)
BC N S (n=9)
BC IIA S (n=44)
BC IIB S (n=18)
BC IIIA S (n=16)
BC IIIB S (n=5)
BC N E (n=9)
BC IIA E (n=44)
BC IIB E (n=18)
BC IIIA E (n=16)
BC IIIB E (n=5)
F
Relative DUSP1 Protein expression (OD)
p=0.54
p=0.15
p=0.88
p=0.88
p=0.84
p=0.44
Normal Ad (n= 12)
BC IIA (n=44)
TNBC IIA (n=47)
BC IIB (n=18)
TNBC IIB (n=29)
BC IIIA (n=16)
TNBC IIIA (n=8)
BC IIIB (n=5)
TNBC IIIB (n=6)
Storma weak (+)
Storma moderate (++)
Storma strong (+++)
Epithelial weak (+)
Epithelial moderate (++)
Epithelial strong (+++)
% DUSP1 Positive tissue
Normal
IIA
IIB
IIIA
IIIB
BC (HR+) stages
G
Stromal tissues
Epithelial tissues
N
IIA
IIB
IIIA
IIIB
IA
IIIC
H
Relative Stroma and Epithelial area (mm2)
TNBC N S (n=3)
TNBC IA S (n=6)
TNBCIIA S (n=47)
TNBC IIB S(n=29)
TNBC IIIA S(n=8)
TNBC IIIB S (n=6)
TNBC IIIC (n=4)
TNBC N E (n=3)
TNBC IA E (n=6)
TNBC IIA E (n=47)
TNBC IIB E (n=29)
TNBC IIIA E (n=8)
TNBC IIIB E (n=6)
TNBC IIIC E (n=4)
I
Stroma weak (+)
Stroma moderate (++)
Stroma strong (+++)
Epithelial weak (+)
Epithelial moderate (++)
Epithelial strong (+++)
% DUSP1 Positive tissue
Normal
IA
IIA
IIB
IIIA
IIIB
IIIC
TNBC Stages
J
MCF-10A
MCF-7
MDA-MB-231
4T1
40 kDa
DUSP1
55 kDa
pJNK
44 kDa
42 kDa
pERK
37 kDa
GAPDH
Relative Phospho-SAPK/JNK (Thr183/Tyr185)
0.59
0.17
Relative DUSP1 expression
0.13
Relative p44/42 expression
0.10

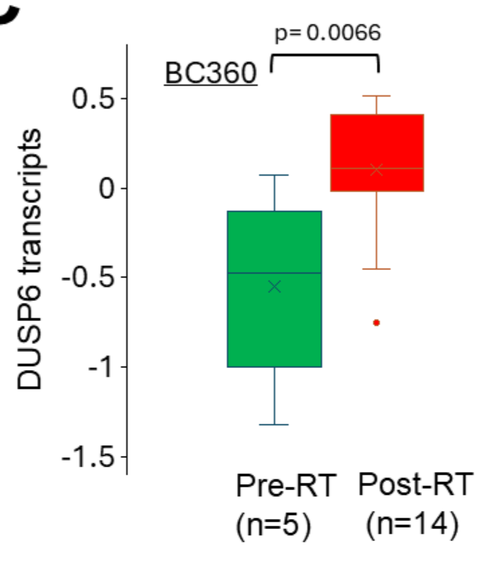
Fig. 2

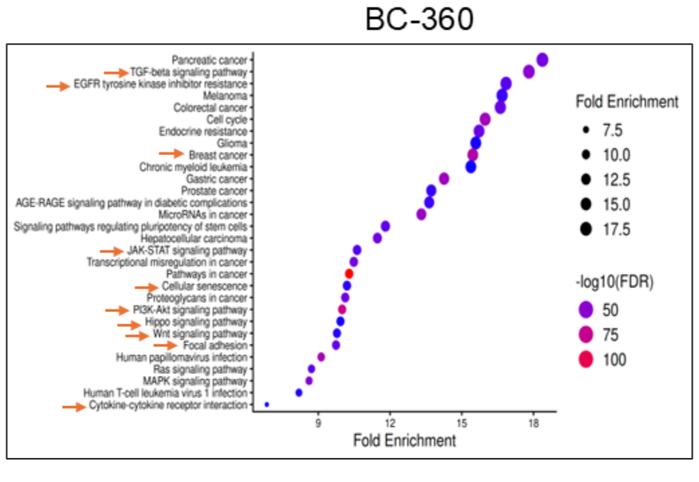

A
Breast cancer patient tumors
Pre-RT
(Biopsy)
5 Gy
Post-RT
(Surgery)
Weeks 4-8
n = 5
n = 14 or 15
Nano-String-RNA analysis
BC360 & IO360

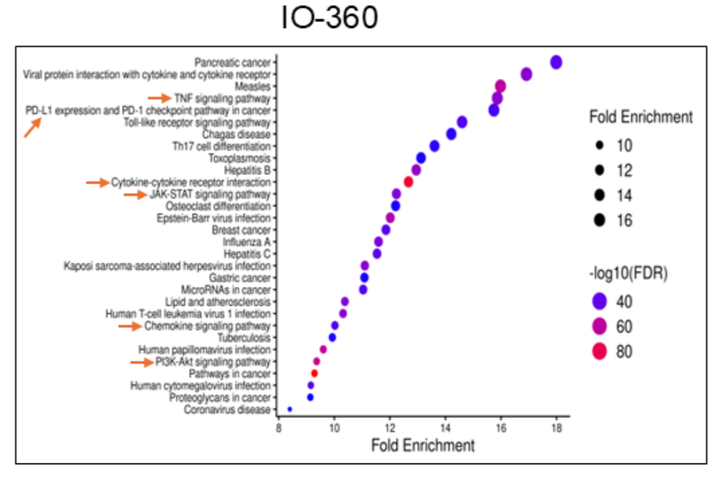

BC360
Biopsy vs Surgery
-Log10 (FDR- Ad p)
Log 2 (fold change)
p<0.05
BAX
CDKN1A
FOS
JUN
COL7A1
PDK4
MDM2
LIF
MTOR
SIGIRR
SRPX
VIM
DCN
DUSP6
HBB
AB
CDH1
MUC1
DPT
OGN
PRKCB
PLA2G2A
BMPR1B

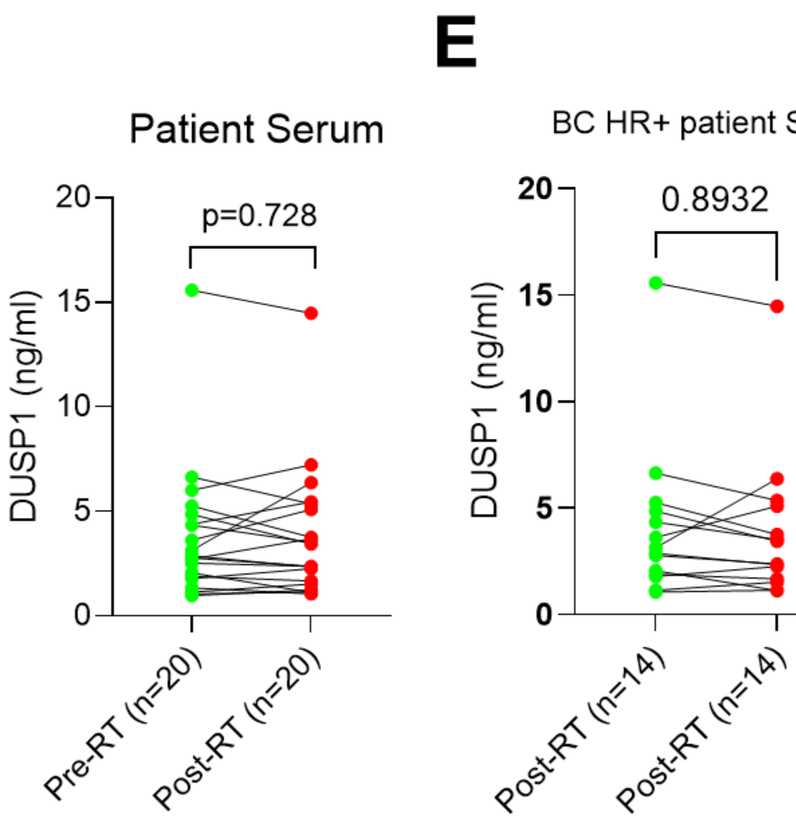

B
IO360
Biospy vs Syrgery
-Log10 (FDR- Ad p)
Log 2(fold change)
p<0.05
CDKN1A
DUSP1
EGR1
BAX
ATF3
BBC3
MS4A4A
SMAP1
CD163
MRC1
SREBF1
EPCAM
ESR1
SERPINA1

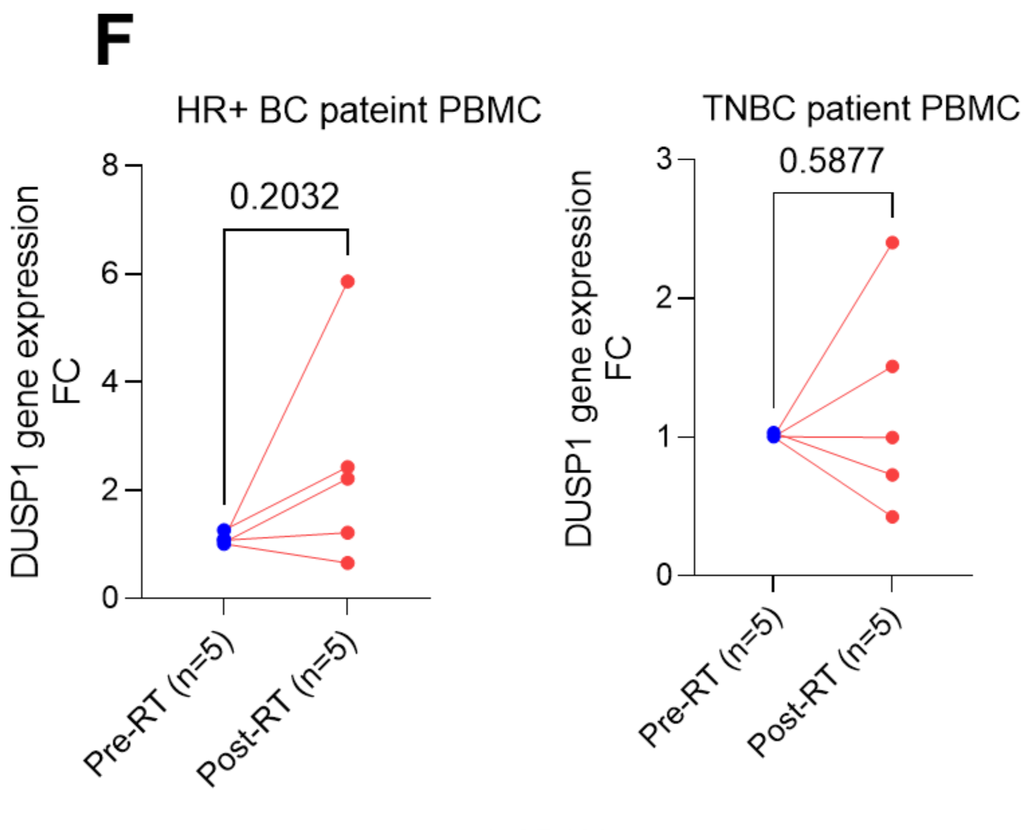

C
p= 0.0001
IO360
DUSP1 transcripts
Pre-RT
(n=5)
Post-RT
(n=15)

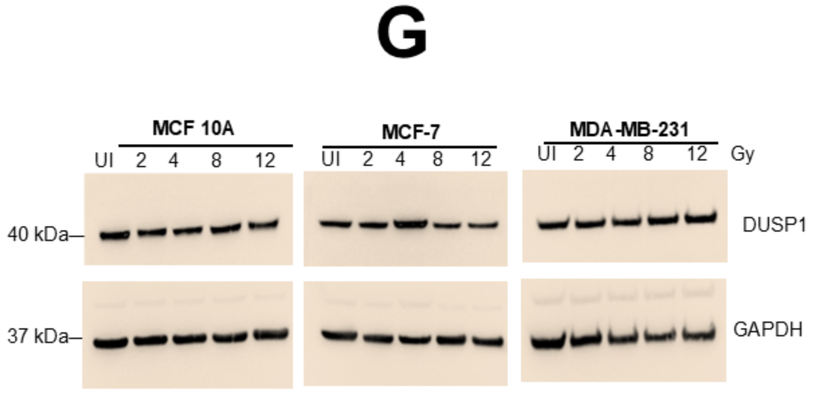

p= 0.0066
BC360
DUSP6 transcripts
Pre-RT
(n=5)
Post-RT
(n=14)

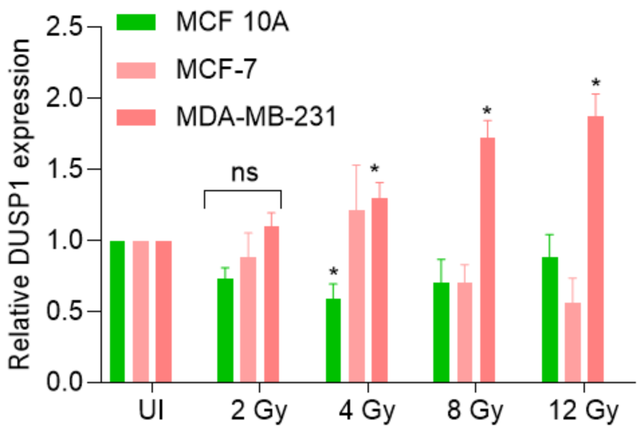

D
BC-360
Fold Enrichment
-log10(FDR)
Pancreatic cancer
TGF-beta signaling pathway
EGFR tyrosine kinase inhibitor resistance
Melanoma
Colorectal cancer
Cell cycle
Endocrine resistance
Glioma
Breast cancer
Chronic myeloid leukemia
Gastric cancer
Prostate cancer
AGE-RAGE signaling pathway in diabetic complications
MicroRNAs in cancer
Signaling pathways regulating pluripotency of stem cells
Hepatocellular carcinoma
JAK-STAT signaling pathway
Transcriptional misregulation in cancer
Pathways in cancer
Cellular senescence
Proteoglycans in cancer
PI3K-Akt signaling pathway
Hippo signaling pathway
Wnt signaling pathway
Focal adhesion
Human papillomavirus infection
Ras signaling pathway
MAPK signaling pathway
Human T-cell leukemia virus 1 infection
Cytokine-cytokine receptor interaction


IO-360
Fold Enrichment
-log10(FDR)
Pancreatic cancer
Viral protein interaction with cytokine and cytokine receptor
Measles
TNF signaling pathway
PD-L1 expression and PD-1 checkpoint pathway in cancer
Toll-like receptor signaling pathway
Chagas disease
Th17 cell differentiation
Toxoplasmosis
Hepatitis B
Cytokine-cytokine receptor interaction
JAK-STAT signaling pathway
Osteoclast differentiation
Epstein-Barr virus infection
Breast cancer
Influenza A
Hepatitis C
Kaposi sarcoma-associated herpesvirus infection
Gastric cancer
MicroRNAs in cancer
Lipid and atherosclerosis
Human T-cell leukemia virus 1 infection
Chemokine signaling pathway
Tuberculosis
Human papillomavirus infection
PI3K-Akt signaling pathway
Pathways in cancer
Human cytomegalovirus infection
Proteoglycans in cancer
Coronavirus disease


E
Patient Serum
DUSP1 (ng/ml)
p=0.728
Pre-RT (n=20)
Post-RT (n=20)
BC HR+ patient Serum
0.8932
Post-RT (n=14)
Post-RT (n=14)
TNBC patient Serum
0.7324
Pre-RT (n=6)
Post-RT (n=6)


F
HR+ BC pateint PBMC
DUSP1 gene expression
FC
0.2032
Pre-RT (n=5)
Post-RT (n=5)
TNBC patient PBMC
0.5877
Pre-RT (n=5)
Post-RT (n=5)


G
MCF 10A
MCF-7
MDA-MB-231
UI 2 4 8 12 Gy
40 kDa
37 kDa
DUSP1
GAPDH


MCF 10A
MCF-7
MDA-MB-231
Relative DUSP1 expression
ns
UI
2 Gy
4 Gy
8 Gy
12 Gy

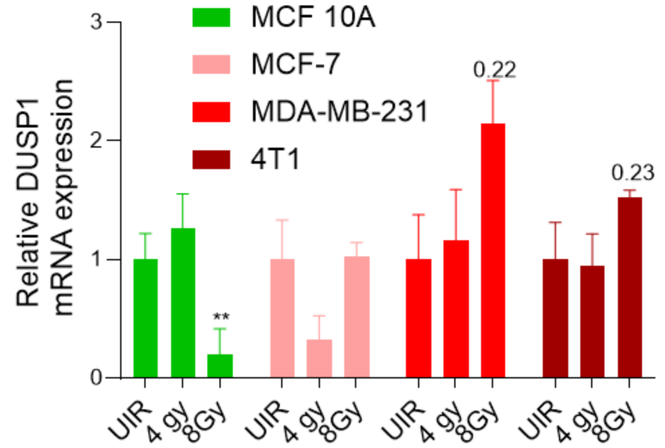

MCF 10A
MCF-7
MDA-MB-231
4T1
Relative DUSP1
mRNA expression
0.22
0.23
UIR
4 gy
8Gy

Fig. 3

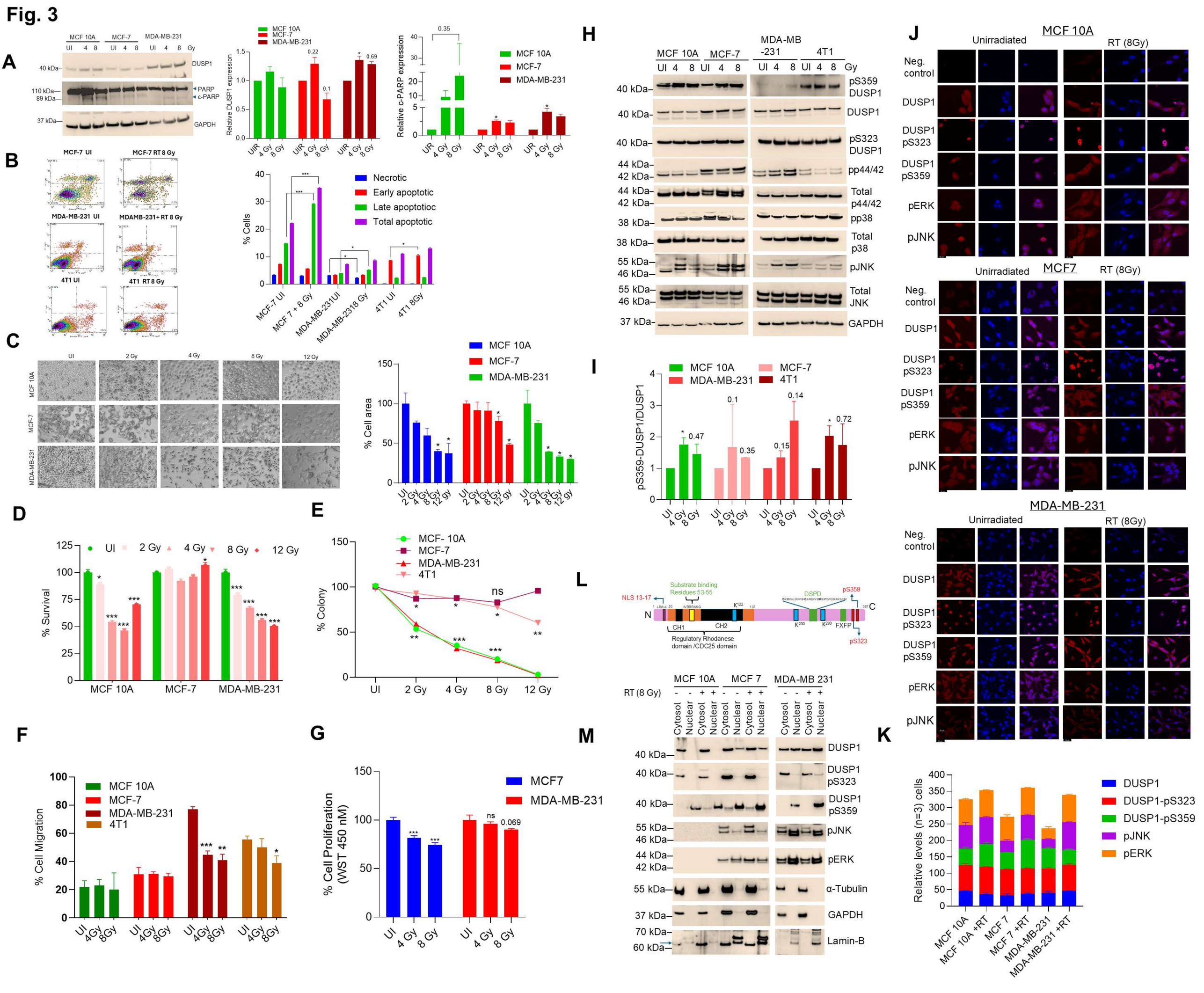
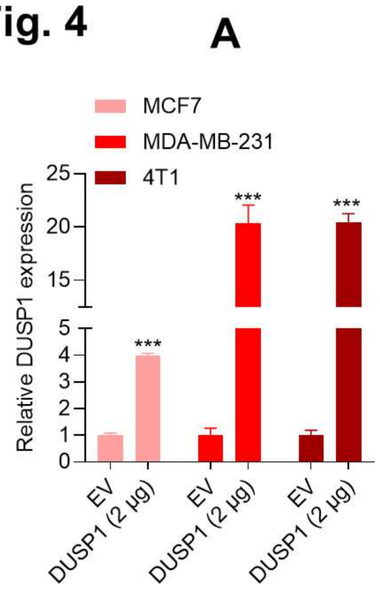
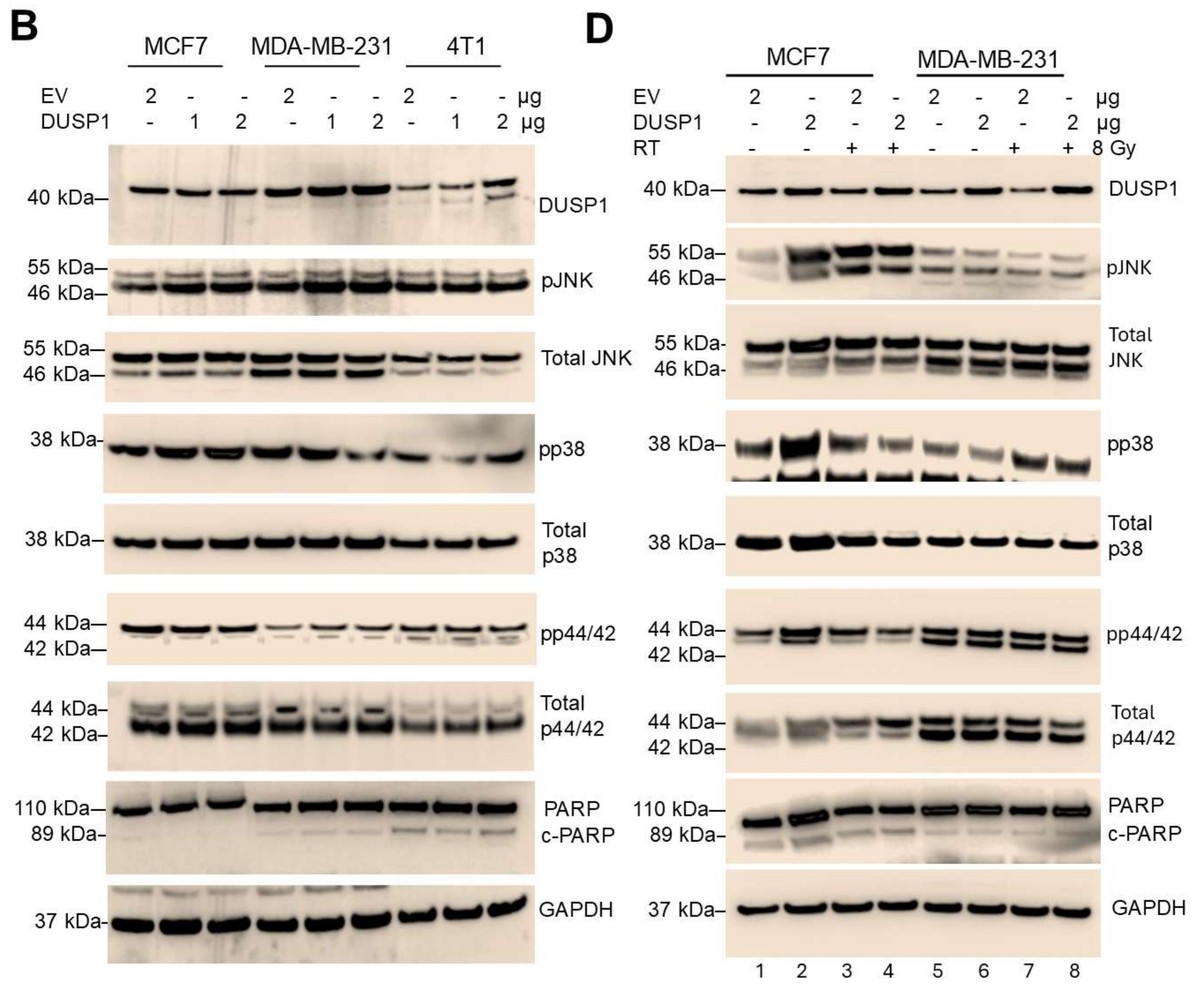
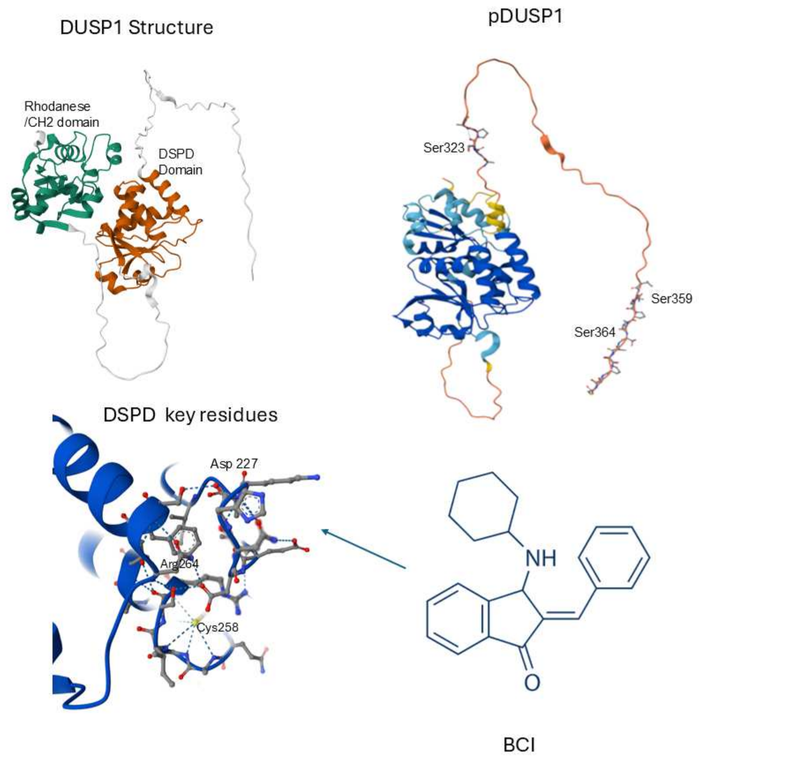

A
MCF 10A
MCF-7
MDA-MB-231
UI 4 8 UI 4 8 UI 4 8 Gy
40 kDa
DUSP1
110 kDa
89 kDa
PARP
c-PARP
37 kDa
GAPDH
Relative DUSP1 expression
0.22
0.1
0.69
UIR 4 Gy 8 Gy
Relative c-PARP expression
0.35
B
MCF-7 UI
MCF-7 RT 8 Gy
MDA-MB-231 UI
MDAMB-231+ RT 8 Gy
4T1 UI
4T1 RT 8 Gy
Necrotic
Early apoptotic
Late apoptotioc
Total apoptotic
% Cells
MCF-7 UI
MCF 7 + 8 Gy
MDA-MB-231UI
MDA-MB-2318 Gy
4T1 UI
4T1 8Gy
C
UI
2 Gy
4 Gy
8 Gy
12 Gy
MCF 10A
MCF-7
MDA-MB-231
% Cell area
D
% Survival
E
MCF- 10A
MCF-7
MDA-MB-231
4T1
% Colony
ns
F
% Cell Migration
4Gy
8Gy
G
MCF7
MDA-MB-231
% Cell Proliferation (WST 450 nM)
0.069
H
MDA-MB -231
4T1
pS359 DUSP1
DUSP1
pS323 DUSP1
pp44/42
Total p44/42
pp38
Total p38
pJNK
Total JNK
I
pS359-DUSP1/DUSP1
0.47
0.1
0.35
0.15
0.14
0.72
J
MCF 10A
Unirradiated
RT (8Gy)
Neg. control
DUSP1
DUSP1 pS323
DUSP1 pS359
pERK
pJNK
MCF7
MDA-MB-231
K
Relative levels (n=3) cells
DUSP1
DUSP1-pS323
DUSP1-pS359
pJNK
pERK
MCF 10A
MCF 10A +RT
MCF 7
MCF 7 +RT
MDA-MB-231
MDA-MB-231 +RT
L
NLS 13-17
Substrate binding Residues 53-55
DSPD
pS359
pS323
N
C
CH1
CH2
Regulatory Rhodanese domain /CDC25 domain
M
RT (8 Gy)
Cytosol
Nuclear
DUSP1
DUSP1 pS323
DUSP1 pS359
pJNK
pERK
α-Tubulin
GAPDH
Lamin-B

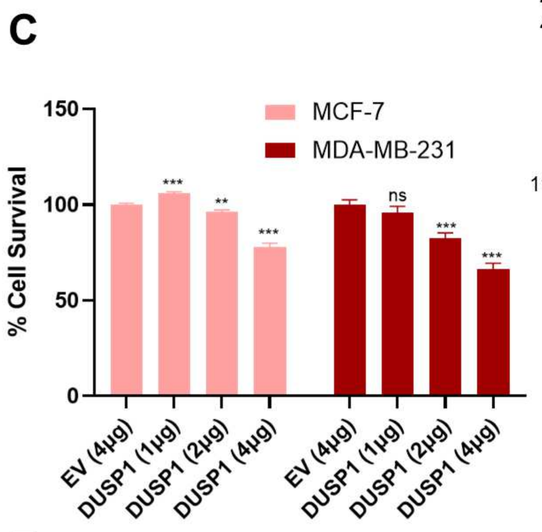
Fig. 4

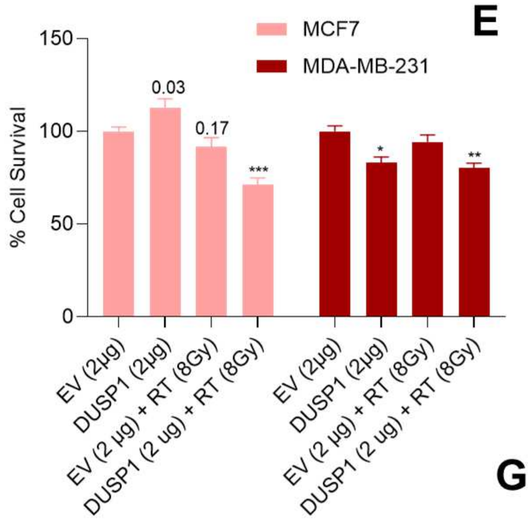

A
MCF7
MDA-MB-231
4T1
Relative DUSP1 expression
EV
DUSP1 (2 µg)

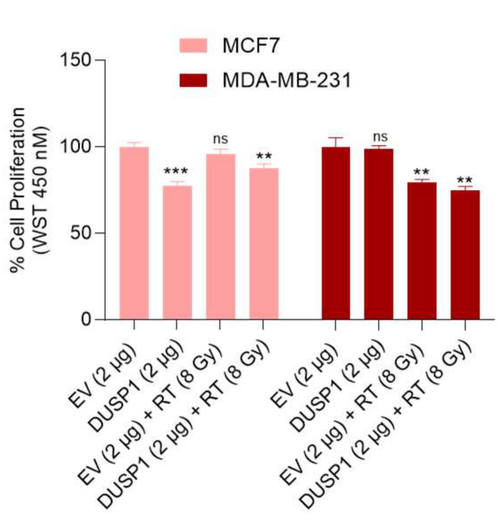

B
MCF7
MDA-MB-231
4T1
EV
DUSP1
µg
40 kDa
DUSP1
55 kDa
46 kDa
pJNK
Total JNK
38 kDa
pp38
Total p38
44 kDa
42 kDa
pp44/42
Total p44/42
110 kDa
89 kDa
PARP
c-PARP
37 kDa
GAPDH

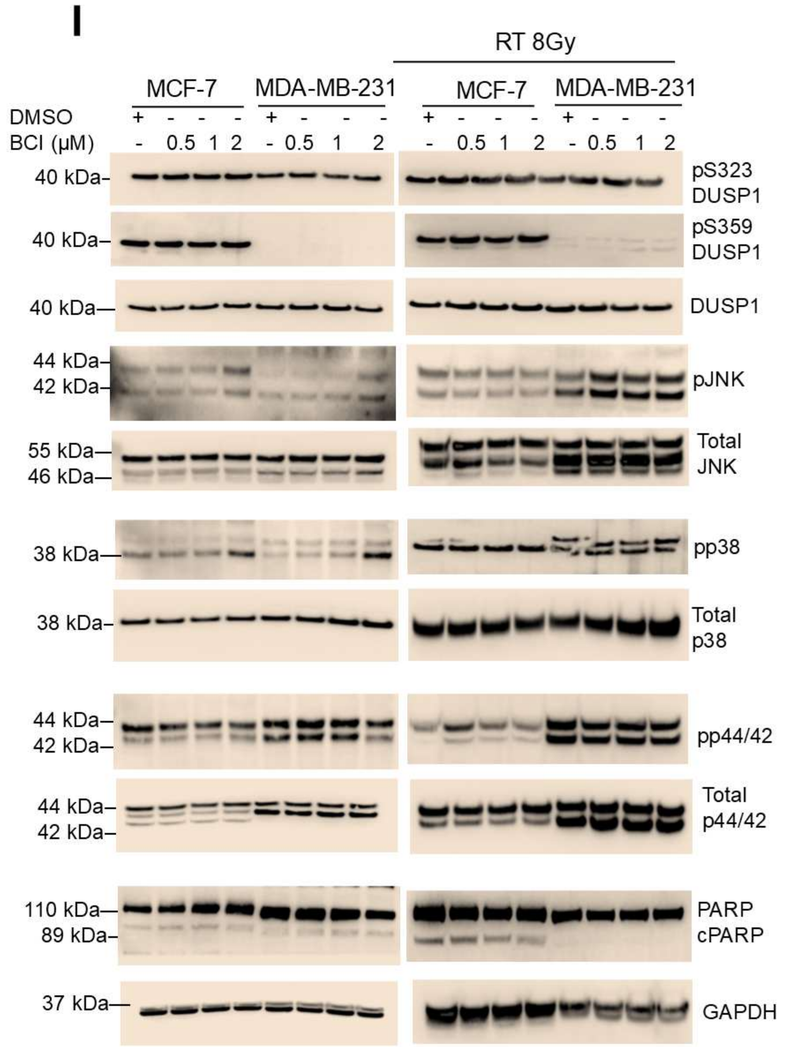
D
MCF7
MDA-MB-231
EV
DUSP1
RT
8 Gy
DUSP1
pJNK
Total JNK
pp38
Total p38
pp44/42
Total p44/42
PARP
c-PARP
GAPDH
1 2 3 4 5 6 7 8

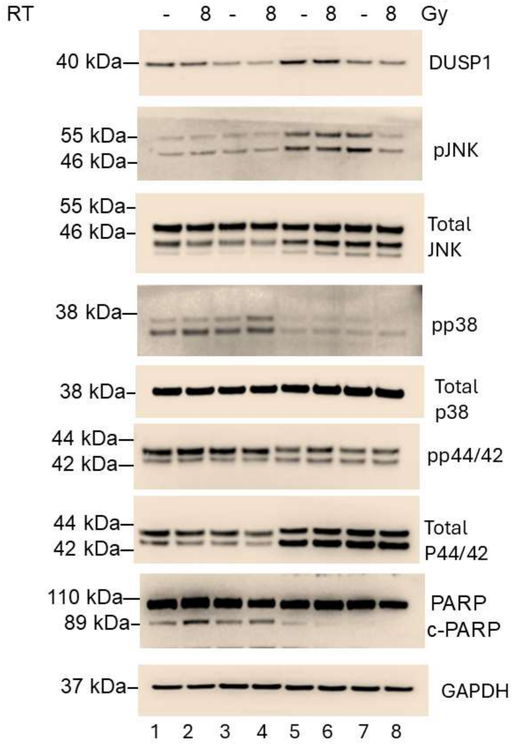

H
DUSP1 Structure
Rhodanese /CH2 domain
DSPD Domain
pDUSP1
Ser323
Ser359
Ser364
DSPD key residues
Asp 227
Arg264
Cys258
NH
O
BCI

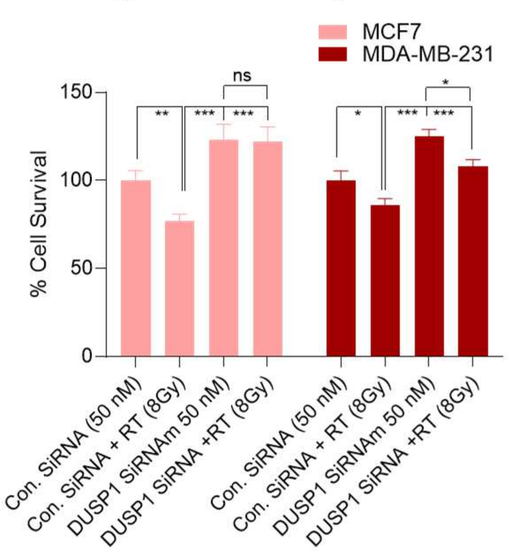

C
MCF-7
MDA-MB-231
% Cell Survival
EV (4µg)
DUSP1 (1µg)
DUSP1 (2µg)
DUSP1 (4µg)

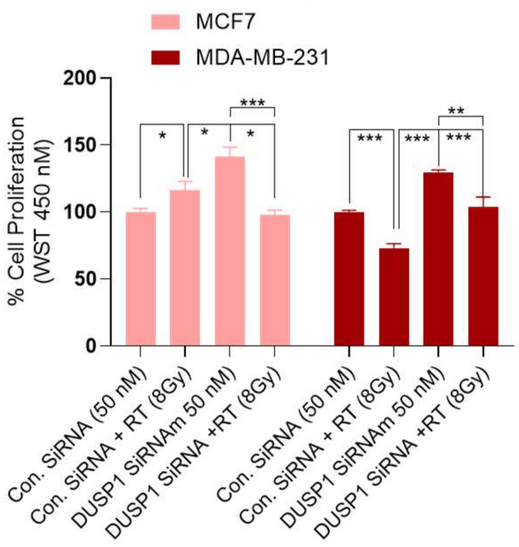

MCF7
MDA-MB-231
% Cell Survival
0.03
0.17
EV (2µg)
DUSP1 (2µg)
EV (2 µg) + RT (8Gy)
DUSP1 (2 ug) + RT (8Gy)

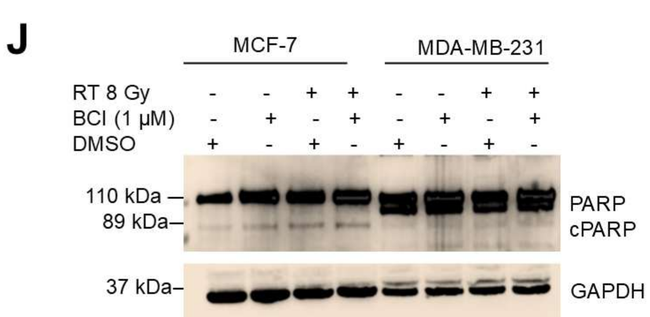

E
MCF7
MDA-MB-231
% Cell Proliferation (WST 450 nM)
EV (2 µg)
DUSP1 (2 µg)
EV (2 µg) + RT (8 Gy)
DUSP1 (2 µg) + RT (8 Gy)

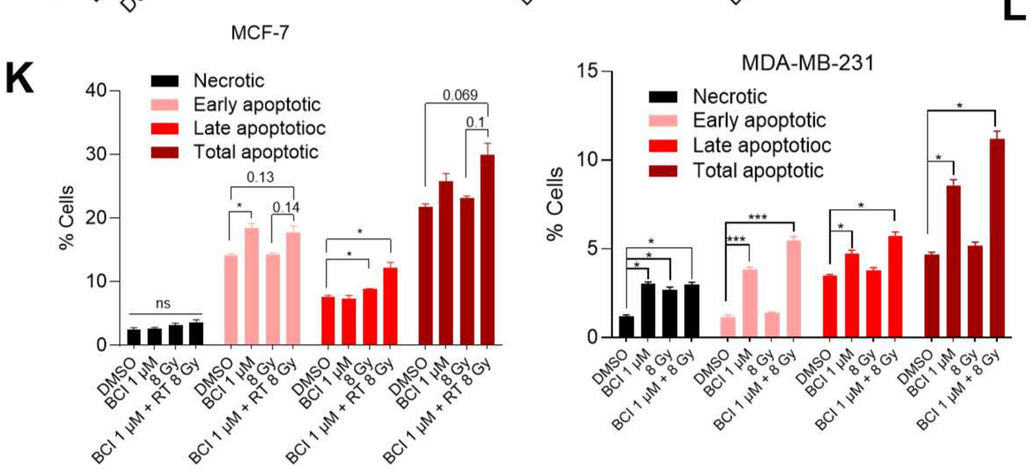

I
RT 8Gy
MCF-7
MDA-MB-231
DMSO
BCI (µM)
40 kDa
pS323 DUSP1
pS359 DUSP1
DUSP1
44 kDa
42 kDa
pJNK
55 kDa
46 kDa
Total JNK
38 kDa
pp38
Total p38
pp44/42
Total p44/42
110 kDa
89 kDa
PARP cPARP
37 kDa
GAPDH


F
MCF-7
MDA-MB-231
Con. si RNA
DUSP1 si RNA
RT
ng
Gy
40 kDa
DUSP1
55 kDa
46 kDa
pJNK
Total JNK
38 kDa
pp38
Total p38
44 kDa
42 kDa
pp44/42
Total P44/42
110 kDa
89 kDa
PARP c-PARP
37 kDa
GAPDH
1 2 3 4 5 6 7 8


MCF7
MDA-MB-231
% Cell Survival
Con. SiRNA (50 nM)
Con. SiRNA + RT (8Gy)
DUSP1 SiRNAm 50 nM)
DUSP1 SiRNA +RT (8Gy)


G
MCF7
MDA-MB-231
% Cell Proliferation (WST 450 nM)
Con. SiRNA (50 nM)
Con. SiRNA + RT (8Gy)
DUSP1 SiRNAm 50 nM)
DUSP1 SiRNA +RT (8Gy)


J
MCF-7
MDA-MB-231
RT 8 Gy
BCI (1 µM)
DMSO
110 kDa
89 kDa
PARP cPARP
37 kDa
GAPDH


K
MCF-7
MDA-MB-231
Necrotic
Early apoptotic
Late apoptotioc
Total apoptotic
% Cells
DMSO
BCI 1 µM
8 Gy
BCI 1 µM + RT 8 Gy

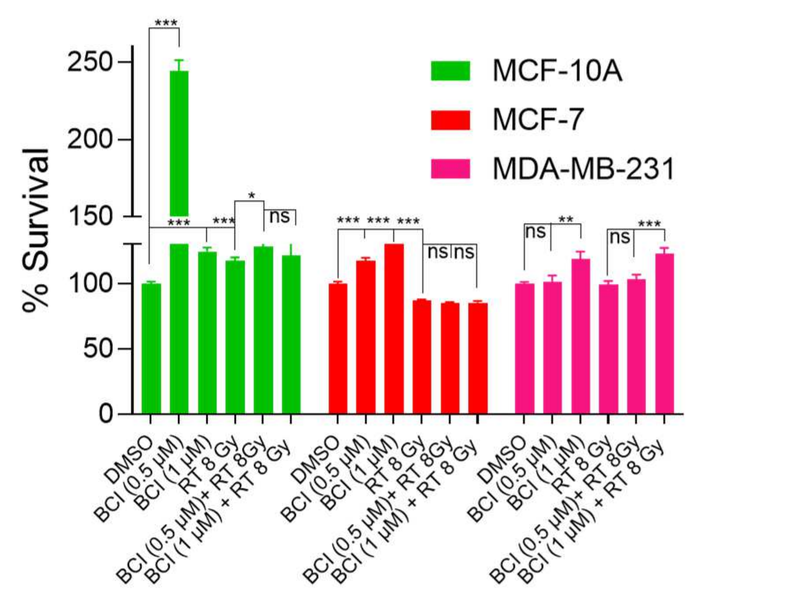
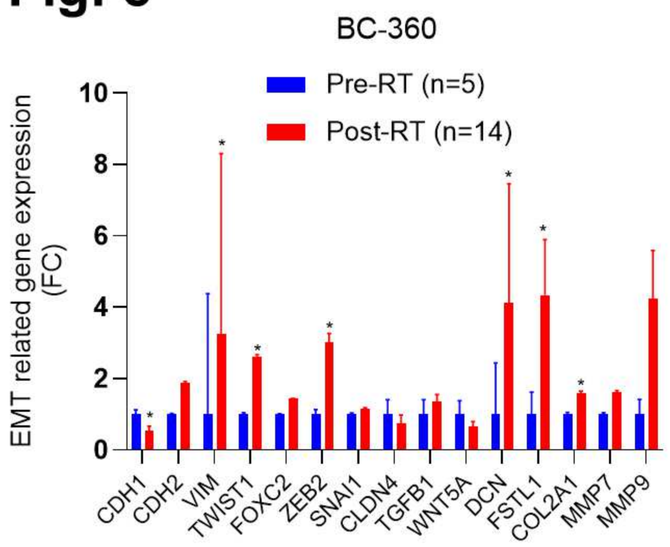
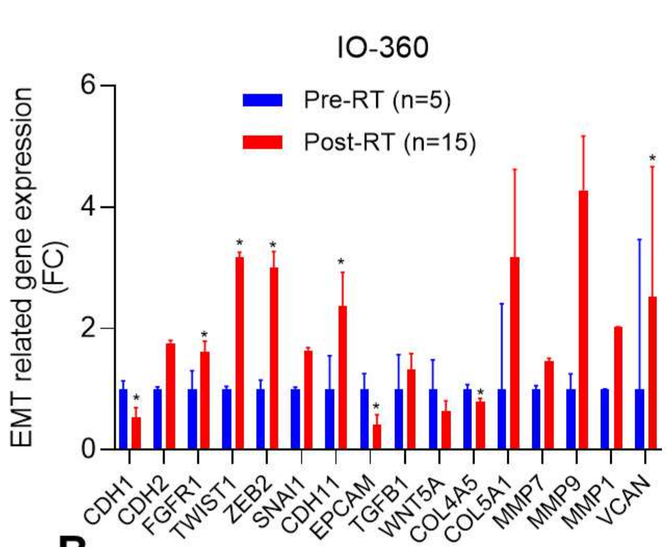
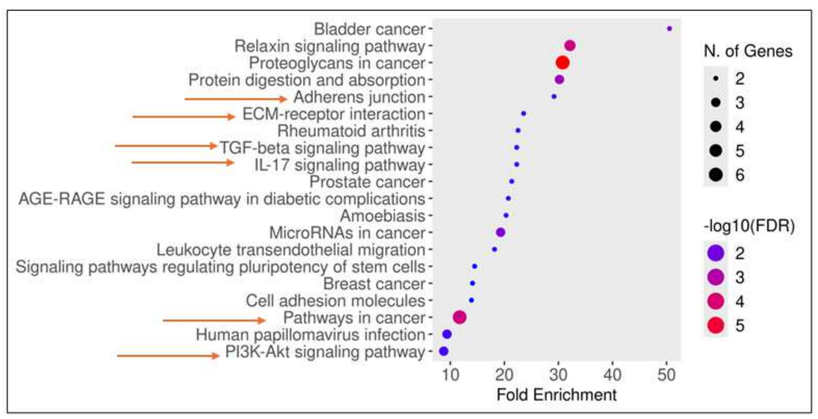
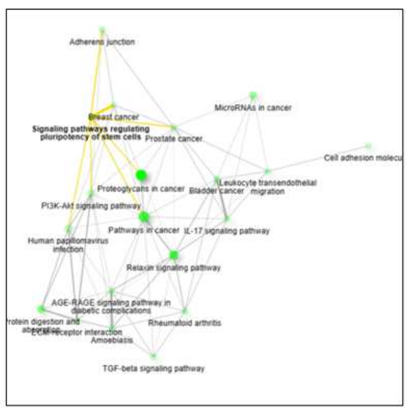

L
MCF-10A
MCF-7
MDA-MB-231
% Survival
DMSO
BCI (0.5 µM)
BCI (1 µM)
RT 8 Gy
BCI (0.5 µM)+ RT 8Gy
BCI (1 µM) + RT 8 Gy

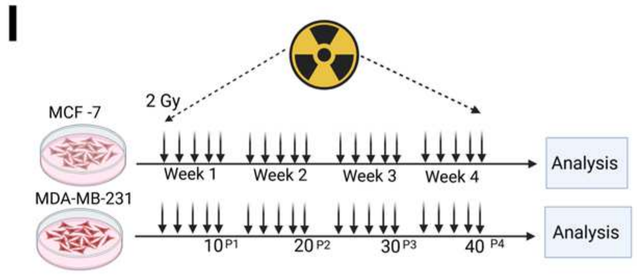
Fig. 5

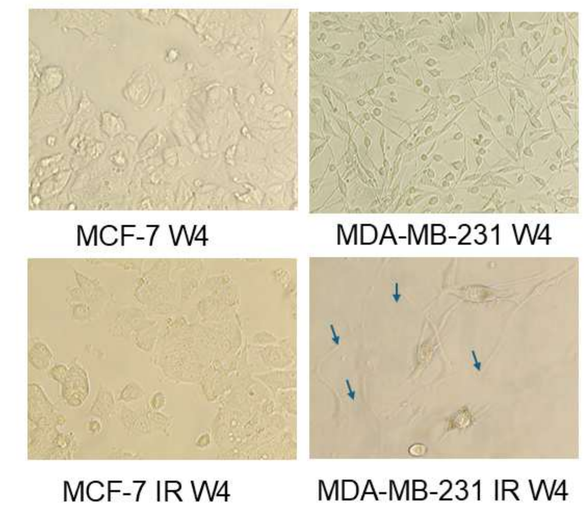

BC-360
Pre-RT (n=5)
Post-RT (n=14)
EMT related gene expression (FC)
CDH1
CDH2
VIM
TWIST1
FOXC2
ZEB2
SNAI1
CLDN4
TGFB1
WNT5A
DCN
FSTL1
COL2A1
MMP7
MMP9

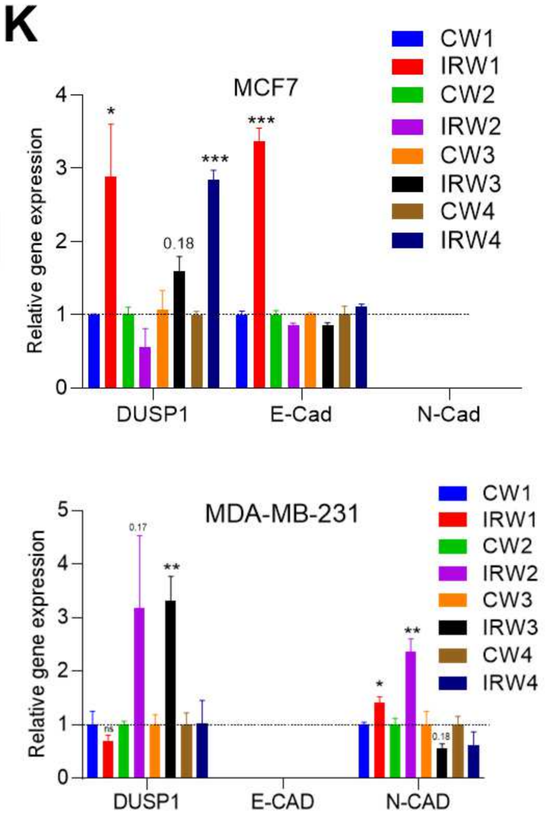

A
IO-360
Pre-RT (n=5)
Post-RT (n=15)
EMT related gene expression (FC)
CDH1
CDH2
FGFR1
TWIST1
ZEB2
SNAI1
CDH11
EPCAM
TGFB1
WNT5A
COL4A5
COL5A1
MMP7
MMP9
MMP1
VCAN

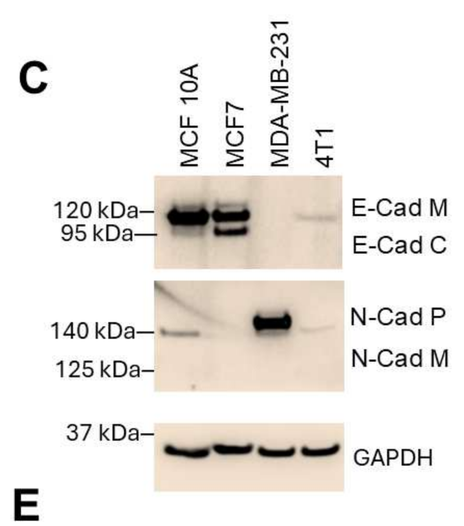

B
Bladder cancer
Relaxin signaling pathway
Proteoglycans in cancer
Protein digestion and absorption
Adherens junction
ECM-receptor interaction
Rheumatoid arthritis
TGF-beta signaling pathway
IL-17 signaling pathway
Prostate cancer
AGE-RAGE signaling pathway in diabetic complications
Amoebiasis
MicroRNAs in cancer
Leukocyte transendothelial migration
Signaling pathways regulating pluripotency of stem cells
Breast cancer
Cell adhesion molecules
Pathways in cancer
Human papillomavirus infection
PI3K-Akt signaling pathway
Fold Enrichment
N. of Genes
-log10(FDR)

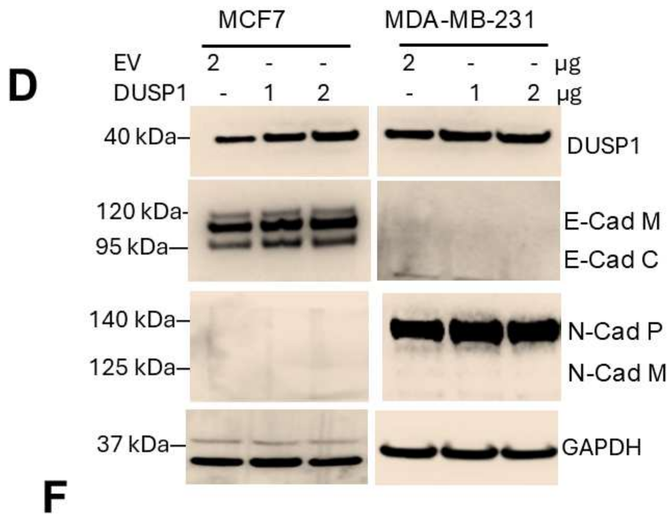


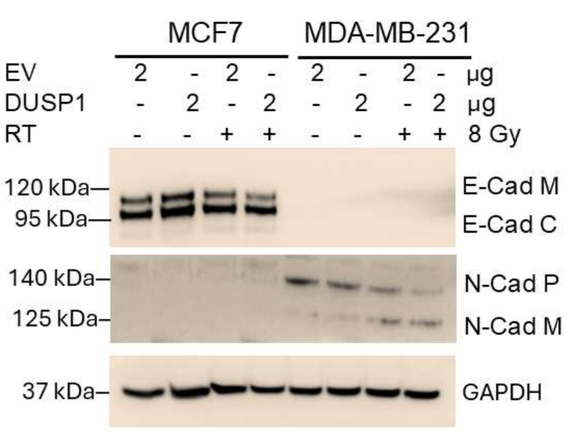

I
MCF -7
2 Gy
Week 1
Week 2
Week 3
Week 4
Analysis
MDA-MB-231
10 P1
20 P2
30 P3
40 P4
Analysis

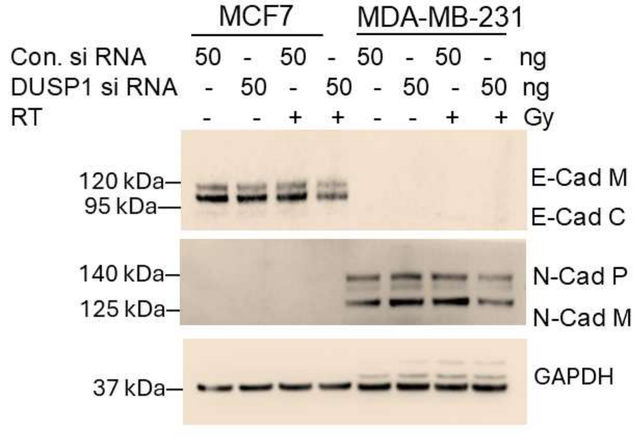

J
MCF-7 W4
MDA-MB-231 W4
MCF-7 IR W4
MDA-MB-231 IR W4

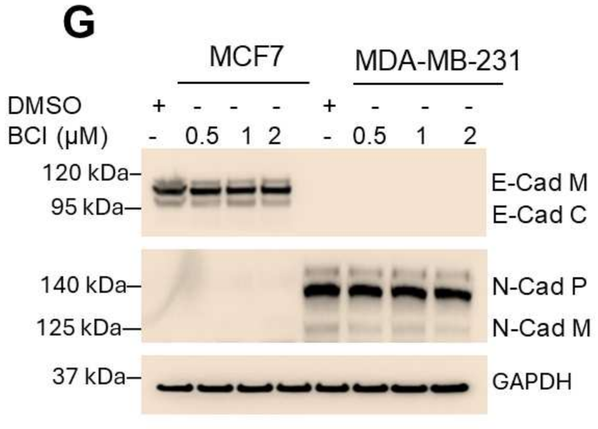

K
MCF7
CW1
IRW1
CW2
IRW2
CW3
IRW3
CW4
IRW4
Relative gene expression
DUSP1
E-Cad
N-Cad
MDA-MB-231
DUSP1
E-CAD
N-CAD

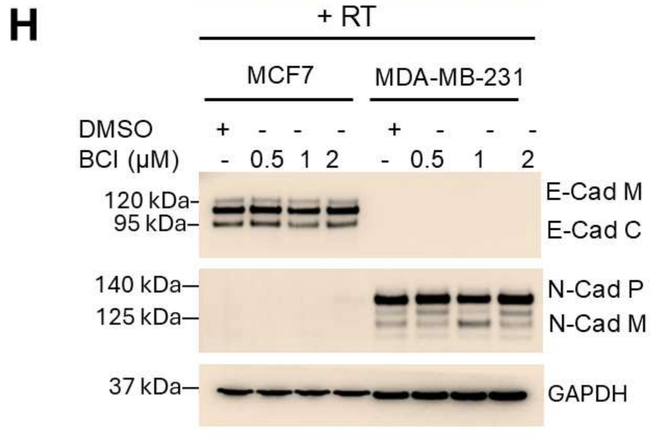

C
MCF 10A
MCF7
MDA-MB-231
4T1
E-Cad M
E-Cad C
N-Cad P
N-Cad M
GAPDH

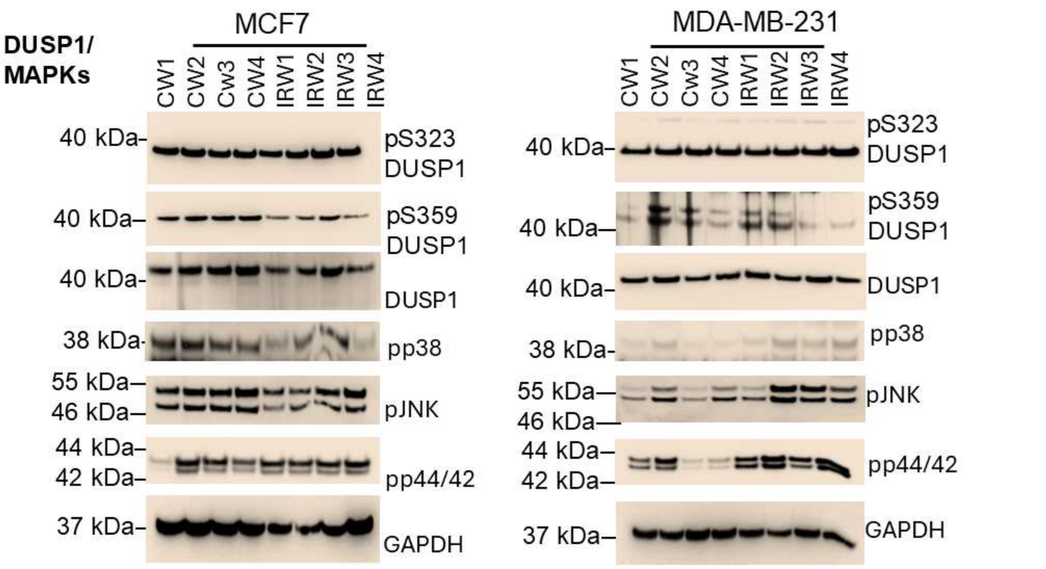

D
MCF7
MDA-MB-231
EV
DUSP1
DUSP1
E-Cad M
E-Cad C
N-Cad P
N-Cad M
GAPDH

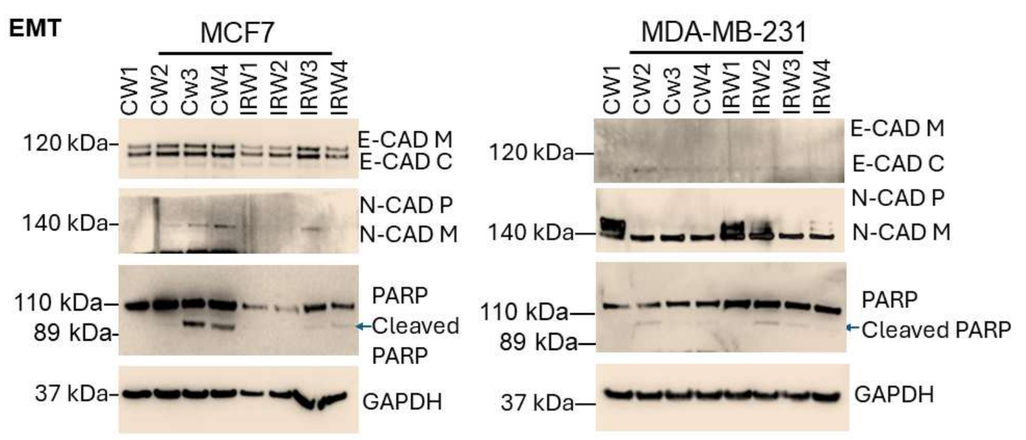

E
MCF7
MDA-MB-231
EV
DUSP1
RT
8 Gy
E-Cad M
E-Cad C
N-Cad P
N-Cad M
GAPDH


F
MCF7
MDA-MB-231
Con. si RNA
DUSP1 si RNA
RT
ng
Gy
E-Cad M
E-Cad C
N-Cad P
N-Cad M
GAPDH


G
MCF7
MDA-MB-231
DMSO
BCI (μM)
E-Cad M
E-Cad C
N-Cad P
N-Cad M
GAPDH


H
+ RT
MCF7
MDA-MB-231
DMSO
BCI (μM)
E-Cad M
E-Cad C
N-Cad P
N-Cad M
GAPDH


L
DUSP1/ MAPKs
MCF7
MDA-MB-231
CW1
CW2
Cw3
CW4
IRW1
IRW2
IRW3
IRW4
pS323 DUSP1
pS359 DUSP1
DUSP1
pp38
pJNK
pp44/42
GAPDH


M
EMT
MCF7
MDA-MB-231
E-CAD M
E-CAD C
N-CAD P
N-CAD M
PARP
Cleaved PARP
GAPDH

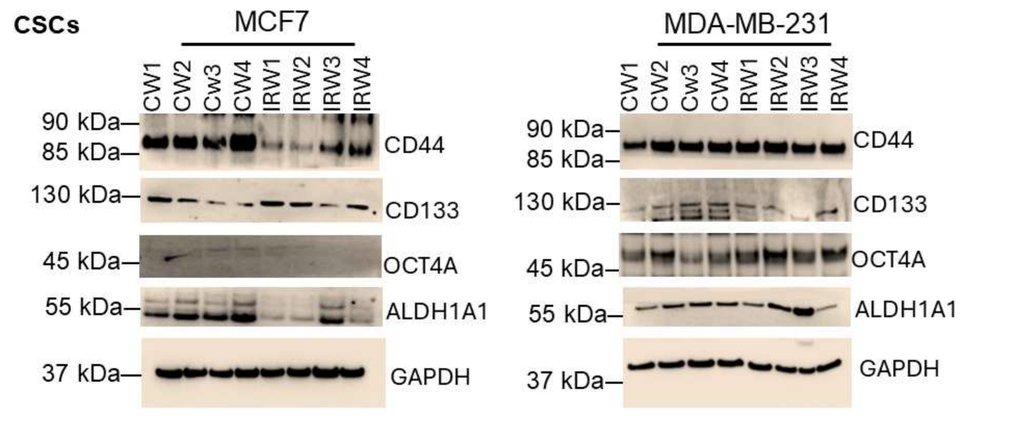
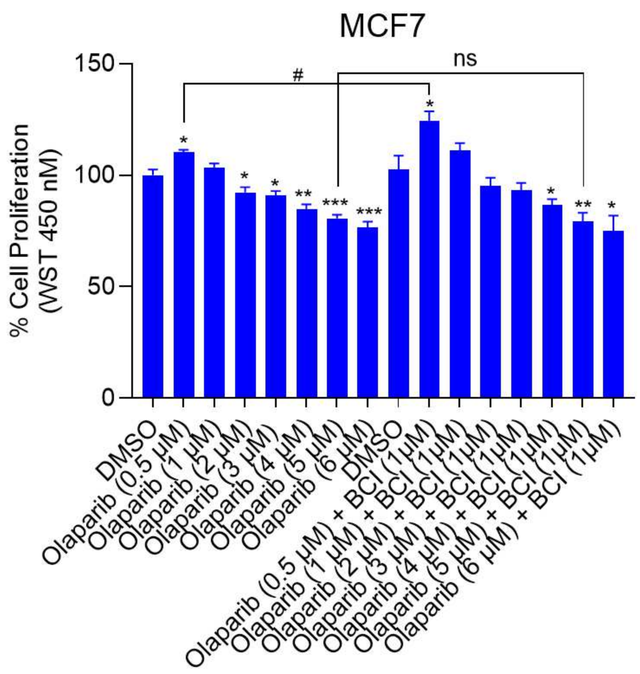
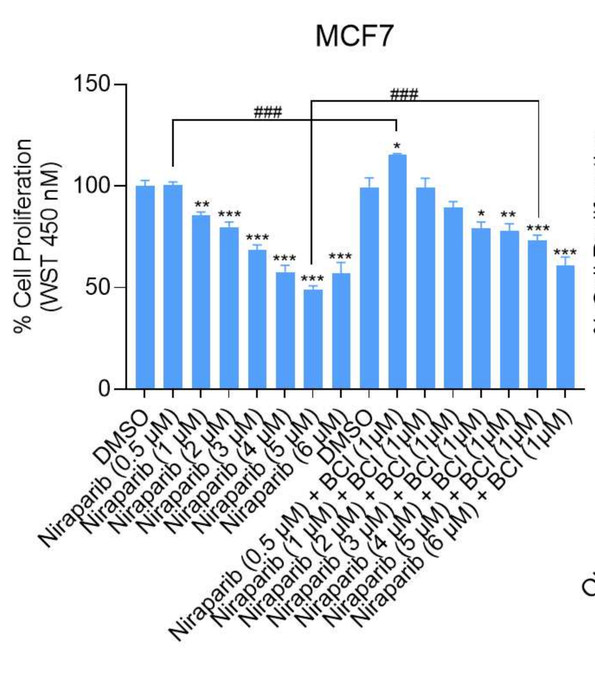
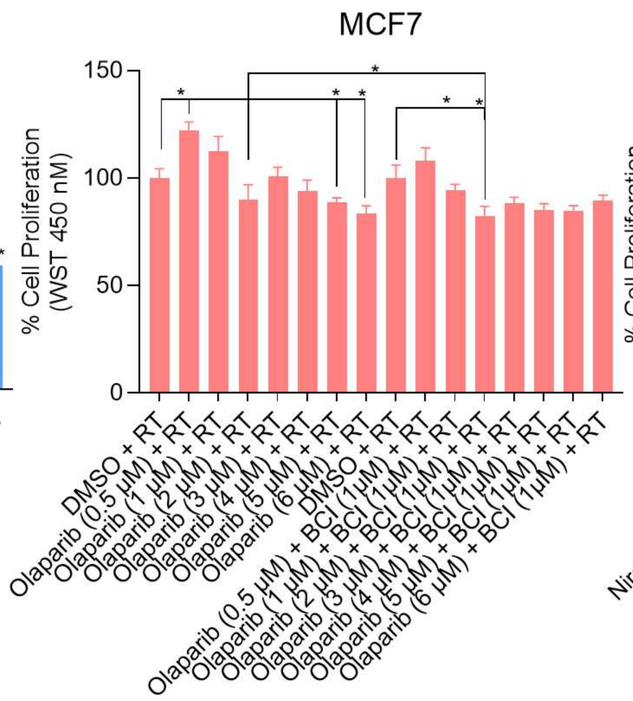

N
CSCs
MCF7
MDA-MB-231
CD44
CD133
OCT4A
ALDH1A1
GAPDH

Fig. 6

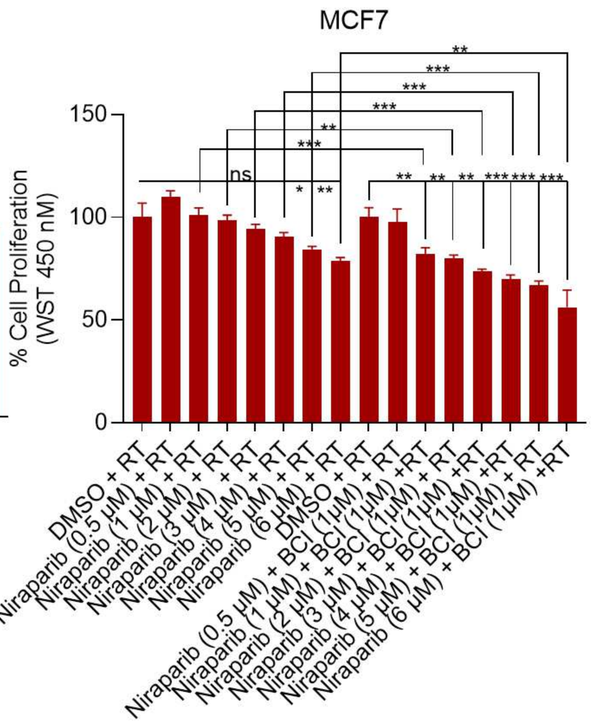

MCF7
% Cell Proliferation (WST 450 nM)
150
100
50
0
#
ns
*
DMSO
Olaparib (0.5 μM)
Olaparib (1 μM)
Olaparib (2 μM)
Olaparib (3 μM)
Olaparib (4 μM)
Olaparib (5 μM)
Olaparib (6 μM)
DMSO
Olaparib (0.5 μM) + BCl (1μM)
Olaparib (1 μM) + BCl (1μM)
Olaparib (2 μM) + BCl (1μM)
Olaparib (3 μM) + BCl (1μM)
Olaparib (4 μM) + BCl (1μM)
Olaparib (5 μM) + BCl (1μM)
Olaparib (6 μM) + BCl (1μM)

A

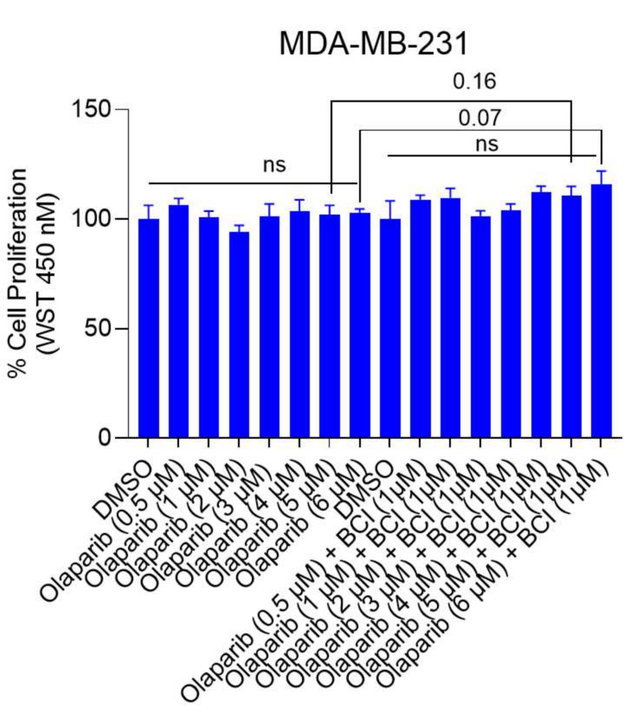

MCF7
% Cell Proliferation (WST 450 nM)
150
100
50
0
###
*
**
***
DMSO
Niraparib (0.5 μM)
Niraparib (1 μM)
Niraparib (2 μM)
Niraparib (3 μM)
Niraparib (4 μM)
Niraparib (5 μM)
Niraparib (6 μM)
DMSO
Niraparib (0.5 μM) + BCl (1μM)
Niraparib (1 μM) + BCl (1μM)
Niraparib (2 μM) + BCl (1μM)
Niraparib (3 μM) + BCl (1μM)
Niraparib (4 μM) + BCl (1μM)
Niraparib (5 μM) + BCl (1μM)
Niraparib (6 μM) + BCl (1μM)

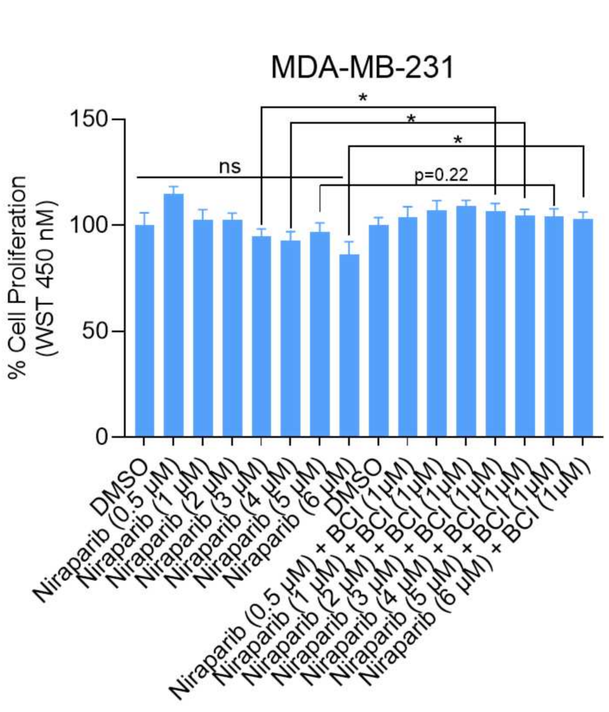

MCF7
% Cell Proliferation (WST 450 nM)
150
100
50
0
*
DMSO + RT
Olaparib (0.5 μM) + RT
Olaparib (1 μM) + RT
Olaparib (2 μM) + RT
Olaparib (3 μM) + RT
Olaparib (4 μM) + RT
Olaparib (5 μM) + RT
Olaparib (6 μM) + RT
DMSO + RT
Olaparib (0.5 μM) + BCl (1μM) + RT
Olaparib (1 μM) + BCl (1μM) + RT
Olaparib (2 μM) + BCl (1μM) + RT
Olaparib (3 μM) + BCl (1μM) + RT
Olaparib (4 μM) + BCl (1μM) + RT
Olaparib (5 μM) + BCl (1μM) + RT
Olaparib (6 μM) + BCl (1μM) + RT

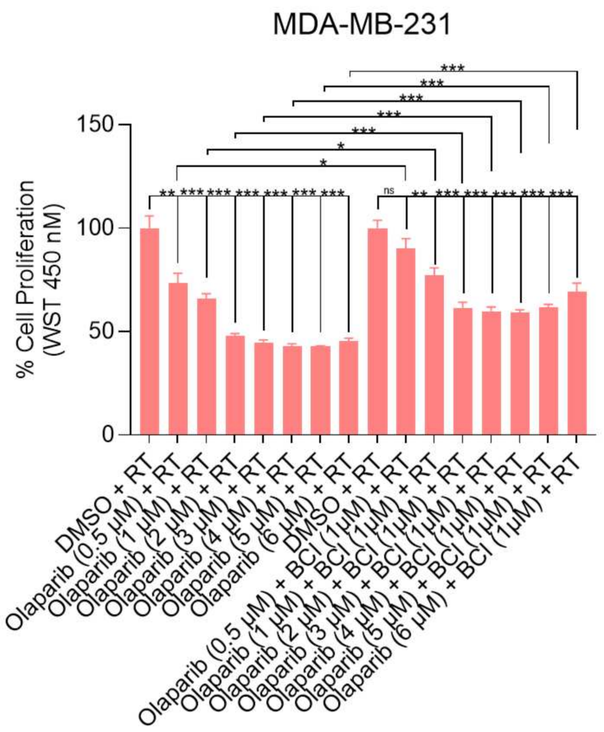
B


MCF7
% Cell Proliferation (WST 450 nM)
150
100
50
0
ns
*
**
***
DMSO + RT
Niraparib (0.5 μM) + RT
Niraparib (1 μM) + RT
Niraparib (2 μM) + RT
Niraparib (3 μM) + RT
Niraparib (4 μM) + RT
Niraparib (5 μM) + RT
Niraparib (6 μM) + RT
DMSO + RT
Niraparib (0.5 μM) + BCl (1μM) + RT
Niraparib (1 μM) + BCl (1μM) + RT
Niraparib (2 μM) + BCl (1μM) + RT
Niraparib (3 μM) + BCl (1μM) + RT
Niraparib (4 μM) + BCl (1μM) + RT
Niraparib (5 μM) + BCl (1μM) + RT
Niraparib (6 μM) + BCl (1μM) + RT

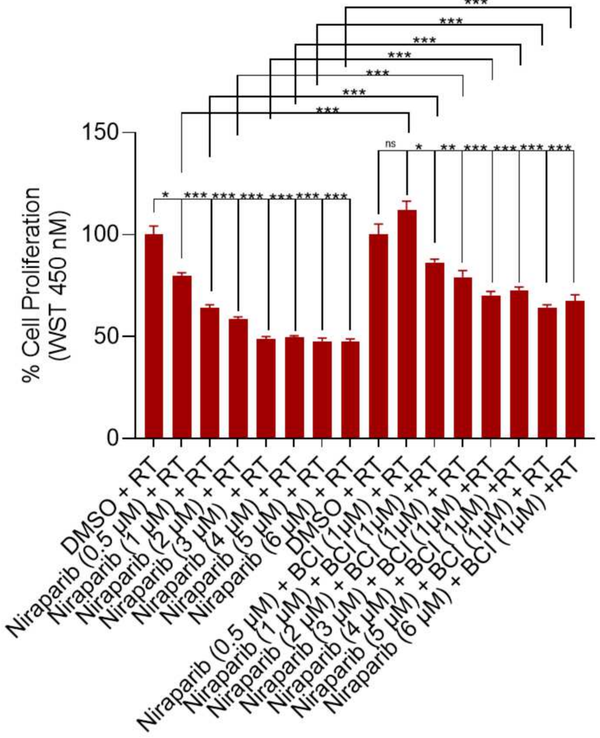
C


MDA-MB-231
% Cell Proliferation (WST 450 nM)
150
100
50
0
0.16
0.07
ns
ns
DMSO
Olaparib (0.5 μM)
Olaparib (1 μM)
Olaparib (2 μM)
Olaparib (3 μM)
Olaparib (4 μM)
Olaparib (5 μM)
Olaparib (6 μM)
DMSO
Olaparib (0.5 μM) + BCl (1μM)
Olaparib (1 μM) + BCl (1μM)
Olaparib (2 μM) + BCl (1μM)
Olaparib (3 μM) + BCl (1μM)
Olaparib (4 μM) + BCl (1μM)
Olaparib (5 μM) + BCl (1μM)
Olaparib (6 μM) + BCl (1μM)

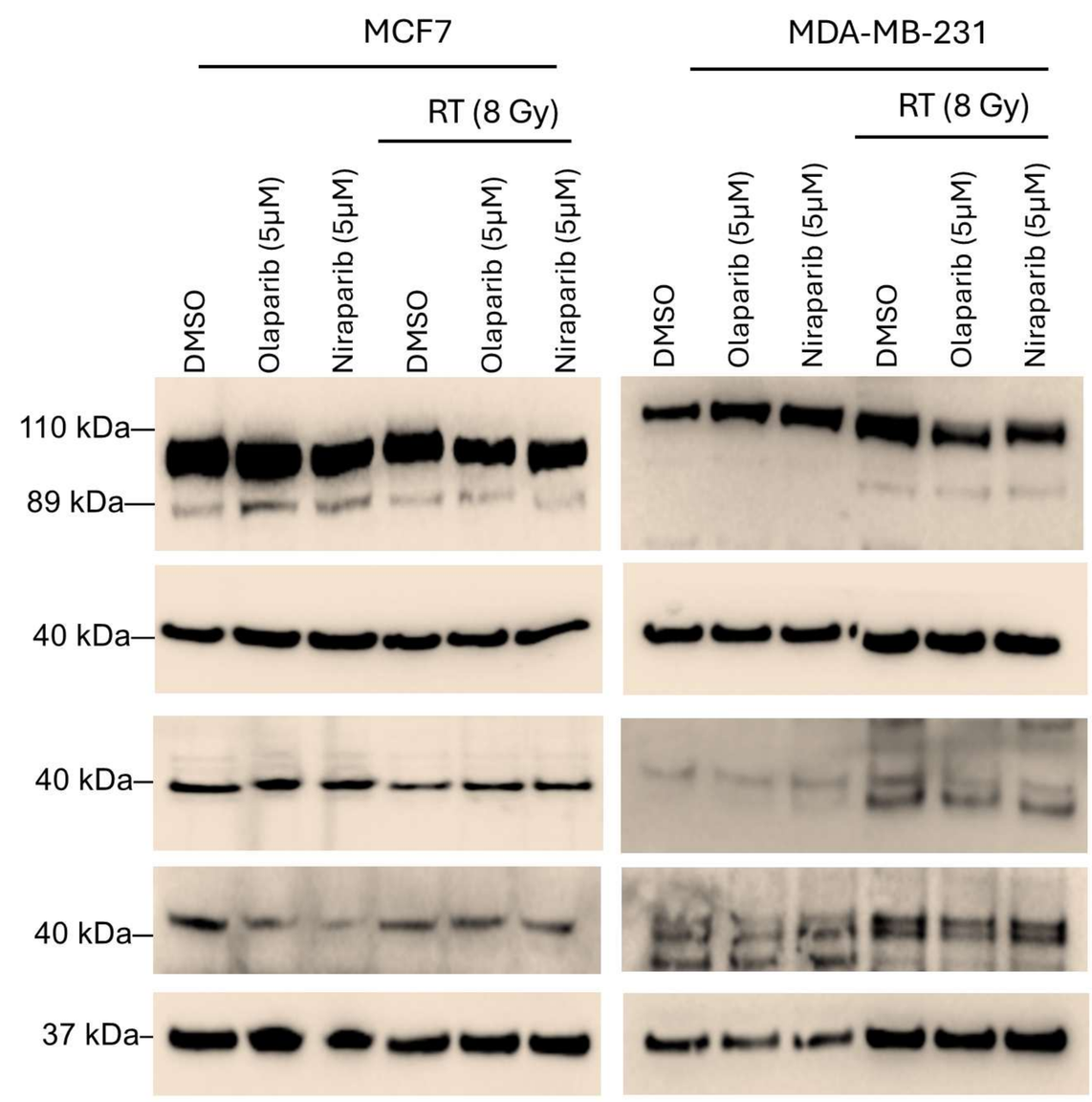

MDA-MB-231
% Cell Proliferation (WST 450 nM)
150
100
50
0
ns
*
p=0.22
DMSO
Niraparib (0.5 μM)
Niraparib (1 μM)
Niraparib (2 μM)
Niraparib (3 μM)
Niraparib (4 μM)
Niraparib (5 μM)
Niraparib (6 μM)
DMSO
Niraparib (0.5 μM) + BCl (1μM)
Niraparib (1 μM) + BCl (1μM)
Niraparib (2 μM) + BCl (1μM)
Niraparib (3 μM) + BCl (1μM)
Niraparib (4 μM) + BCl (1μM)
Niraparib (5 μM) + BCl (1μM)
Niraparib (6 μM) + BCl (1μM)


MDA-MB-231
% Cell Proliferation (WST 450 nM)
150
100
50
0
*
**
***
ns
DMSO + RT
Olaparib (0.5 μM) + RT
Olaparib (1 μM) + RT
Olaparib (2 μM) + RT
Olaparib (3 μM) + RT
Olaparib (4 μM) + RT
Olaparib (5 μM) + RT
Olaparib (6 μM) + RT
DMSO + RT
Olaparib (0.5 μM) + BCl (1μM) + RT
Olaparib (1 μM) + BCl (1μM) + RT
Olaparib (2 μM) + BCl (1μM) + RT
Olaparib (3 μM) + BCl (1μM) + RT
Olaparib (4 μM) + BCl (1μM) + RT
Olaparib (5 μM) + BCl (1μM) + RT
Olaparib (6 μM) + BCl (1μM) + RT

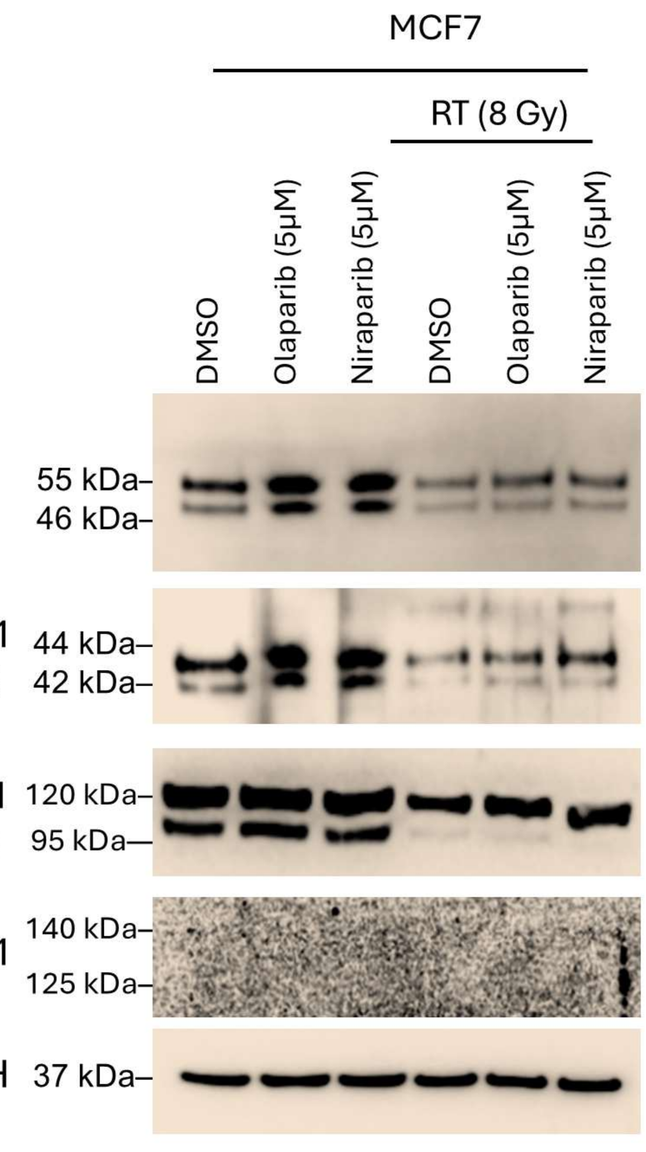
D


MDA-MB-231
% Cell Proliferation (WST 450 nM)
150
100
50
0
*
**
***
ns
DMSO + RT
Niraparib (0.5 μM) + RT
Niraparib (1 μM) + RT
Niraparib (2 μM) + RT
Niraparib (3 μM) + RT
Niraparib (4 μM) + RT
Niraparib (5 μM) + RT
Niraparib (6 μM) + RT
DMSO + RT
Niraparib (0.5 μM) + BCl (1μM) + RT
Niraparib (1 μM) + BCl (1μM) + RT
Niraparib (2 μM) + BCl (1μM) + RT
Niraparib (3 μM) + BCl (1μM) + RT
Niraparib (4 μM) + BCl (1μM) + RT
Niraparib (5 μM) + BCl (1μM) + RT
Niraparib (6 μM) + BCl (1μM) + RT

E


MCF7
RT (8 Gy)
DMSO
Olaparib (5μM)
Niraparib (5μM)
110 kDa
89 kDa
PARP
cPARP
40 kDa
DUSP1
pS323
40 kDa
DUSP1
pS359
40 kDa
DUSP1
37 kDa
GAPDH

MDA-MB-231
RT (8 Gy)
DMSO
Olaparib (5μM)
Niraparib (5μM)
PARP
cPARP
DUSP1
pS323
DUSP1
pS359
DUSP1
GAPDH


MCF7
RT (8 Gy)
DMSO
Olaparib (5μM)
Niraparib (5μM)
55 kDa
46 kDa
pJNK
44 kDa
42 kDa
pERK
120 kDa
95 kDa
E-Cad M
E-Cad C
140 kDa
125 kDa
N-Cad P
N-Cad M
37 kDa
GAPDH

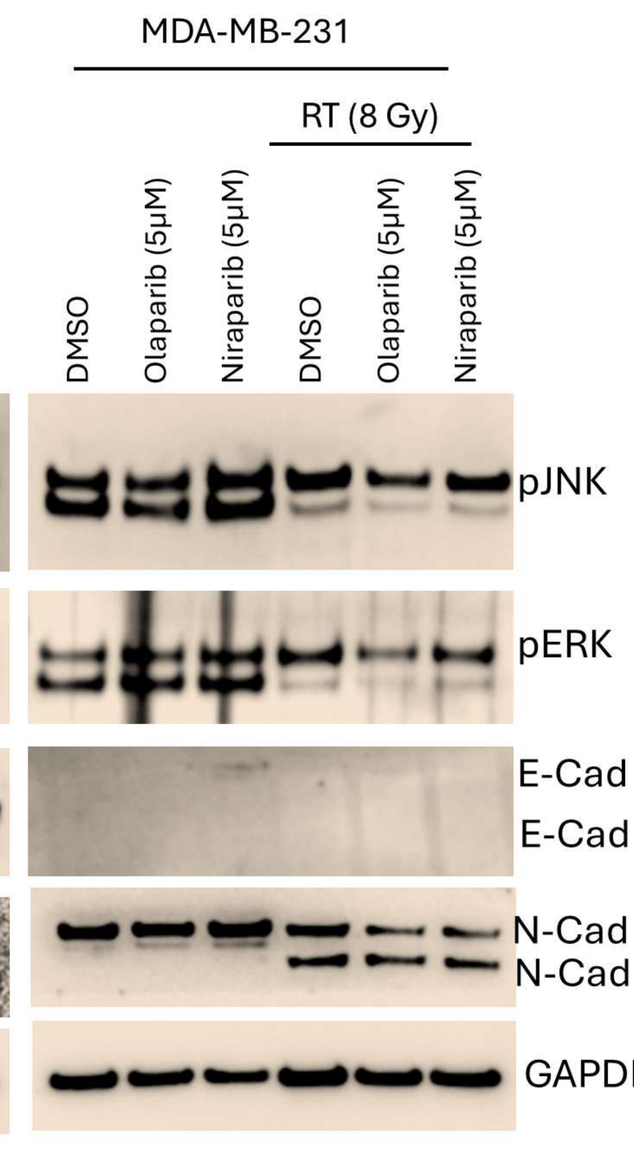
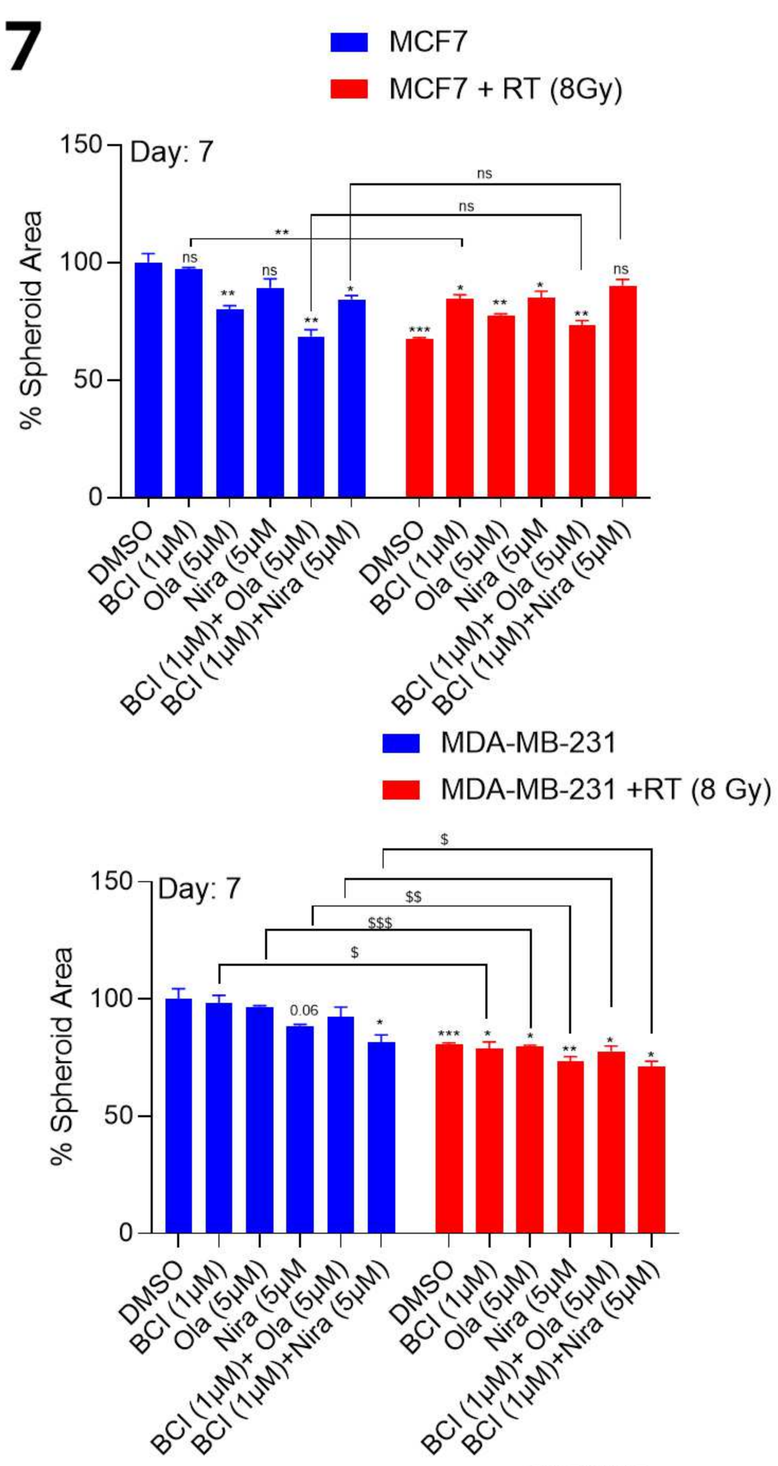
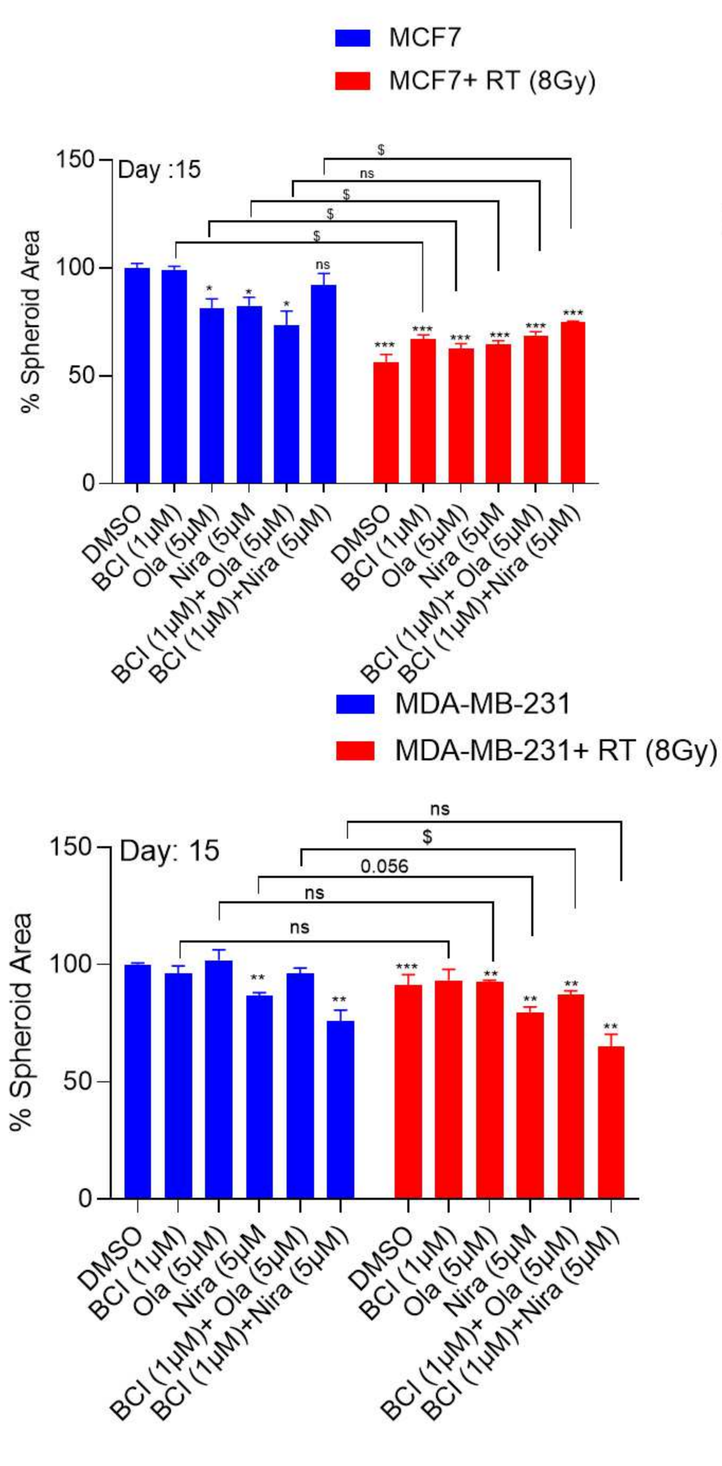

MDA-MB-231
RT (8 Gy)
DMSO
Olaparib (5μM)
Niraparib (5μM)
pJNK
pERK
E-Cad M
E-Cad C
N-Cad P
N-Cad M
GAPDH

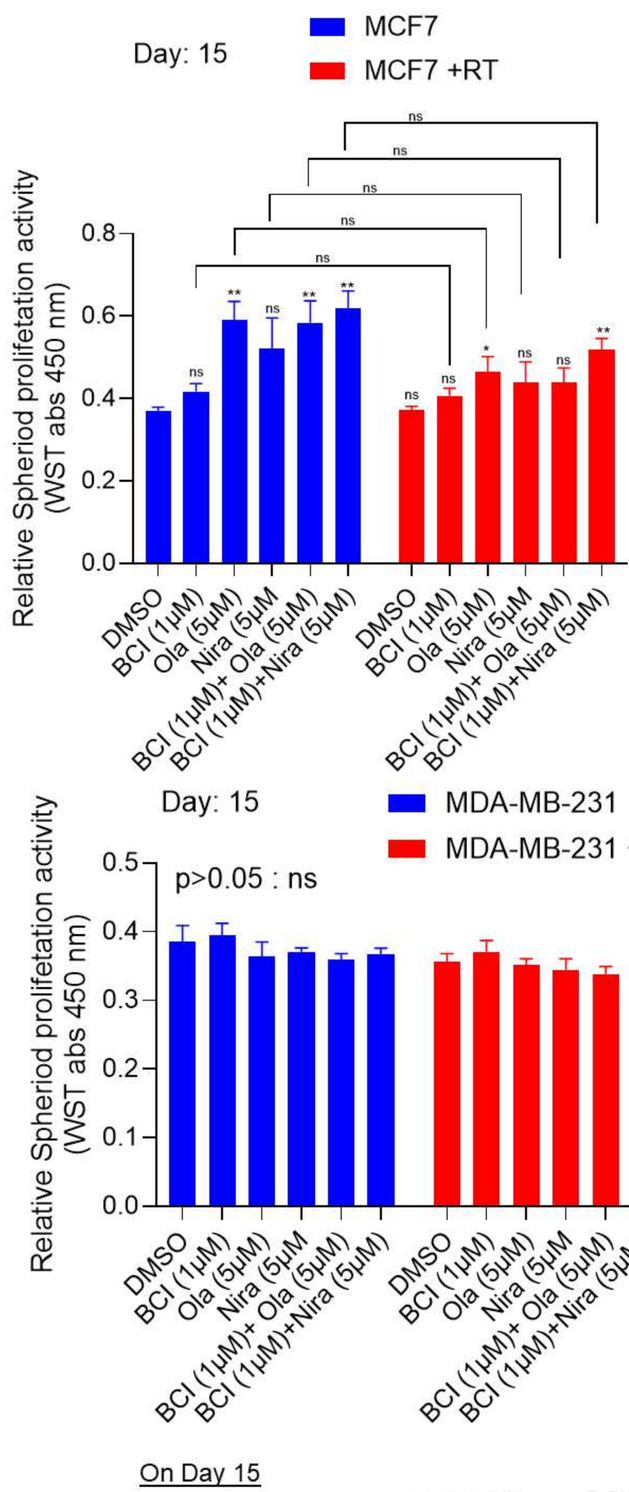
Fig. 7

A


MCF7
MCF7 + RT (8Gy)
Day: 7
% Spheroid Area
150
100
50
0
ns
**
*
***
DMSO
BCl (1μM)
Ola (5μM)
Nira (5μM
BCl (1μM)+ Ola (5μM)
BCl (1μM)+Nira (5μM)
MDA-MB-231
MDA-MB-231 +RT (8 Gy)


MCF7
MCF7+ RT (8Gy)
Day :15
% Spheroid Area
150
100
50
0
$
ns
*
***
DMSO
BCl (1μM)
Ola (5μM)
Nira (5μM
BCl (1μM)+ Ola (5μM)
BCl (1μM)+Nira (5μM)
MDA-MB-231
MDA-MB-231+ RT (8Gy)

C


Day: 15
MCF7
MCF7 +RT
Relative Spheriod prolifetation activity
(WST abs 450 nm)
0.8
0.6
0.4
0.2
0.0
ns
**
*
DMSO
BCl (1μM)
Ola (5μM)
Nira (5μM
BCl (1μM)+ Ola (5μM)
BCl (1μM)+Nira (5μM)

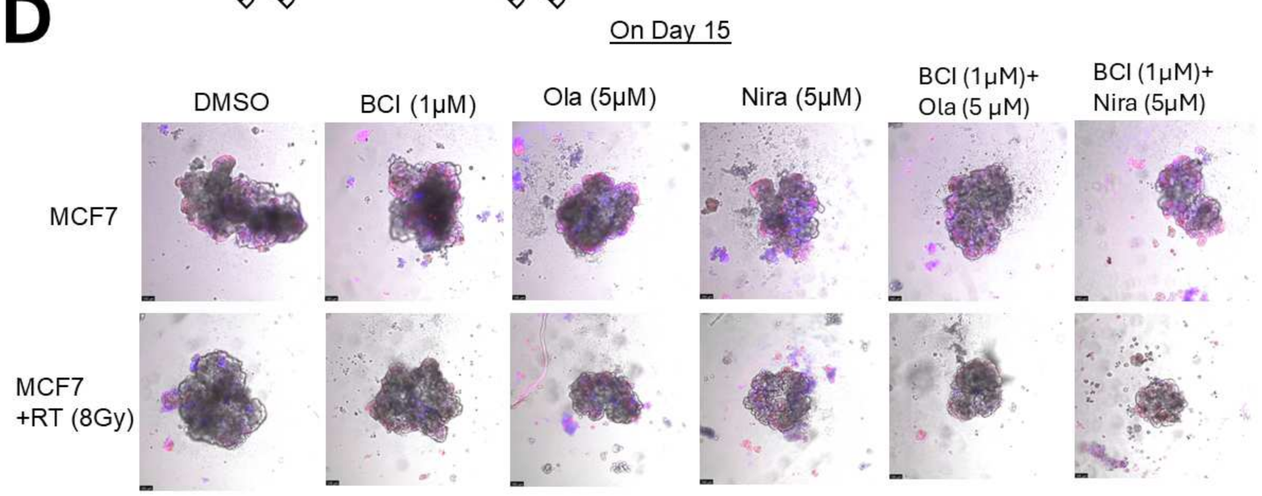
B

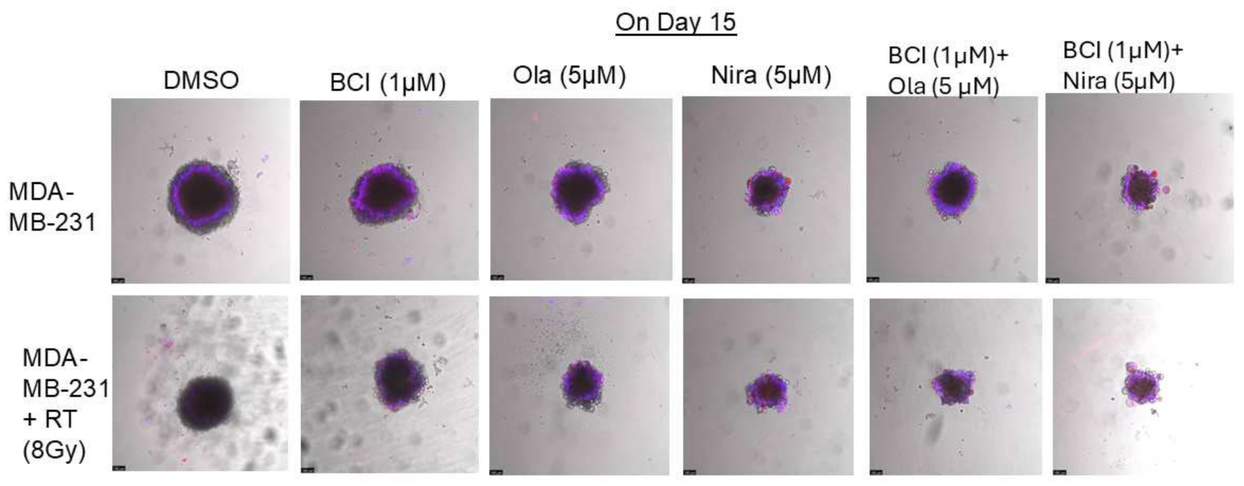
Day: 7
% Spheroid Area
150
100
50
0
$
$$
$$$
0.06
*
DMSO
BCl (1μM)
Ola (5μM)
Nira (5μM
BCl (1μM)+ Ola (5μM)
BCl (1μM)+Nira (5μM)

Day: 15
% Spheroid Area
150
100
50
0
$
0.056
ns
**
***
DMSO
BCl (1μM)
Ola (5μM)
Nira (5μM
BCl (1μM)+ Ola (5μM)
BCl (1μM)+Nira (5μM)

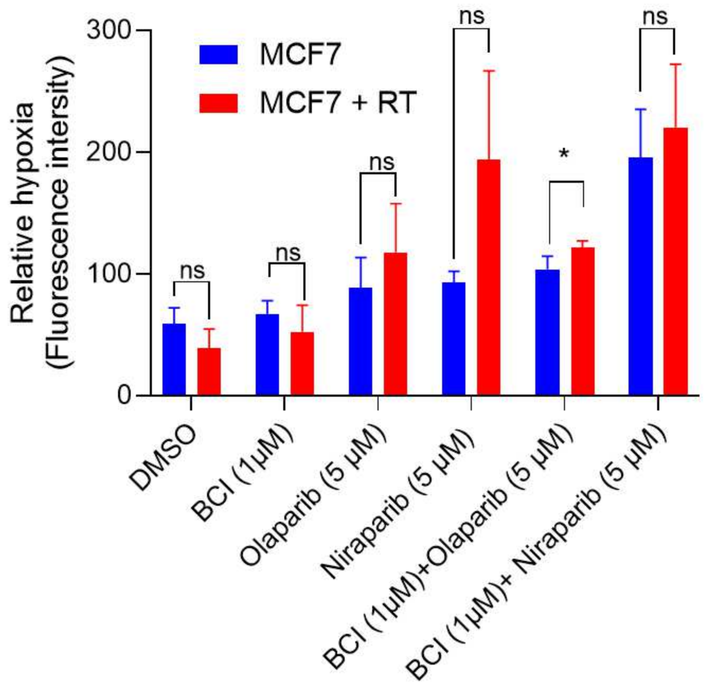
Day: 15
MDA-MB-231
MDA-MB-231 + RT
p>0.05 : ns
Relative Spheriod prolifetation activity
(WST abs 450 nm)
0.5
0.4
0.3
0.2
0.1
0.0
DMSO
BCl (1μM)
Ola (5μM)
Nira (5μM
BCl (1μM)+ Ola (5μM)
BCl (1μM)+Nira (5μM)

D


On Day 15
DMSO
BCl (1μM)
Ola (5μM)
Nira (5μM)
BCl (1μM)+ Ola (5 μM)
BCl (1μM)+ Nira (5μM)
MCF7
MCF7 +RT (8Gy)


On Day 15
DMSO
BCl (1μM)
Ola (5μM)
Nira (5μM)
BCl (1μM)+ Ola (5 μM)
BCl (1μM)+ Nira (5μM)
MDA-MB-231
MDA-MB-231 + RT (8Gy)

E


MCF7
MCF7 + RT
Relative hypoxia
(Fluorescence intersity)
300
200
100
0
ns
*
DMSO
BCl (1μM)
Olaparib (5 μM)
Niraparib (5 μM)
BCl (1μM)+Olaparib (5 μM)
BCl (1μM)+ Niraparib (5 μM)

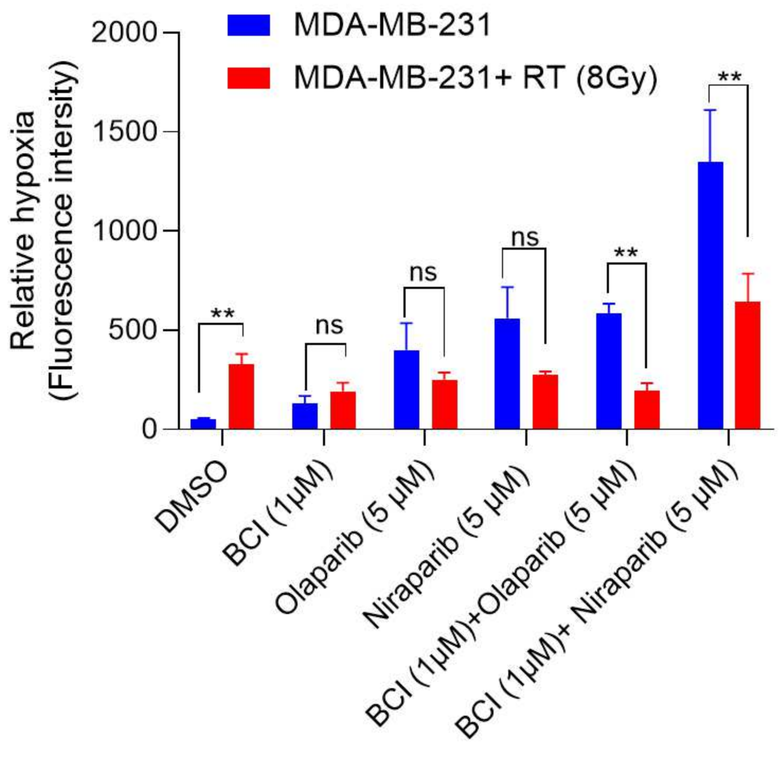
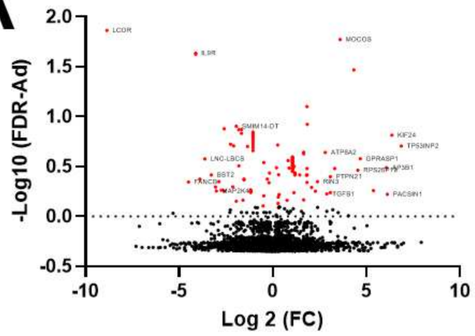
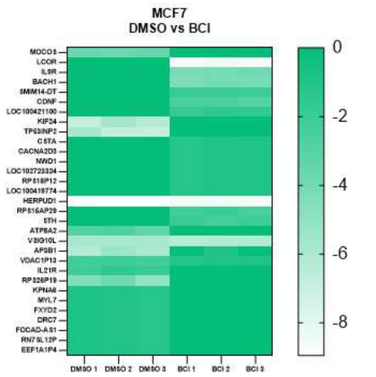
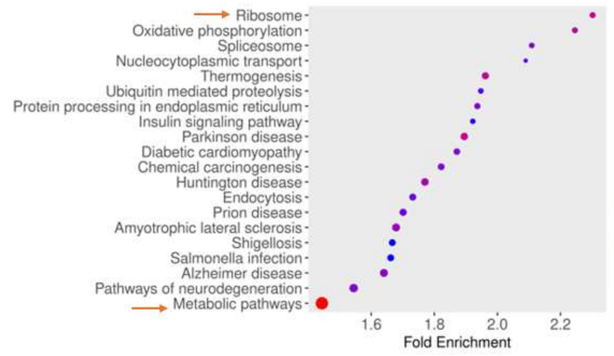

MDA-MB-231
MDA-MB-231+ RT (8Gy)
Relative hypoxia
(Fluorescence intersity)
2000
1500
1000
500
0
**
ns
DMSO
BCl (1μM)
Olaparib (5 μM)
Niraparib (5 μM)
BCl (1μM)+Olaparib (5 μM)
BCl (1μM)+ Niraparib (5 μM)

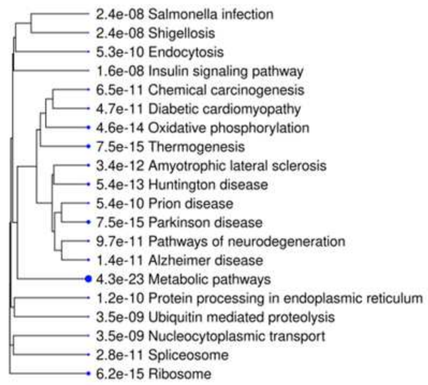
Fig 8

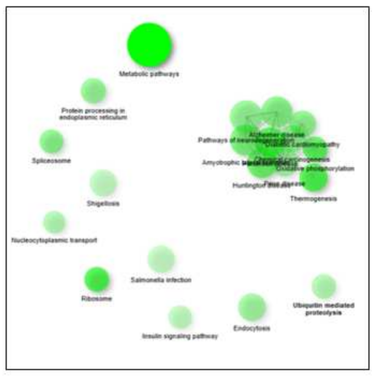
A


MCF7
DMSO vs BCI
-Log10 (FDR-Ad)
Log 2 (FC)

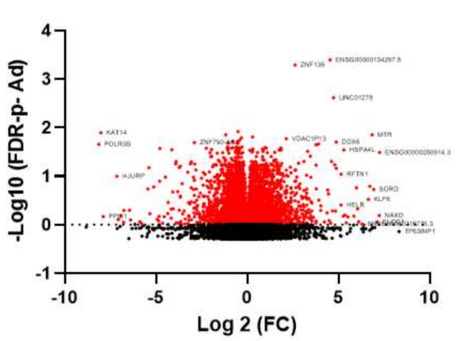

MCF7
DMSO vs BCI
DMSO 1
DMSO 2
DMSO 3
BCI 1
BCI 2
BCI 3

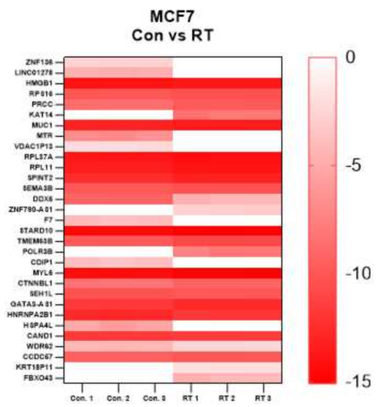

Ribosome
Oxidative phosphorylation
Spliceosome
Nucleocytoplasmic transport
Thermogenesis
Ubiquitin mediated proteolysis
Protein processing in endoplasmic reticulum
Insulin signaling pathway
Parkinson disease
Diabetic cardiomyopathy
Chemical carcinogenesis
Huntington disease
Endocytosis
Prion disease
Amyotrophic lateral sclerosis
Shigellosis
Salmonella infection
Alzheimer disease
Pathways of neurodegeneration
Metabolic pathways
Fold Enrichment
N. of Genes
-log10(FDR)

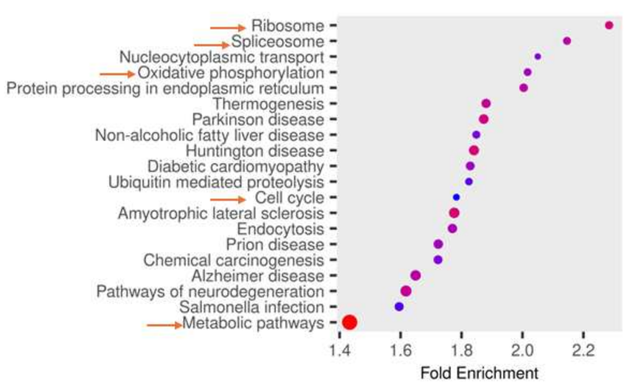

2.4e-08 Salmonella infection
2.4e-08 Shigellosis
5.3e-10 Endocytosis
1.6e-08 Insulin signaling pathway
6.5e-11 Chemical carcinogenesis
4.7e-11 Diabetic cardiomyopathy
4.6e-14 Oxidative phosphorylation
7.5e-15 Thermogenesis
3.4e-12 Amyotrophic lateral sclerosis
5.4e-13 Huntington disease
5.4e-10 Prion disease
7.5e-15 Parkinson disease
9.7e-11 Pathways of neurodegeneration
1.4e-11 Alzheimer disease
4.3e-23 Metabolic pathways
1.2e-10 Protein processing in endoplasmic reticulum
3.5e-09 Ubiquitin mediated proteolysis
3.5e-09 Nucleocytoplasmic transport
2.8e-11 Spliceosome
6.2e-15 Ribosome

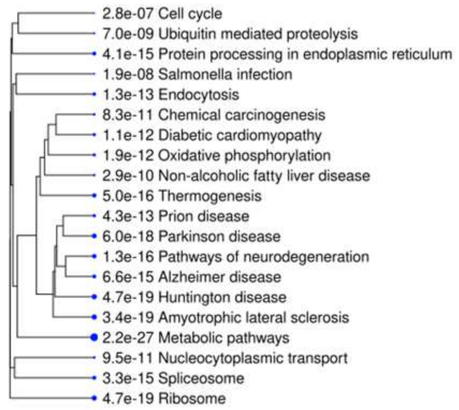


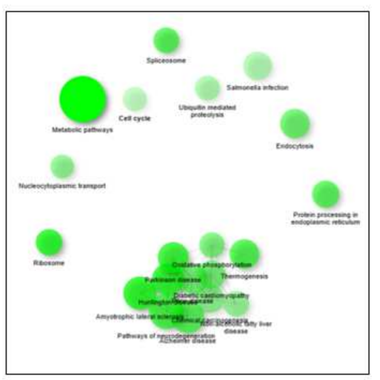
B


MCF7
DMSO vs RT
-Log10 (FDR-p- Ad)
Log 2 (FC)

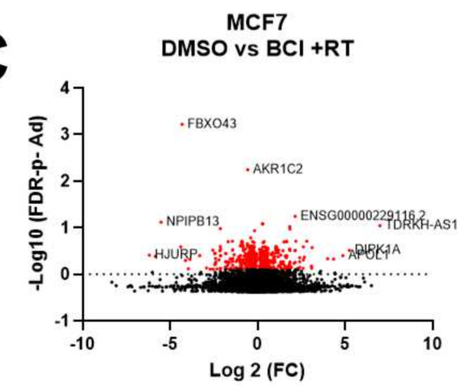

MCF7
Con vs RT
Con. 1
Con. 2
Con. 3
RT 1
RT 2
RT 3

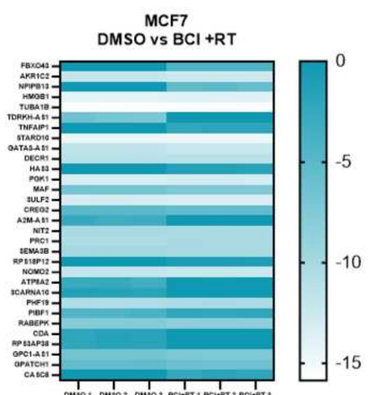

Ribosome
Spliceosome
Nucleocytoplasmic transport
Oxidative phosphorylation
Protein processing in endoplasmic reticulum
Thermogenesis
Parkinson disease
Non-alcoholic fatty liver disease
Huntington disease
Diabetic cardiomyopathy
Ubiquitin mediated proteolysis
Cell cycle
Amyotrophic lateral sclerosis
Endocytosis
Prion disease
Chemical carcinogenesis
Alzheimer disease
Pathways of neurodegeneration
Salmonella infection
Metabolic pathways
Fold Enrichment
N. of Genes
-log10(FDR)

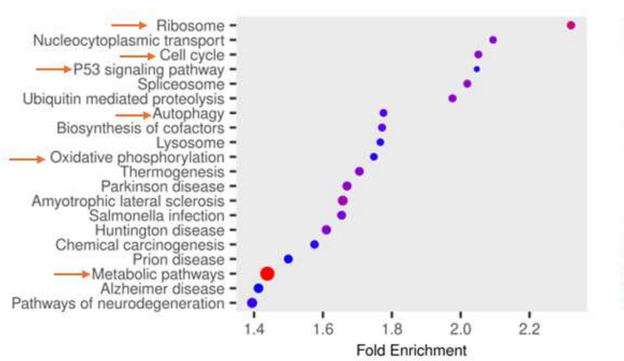

2.8e-07 Cell cycle
7.0e-09 Ubiquitin mediated proteolysis
4.1e-15 Protein processing in endoplasmic reticulum
1.9e-08 Salmonella infection
1.3e-13 Endocytosis
8.3e-11 Chemical carcinogenesis
1.1e-12 Diabetic cardiomyopathy
1.9e-12 Oxidative phosphorylation
2.9e-10 Non-alcoholic fatty liver disease
5.0e-16 Thermogenesis
4.3e-13 Prion disease
6.0e-18 Parkinson disease
1.3e-16 Pathways of neurodegeneration
6.6e-15 Alzheimer disease
4.7e-19 Huntington disease
3.4e-19 Amyotrophic lateral sclerosis
2.2e-27 Metabolic pathways
9.5e-11 Nucleocytoplasmic transport
3.3e-15 Spliceosome
4.7e-19 Ribosome

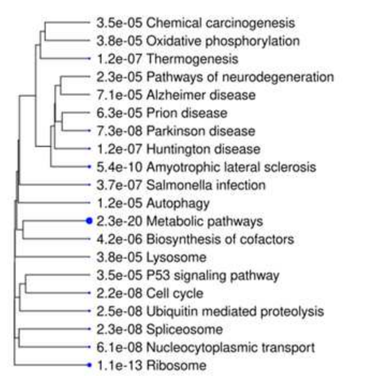


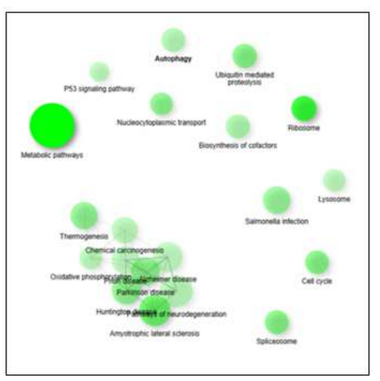
C


MCF7
DMSO vs BCI +RT
FBXO43
AKR1C2
NPIPB13
ENSG00000229116.2
TDRKH-AS1
HJURP
DIPK1A
APOL1
-Log10 (FDR-p- Ad)
Log 2 (FC)

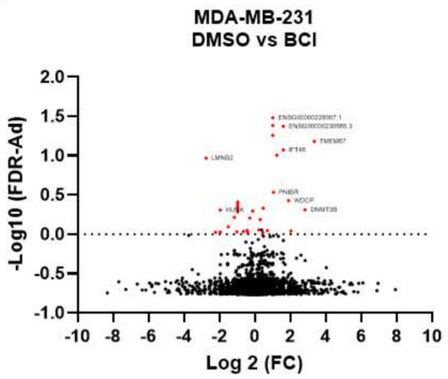

MCF7
DMSO vs BCI +RT
DMSO 1
DMSO 2
DMSO 3
BCI+RT 1
BCI+RT 2
BCI+RT 3

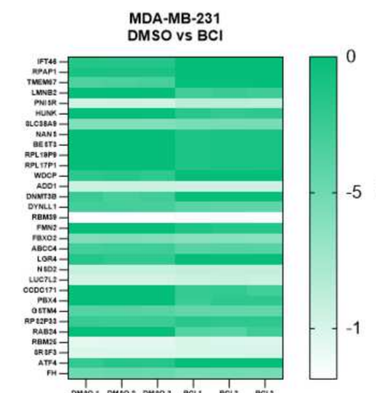

Ribosome
Nucleocytoplasmic transport
Cell cycle
P53 signaling pathway
Spliceosome
Ubiquitin mediated proteolysis
Autophagy
Biosynthesis of cofactors
Lysosome
Oxidative phosphorylation
Thermogenesis
Parkinson disease
Amyotrophic lateral sclerosis
Salmonella infection
Huntington disease
Chemical carcinogenesis
Prion disease
Metabolic pathways
Alzheimer disease
Pathways of neurodegeneration
Fold Enrichment
N. of Genes
-log10(FDR)

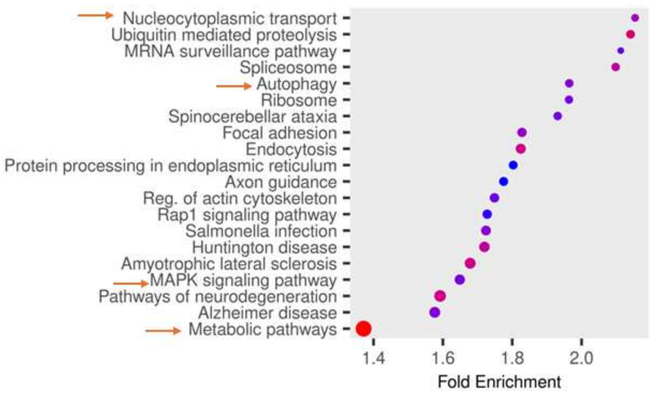

3.5e-05 Chemical carcinogenesis
3.8e-05 Oxidative phosphorylation
1.2e-07 Thermogenesis
2.3e-05 Pathways of neurodegeneration
7.1e-05 Alzheimer disease
6.3e-05 Prion disease
7.3e-08 Parkinson disease
1.2e-07 Huntington disease
5.4e-10 Amyotrophic lateral sclerosis
3.7e-07 Salmonella infection
1.2e-05 Autophagy
2.3e-20 Metabolic pathways
4.2e-06 Biosynthesis of cofactors
3.8e-05 Lysosome
3.5e-05 P53 signaling pathway
2.2e-08 Cell cycle
2.5e-08 Ubiquitin mediated proteolysis
2.3e-08 Spliceosome
6.1e-08 Nucleocytoplasmic transport
1.1e-13 Ribosome

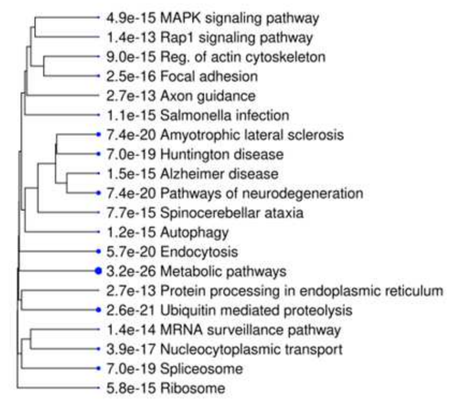


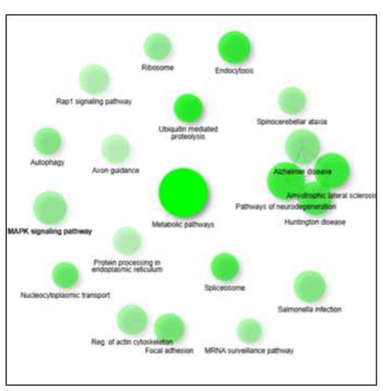
D


MDA-MB-231
DMSO vs BCI
-Log10 (FDR-Ad)
Log 2 (FC)

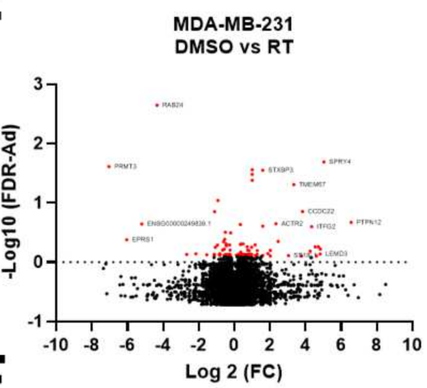

MDA-MB-231
DMSO vs BCI
DMSO 1
DMSO 2
DMSO 3
BCI 1
BCI 2
BCI 3

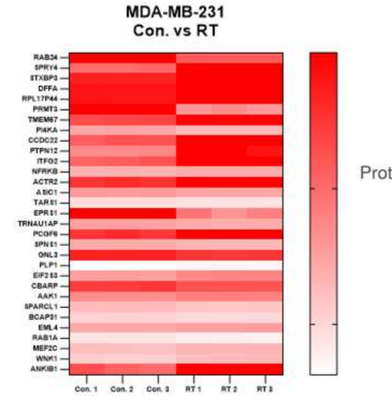

Nucleocytoplasmic transport
Ubiquitin mediated proteolysis
MRNA surveillance pathway
Spliceosome
Autophagy
Ribosome
Spinocerebellar ataxia
Focal adhesion
Endocytosis
Protein processing in endoplasmic reticulum
Axon guidance
Reg. of actin cytoskeleton
Rap1 signaling pathway
Salmonella infection
Huntington disease
Amyotrophic lateral sclerosis
MAPK signaling pathway
Pathways of neurodegeneration
Alzheimer disease
Metabolic pathways
Fold Enrichment
N. of Genes
-log10(FDR)

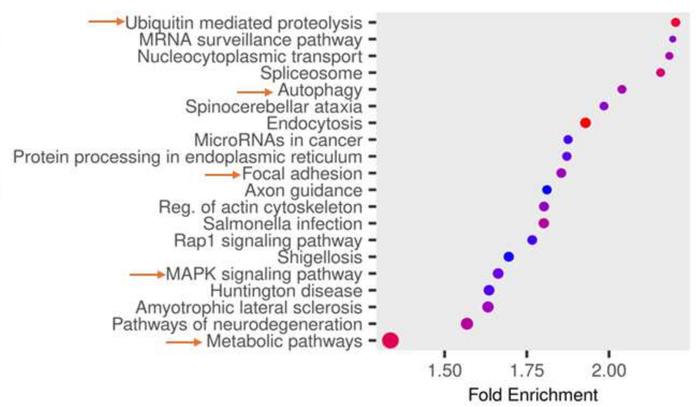

4.9e-15 MAPK signaling pathway
1.4e-13 Rap1 signaling pathway
9.0e-15 Reg. of actin cytoskeleton
2.5e-16 Focal adhesion
2.7e-13 Axon guidance
1.1e-15 Salmonella infection
7.4e-20 Amyotrophic lateral sclerosis
7.0e-19 Huntington disease
1.5e-15 Alzheimer disease
7.4e-20 Pathways of neurodegeneration
7.7e-15 Spinocerebellar ataxia
1.2e-15 Autophagy
5.7e-20 Endocytosis
3.2e-26 Metabolic pathways
2.7e-13 Protein processing in endoplasmic reticulum
2.6e-21 Ubiquitin mediated proteolysis
1.4e-14 MRNA surveillance pathway
3.9e-17 Nucleocytoplasmic transport
7.0e-19 Spliceosome
5.8e-15 Ribosome

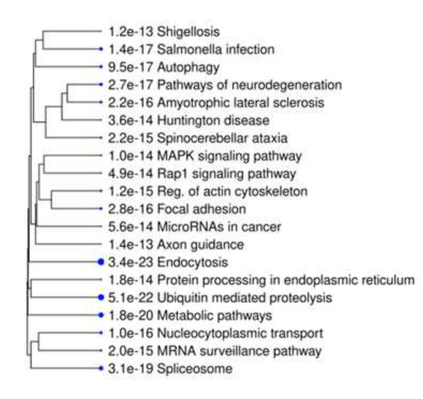


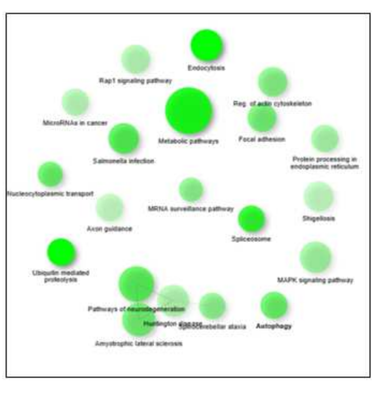
E


MDA-MB-231
DMSO vs RT
-Log10 (FDR-Ad)
Log 2 (FC)

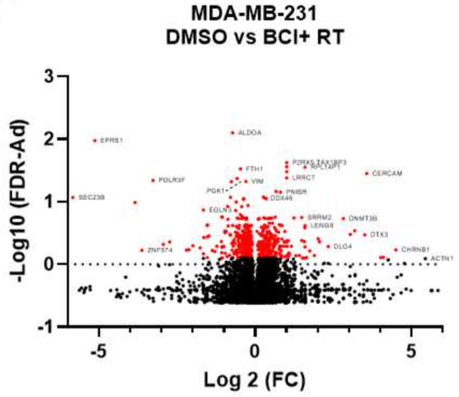

MDA-MB-231
Con. vs RT
Con. 1
Con. 2
Con. 3
RT 1
RT 2
RT 3

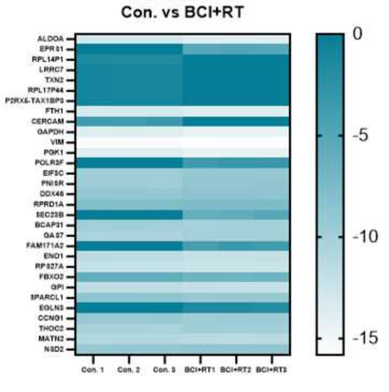

Ubiquitin mediated proteolysis
MRNA surveillance pathway
Nucleocytoplasmic transport
Spliceosome
Autophagy
Spinocerebellar ataxia
Endocytosis
MicroRNAs in cancer
Protein processing in endoplasmic reticulum
Focal adhesion
Axon guidance
Reg. of actin cytoskeleton
Salmonella infection
Rap1 signaling pathway
Shigellosis
MAPK signaling pathway
Huntington disease
Amyotrophic lateral sclerosis
Pathways of neurodegeneration
Metabolic pathways
Fold Enrichment
N. of Genes
-log10(FDR)

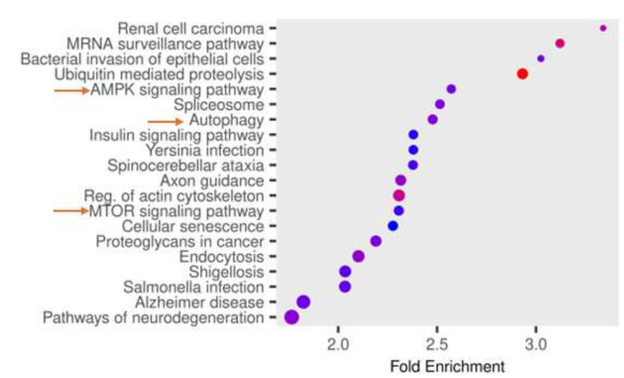

1.2e-13 Shigellosis
1.4e-17 Salmonella infection
9.5e-17 Autophagy
2.7e-17 Pathways of neurodegeneration
2.2e-16 Amyotrophic lateral sclerosis
3.6e-14 Huntington disease
2.2e-15 Spinocerebellar ataxia
1.0e-14 MAPK signaling pathway
4.9e-14 Rap1 signaling pathway
1.2e-15 Reg. of actin cytoskeleton
2.8e-16 Focal adhesion
5.6e-14 MicroRNAs in cancer
1.4e-13 Axon guidance
3.4e-23 Endocytosis
1.8e-14 Protein processing in endoplasmic reticulum
5.1e-22 Ubiquitin mediated proteolysis
1.8e-20 Metabolic pathways
1.0e-16 Nucleocytoplasmic transport
2.0e-15 MRNA surveillance pathway
3.1e-19 Spliceosome

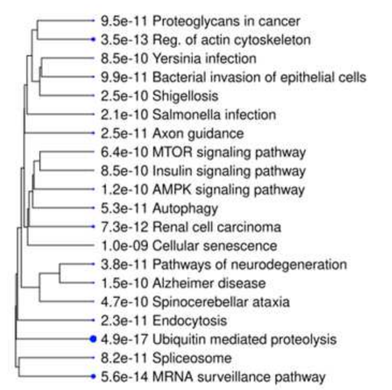


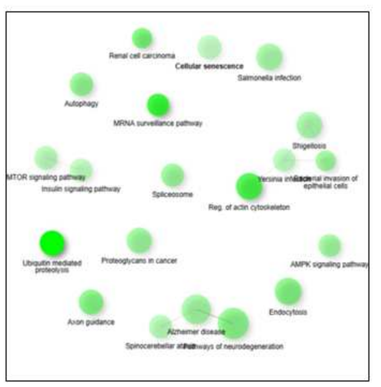
F


MDA-MB-231
DMSO vs BCI+ RT
-Log10 (FDR-Ad)
Log 2 (FC)


MDA-MB-231
Con. vs BCI+RT
Con. 1
Con. 2
Con. 3
BCI+RT1
BCI+RT2
BCI+RT3


Renal cell carcinoma
MRNA surveillance pathway
Bacterial invasion of epithelial cells
Ubiquitin mediated proteolysis
AMPK signaling pathway
Spliceosome
Autophagy
Insulin signaling pathway
Yersinia infection
Spinocerebellar ataxia
Axon guidance
Reg. of actin cytoskeleton
MTOR signaling pathway
Cellular senescence
Proteoglycans in cancer
Endocytosis
Shigellosis
Salmonella infection
Alzheimer disease
Pathways of neurodegeneration
Fold Enrichment
N. of Genes
-log10(FDR)


9.5e-11 Proteoglycans in cancer
3.5e-13 Reg. of actin cytoskeleton
8.5e-10 Yersinia infection
9.9e-11 Bacterial invasion of epithelial cells
2.5e-10 Shigellosis
2.1e-10 Salmonella infection
2.5e-11 Axon guidance
6.4e-10 MTOR signaling pathway
8.5e-10 Insulin signaling pathway
1.2e-10 AMPK signaling pathway
5.3e-11 Autophagy
7.3e-12 Renal cell carcinoma
1.0e-09 Cellular senescence
3.8e-11 Pathways of neurodegeneration
1.5e-10 Alzheimer disease
4.7e-10 Spinocerebellar ataxia
2.3e-11 Endocytosis
4.9e-17 Ubiquitin mediated proteolysis
8.2e-11 Spliceosome
5.6e-14 MRNA surveillance pathway



Supplementary Files

This is a list of supplementary files associated with this preprint. Click to download.

- Fig.S1.tif
- Fig.S5.tif
- Fig.S4.tif
- Fig.S3.tif
- Fig.S10.tif
- Fig.S2.tif
- Fig.S6.tif
- TableS2.pdf
- Fig.S11.tif
- Fig.S9.tif
- OriginalImmunoblotsforSub.pdf
- Fig.S8.tif
- Fig.S7.tif
- TableS1.pdf